LULEÅ
UNIVERSITY
OF TECHNOLOGY

Cosmic dust and heavy neutrinos

Erik Elfgren

Doctoral Thesis 2007:75
Division of Physics
Department of Applied Physics and Experimental Mechanics
Luleå University of Technology
SE-971 87 Luleå
Sweden

Luleå 2007

The photo on the front page shows the Eagle nebula, which is a dust region of active star formation about 7,000 light-years away.
Source: The Hubble Space Telescope, NASA

Dust in the wind

I close my eyes, only for a moment, and the moment's gone
All my dreams, pass before my eyes, a curiosity
Dust in the wind, all they are is dust in the wind.
Same old song, just a drop of water in an endless sea
All we do, crumbles to the ground, though we refuse to see

Dust in the wind, all we are is dust in the wind

Don't hang on, nothing lasts forever but the earth and sky
It slips away, and all your money won't another minute buy.

Dust in the wind, all we are is dust in the wind
Dust in the wind, everything is dust in the wind.

- *Kansas*

Preface

The work presented in this doctoral thesis is a result of a collaboration between Luleå University of Technology, Laboratoire d'Astrophysique de l'Observatoire de Grenoble, Institut d'Astrophysique de Paris and Centre de Recherche Astronomique de Lyon. My supervisor at Luleå University of Technology has been Sverker Fredriksson and my co-supervisors have been first Johnny Ejemalm and then Hans Weber.

I would like to express my gratitude towards the universe in general for being such a beautiful place, and towards my collaborators in particular for having helped me in my quest for knowledge and understanding of the workings of the universe. Of my collaborators I especially would like to thank François-Xavier Désert for his ideas, his concrete approach to problem solving and all the verifications he proposed to corroborate our results. Furthermore, I thank Bruno Guiderdoni for his invaluable support in the field of dark matter simulations. Of course, my supervisor Sverker Fredriksson has been of much help with his good general knowledge of particle and astrophysics and his invaluable support. My thanks also to Hans Weber, who gave me support at a crucial time.

A special thanks to my coauthors: François-Xavier Désert for Paper I and Paper II, Bruno Guiderdoni for Paper II and Sverker Fredriksson for Paper III and Paper IV.

I am grateful to my office-mate, Fredrik Sandin, for our discussions and his help with practical as well as theoretical issues and to Tiia Grenman and Johan Hansson for the exchanges we have had. I would also like to thank Henrik Andrén for his help in the matter of geometry and I thank all my friends for our friendship.

I am happy and grateful for having been a part of the National Graduate School in Space Technology, which has provided the financial support for my research, a most interesting set of workshops and course-work, and also a good network of fellow PhD-students.

Finally, a special thank to my wonderful, supporting wife, Nathalie, who is with me in my moments of defeat as well as of victory, and to my parents, who have helped me all along and brought me up to who I am today.

Luleå in December 2007

Erik Elfgren

Abstract

This doctoral thesis treats two subjects.

The first subject is the impact of early dust on the cosmic microwave background (CMB). The dust that is studied comes from the first generation of stars, which were hot and short-lived, ending their lives as giant supernovæ. In the supernova explosions, heavy elements, produced through the fusion in the stars, were ejected into the interstellar medium. These heavy elements condensed to form dust, which can absorb and thus perturb the CMB radiation. The dust contribution to this radiation is calculated and found negligible. However, since the dust is produced within structures (like galaxy clusters), it will have a spatial correlation that could be used to detect it. This correlation is calculated with relevant assumptions. The planned Planck satellite might detect and thus confirm this correlation.

The second subject is heavy neutrinos and their impact on the diffuse gamma ray background. Neutrinos heavier than $M_Z/2 \sim 45$ GeV are not excluded by particle physics data. Stable neutrinos heavier than this might contribute to the cosmic gamma ray background through annihilation in distant galaxies. They can also contribute to the dark matter content of the universe. The evolution of the heavy neutrino density in the universe is calculated as a function of the neutrino mass, M_N. The subsequent gamma ray spectrum from annihilation of distant neutrinos-antineutrinos (from $0 < z < 5$) is also calculated. The evolution of the heavy neutrino density in the universe is calculated numerically. In order to obtain the enhancement due to structure formation in the universe, the distribution of N is approximated to be proportional to that of dark matter in the GalICS model. The calculated gamma ray spectrum is compared to the measured EGRET data. A conservative exclusion region for the heavy neutrino mass is 100 to 200 GeV, both from EGRET data and our re-evalutation of the Kamiokande data. The heavy neutrino contribution to dark matter is found to be at most 15%.

Finally, heavy neutrinos are considered within the context of a preon model for composite leptons and quarks, where such particles are natural. The consequences of these are discussed, with emphasis on existing data from the particle accelerator LEP at CERN. A numerical method for optimizing variable cuts in particle physics is also included in the thesis.

Keywords: *Dust – CMB – Reionization – Power spectrum – Heavy leptons – Gamma rays – Preons*

Papers

The following papers are appended to this doctoral thesis:

Paper I: **Dust from reionization**
The production of dust in the early universe is estimated from the number of stars needed to achieve reionization. The spectral signature of the dust is calculated and compared to measurements. The contribution from the dust layer to the Cosmic microwave background is found to be small.
Elfgren, Erik and Désert, François-Xavier, 2004, Astronomy and Astrophysics, **425**, 9-14.

Paper II: **Dust distribution during reionization**
The spatial distribution of the dust is estimated using simulations of dark matter density evolution. Combining the calculated intensity from Paper I with this density and integrating along the line of sight, the spatial signature of the dust is obtained. The distribution of the dust gives a detectable signal.
Elfgren, Erik, Désert, François-Xavier and Guiderdoni, Bruno, 2007, Astronomy and Astrophysics, **476**, 1145-1150.

Paper III: **Mass limits for heavy neutrinos**
If fourth generation neutrinos exist and have a mass higher than 50 GeV they would produce a gamma ray signal due to annihilation within dense parts of the universe. We show that if the neutrino mass is $\sim 100 - 200$ GeV, this signal would already have manifested itself in data, and thus such masses can be excluded. We also show that in the edges of this region an eventual neutrino would give a small bump in the gamma ray spectrum.
Elfgren, Erik and Fredriksson, Sverker, accepted for publication (December 10, 2007) in Astronomy and Astrophysics. (astro-ph/0710.3893)

Paper IV: **Are there indications of compositeness of leptons and quarks in CERN LEP data?**
The implications of a substructure of fermions are investigated within a particular preon model, and possible signal characteristics are evaluated at the fairly “low” energies of the existing CERN LEP data.
Elfgren, Erik and Fredriksson, Sverker, submitted to Physical Review D. (hep-ph/0712.3342)

Paper V: **Using Monte Carlo to optimize variable cuts**
Optimization for finding signals of exotic particles are made by carefully choosing cuts on variables in order to reduce the background while keeping the signal. A method is proposed for optimizing these cuts by the use of cuts chosen with a *Monte Carlo* method.
Elfgren, Erik, submitted to Physics Letters B. (hep-ph/0712.3340)

(Most of the work in Paper I-III was done by the author with supervision and comments by the coauthors. In Paper IV a substantial part of the work was done by Sverker Fredriksson.)

Other publications with significant contributions by the author (not appended to this thesis):

- Azuelos, G.; Elfgren E.; Karapetian, G. (2001): Search for the FCNC decay $Z \to tq$ in the channel $t \to l\nu b$. OPAL Technical Note 693. This note and OPAL Papers and Preprints PR345 provide part of the background material to: Abbiendi, G. et al. (2001): The OPAL Collaboration. Search for Single Top Quark Production at LEP2. CERN-EP-2001-066. Physics Letters B521 (2001), pp 181-194.
- Azuelos, G.; Benchekroun, D.; Cakir, O.; Elfgren, E.; Gianotti, F.; Hansen, J.-B; Hinchliffe, I.; Hohlfeld, M.; Jakobs, K.; Leroy, C.; Mehdiyev, R.; Paige, F.E.; Polesello, G.; Stenzel, H.; Tapprogge, S.; Usubov, Z.; Vacavant, L. (2001): Impact of Energy and Luminosity upgrades at LHC on the Physics program of ATLAS. J. Phys. G28 (2002), pp 2453-2474. (hep-ex/0203019)
- Elfgren, Erik (1998): Moiré Profilometry. Research report for the PCS group, Cavendish Laboratory, University of Cambridge.
- Elfgren, Erik (1999): Control System for the Ion Accelerator at ISOLDE. Student lecture presented on 13 August 1999 at CERN, Geneva, Switzerland. Published in CERN Annual Report 1999, p 347.
- Elfgren, Erik (2000): Detection of a Hypercharge Axion in ATLAS. A Monte-Carlo Simulation of a Pseudo-Scalar Particle (Hypercharge Axion) with Electroweak Interactions for the ATLAS Detector in the Large Hadron Collider at CERN. Master's Thesis 2000:334CIV, Luleå University of Technology, ISSN 1402-1617 (hep-ph/0105290)
- Elfgren, Erik (2001): Detection of a Hypercharge Axion in ATLAS, appearing in "Fundamental Interactions", Proceedings of the 16th Lake Louise Winter Institute, British Colombia, Canada, World Scientific, pp 185-191 (2002).
- Elfgren, Erik (2002): Heavy and Excited Leptons in the OPAL Detector? Master's Thesis, Université de Montréal, Montréal, pp 1-85 (hep-ph/0209238)

Publications with insignificant contributions by the author (not appended to this thesis):

- R. Barate et al. (2003), Search for the standard model higgs boson at LEP. Physics Letters B 565: 61-75.
- G. Abbiendi et al. (2003), Test of noncommutative QED in the process $e^+ e^- \to \gamma\gamma$ at LEP. Physics Letters B 568: 181-190.
- G. Abbiendi et al. (2003), Bose-Einstein correlations of π^0 pairs from hadronic Z^0 decays. Physics Letters B 559: 131-143.
- G. Abbiendi et al. (2003), A measurement of semileptonic B decays to narrow orbitally excited charm mesons. European Physical Journal C 30: 467-475.
- G. Abbiendi et al. (2003), Dijet production in photon-photon collisions at $\sqrt{s_{ee}}$ from 189 to 209 GeV. European Physical Journal C 31: 307-325.
- G. Abbiendi et al. (2003), A measurement of the $\tau^- \to \mu^- \bar{\nu}_\mu \nu_\tau$ Branching Ratio. Physics Letters B 551: 35-48.

- G. Abbiendi et al. (2003), Search for nearly mass degenerate charginos and neutralinos at LEP. European Physical Journal C 29: 479-489.

- G. Abbiendi et al. (2003), Inclusive analysis of the b quark fragmentation function in Z decays at LEP. European Physical Journal C 29: 463-478.

- G. Abbiendi et al. (2003), Multiphoton production in e^+e^- collisions at $\sqrt{s} = 181$ to 209 GeV. European Physical Journal C 26: 331-344.

- G. Abbiendi et al. (2003), Search for the standard model Higgs boson with the OPAL detector at LEP. European Physical Journal C 26: 479-503.

- G. Abbiendi et al. (2003), Search for a low mass CP odd Higgs boson in e^+e^- collisions with the OPAL detector at LEP-2. European Physical Journal C 27: 483-495.

- G. Abbiendi et al. (2003), Measurement of the cross-section for the process $\gamma\gamma \to p\bar{p}$ at $\sqrt{s_{ee}} = 183$ to 189 GeV at LEP. European Physical Journal C 28: 45-54.

- G. Abbiendi et al. (2003), Charged particle momentum spectra in e^+e^- annihilation at $\sqrt{s} = 192$ to 209 GeV. European Physical Journal C 27: 467-481.

- G. Abbiendi et al. (2003), Decay mode independent searches for new scalar bosons with the OPAL detector at LEP. European Physical Journal C 27: 311-329.

- G. Abbiendi et al. (2002), Charged particle multiplicities in heavy and light quark initiated events above the Z^0 peak. Physics Letters B 550: 33-46.

- G. Abbiendi et al. (2002), Measurement of neutral current four fermion production at LEP-2. Physics Letters B 544: 259-273.

- G. Abbiendi et al. (2002), Measurement of the b quark forward backward asymmetry around the Z^0 peak using an inclusive tag. Physics Letters B 546: 29-47.

- G. Abbiendi et al. (2002), Search for scalar top and scalar bottom quarks at LEP. Physics Letters B 545: 272-284, 2002, Erratum-ibid. B548: 258.

- G. Abbiendi et al. (2002), Search for associated production of massive states decaying into two photons in e^+e^- annihilations at $\sqrt{s} = 88$ to 209 GeV. Physics Letters B 544: 44-56.

- G. Abbiendi et al. (2002), Search for charged excited leptons in e^+e^- collisions at $\sqrt{s} = 183$ to 209 GeV. Physics Letters B 544: 57-72.

- G. Abbiendi et al. (2002), Measurement of the charm structure function $F^{\gamma}_{2,c}$ of the photon at LEP. Physics Letters B 539: 13-24.

Contents

1 Introduction **1**

1.1 Background and motivation 1

1.2 Objectives 2

1.3 Research questions 2

1.3.1 Imprint of dust on the CMB 2

1.3.2 Implications and possible origin of hypothetical heavy neutrinos 2

1.3.3 Cut optimization 3

1.4 Thesis guide 3

2 History of the universe **5**

2.1 The big bang 5

2.2 Inflation 7

2.3 Radiation dominated era 7

2.4 Matter dominated era 7

2.5 Decoupling of matter 8

2.6 Structure formation 8

2.7 The first generation of stars 8

2.8 Reionization 9

3 Cosmology **11**

3.1 Introduction 11

3.2 General relativity 11

3.2.1 The equivalence principle 11

3.2.2 The metric 12

3.2.3 The Einstein equations 13

3.3 Standard cosmology 14

3.4 Thermodynamics of the early universe 15

3.4.1 Thermal equilibrium 15

3.4.2 Radiation 16

3.5 Decoupling 17

4 The cosmic microwave background **19**

4.1 Primary anisotropies 20

4.1.1 Gravitational anisotropies 20

4.1.2 Adiabatic anisotropies 20

4.1.3 Doppler anisotropies 21

4.2 Secondary anisotropies 21

4.2.1 Gravitational effects 21

    - 4.2.2 Local reionization . . . 21
    - 4.2.3 Global reionization . . . 22
  - 4.3 Foregrounds . . . 23
    - 4.3.1 Extragalactic foregrounds . . . 23
    - 4.3.2 Galactic foregrounds . . . 23
    - 4.3.3 Local foregrounds . . . 23
  - 4.4 Power spectrum . . . 24
    - 4.4.1 Acoustic oscillations . . . 24
    - 4.4.2 Simulations of the cosmic microwave background . . . 24

5 Introduction to the papers **27**
  - 5.1 Dust . . . 27
    - 5.1.1 Production . . . 27
    - 5.1.2 Properties . . . 27
    - 5.1.3 Destruction . . . 28
  - 5.2 Dark matter . . . 28
  - 5.3 Heavy neutrinos . . . 29
    - 5.3.1 Background . . . 29
    - 5.3.2 Heavy fermions . . . 30
  - 5.4 Preons . . . 32
    - 5.4.1 The standard model vs preons . . . 32
    - 5.4.2 A brief history of preon models . . . 33
    - 5.4.3 Some general arguments . . . 34
    - 5.4.4 There are too many quarks and leptons . . . 35
    - 5.4.5 Unstable fundamental particles? . . . 35
    - 5.4.6 Ad hoc quantum numbers . . . 36
    - 5.4.7 Mixings of fundamental particles? . . . 36
    - 5.4.8 γ/Z mixing . . . 39
    - 5.4.9 What next? . . . 41

6 Discussion and conclusions **43**
  - 6.1 Imprint of dust on the CMB . . . 43
  - 6.2 Implications and possible origin of hypothetical heavy neutrinos . . . 44
  - 6.3 Conclusions . . . 48

7 Outlook **49**

A Cosmology reference **59**
  - A.1 Basic introduction . . . 59
  - A.2 Cosmological equations . . . 60

B Particle physics **61**
  - B.1 The standard model of particle physics . . . 61
  - B.2 Quantum field theory . . . 61
  - B.3 Electroweak interactions . . . 62
  - B.4 Heavy neutrinos . . . 62

C Explanations **65**
C.1 Glossary 65
C.2 Abbreviations 68
C.3 List of variables 68
C.4 List of some cosmological constants 69
C.5 List of some physical constants and units 69

Appended papers

- Paper I: Dust from reionization
- Paper II: Dust distribution during reionization
- Paper III: Mass limits for heavy neutrinos
- Paper IV: Are there indications of compositeness of leptons and quarks in CERN LEP data?
- Paper V: Using Monte Carlo to optimize variable cuts

Chapter 1

Introduction

In this chapter, the background to and motivation for this thesis are explained. The research objectives and research questions are then stated and, finally, a guide to the thesis is presented.

1.1 Background and motivation

The universe is a wonderful place, ranging from smaller than an atom to larger than a galaxy, with complex humans, beautiful flowers, powerful stars, and vast amounts of empty space. But where does it all come from? How did all this diversity come to be?

The universe is generally believed to have started out in the big bang – an immense concentration of energy, expanding and thus diluting. Different particles were created, such as neutrons, protons and electrons, then ions and atoms. A long pause followed during which matter assembled through gravity to form large-scale structures such as stars and galaxies. And in the galaxies, around the stars, planetary systems assembled, which can host life.

But how can we know all this? The truth is that we do not. However, we do have several pieces of indirect evidence. The single most important observation is the so-called cosmic microwave background radiation (CMB for short). This radiation was emitted when the universe was merely 400,000 years old and can be thought of as a kind of photograph taken of the universe at this time. Amazing! Furthermore, this radiation is present everywhere in the universe and has a very characteristic spectrum. The discovery of the CMB single-handedly convinced the scientific community of the validity of the big bang model.

In order to measure the CMB accurately, we must know what it has passed through; our solar system, our galaxy, other galaxies, further and further away until the first generation of stars. Very little is known about these first stars. One plausible hypothesis states that they had very intense and violent lives. This would mean that they finished as supernovæ – giant explosions – thus spreading their contents in space. These left-overs are called star dust, and due to its abundant production and wide spread it clouds the CMB somewhat. It is like looking at the sun through a thin mist.

From my background in particle physics I was also interested in finding out more about the consequences of exotic particles (heavy neutrinos in particular) within the context of astrophysics, cosmology and particle physics. There are three families of particles known today, but there are strong reasons to believe that this is not the whole picture. A fourth family seems like a natural extension, and this was the subject of my Master's thesis in Montréal (Elfgren 2002*b*). In a particle detector, these neutrinos would need to be very short-lived to be distinguishable from ordinary neutrinos. In astrophysics, the reverse is true. Only very long-lived neutrinos would leave a trace today, through annihilations of neutrino-antineutrino pairs, resulting in energetic gamma rays.

Another interesting explanation for the three generations is that they have a substructure – consisting of particles known as preons. These preons have recently gained momentum in the context of astrophysics because of preon stars, a new type of hypothetical astrophysical objects (Ball 2007). These compact stars were proposed by my co-workers Fredrik Sandin and Johan Hansson (Sandin and Hansson 2007). Earlier, a particular preon model was invented by Dugne, Fredriksson and Hansson (2002) and it turns out to be particularly suitable for studying heavy neutrinos.

1.2 Objectives

The objectives of my research have been to investigate

- the imprint of early dust on the CMB and
- the implications and possible origin of hypothetical heavy neutrinos.

1.3 Research questions

In order to meet the objectives, seven research questions have been formulated and they form the core of the research presented in this thesis. The answers to the questions are derived in the appended publications and summarized in chapter 6 in the thesis. The research questions are as follows:

1.3.1 Imprint of dust on the CMB

1. **How did the dust density evolve in the early universe?**
   This question is discussed in Paper I.

2. **What is the spectrum of the thermal emission of dust from population III stars?**
   This question is discussed in Paper I.

3. **What was the spatial distribution of the dust from population III stars?**
   This question is discussed in Paper II.

1.3.2 Implications and possible origin of hypothetical heavy neutrinos

4. **How does the neutrino density evolve with time?**
   This question is discussed in Paper III.

5. **How large is the clumping enhancement for the neutrino-antineutrino signal?**
   This question is discussed in Paper III.

6. **How much would heavy neutrinos contribute to the diffuse gamma ray background?**
   This question is discussed in Paper III.

7. **How would composite leptons and quarks reveal themselves in existing data?**
   This question is discussed in Paper IV.

1.3.3 Cut optimization

While doing research in particle physics (Elfgren 2002*b*), within the CERN OPAL collaboration, I invented a method of cut optimization. Such cuts are traditionally found by hand, while I use a Monte Carlo method to optimize them. This greatly improves the signal-over-background ratio obtained. While this method was developed in the context of particle physics, it can be just as useful in astrophysics, at least in the case of a weak signal with several variables describing the same object. The method is presented in a short letter, paper V.

1.4 Thesis guide

In chapter 2, the early history of the universe is outlined, from the big bang until the formation of the first galaxies. This part of the thesis is intended as an introduction for the general public and is thus rather elementary.

In chapter 3 follows some basics of cosmology and the more technical parts of the early universe. Some general relativity and thermodynamics are treated as an introduction to Paper III. This chapter should be understandable for physicists in general.

In chapter 4, the CMB with its properties and its different foregrounds is described in some detail. This is also rather technical, but mostly descriptive. Some knowledge of astrophysics is required to fully understand this chapter.

In chapter 5, I present a brief introduction that is useful for the understanding of some of the particulars of the five appended papers. This includes a description of our general knowledge of dust and some concepts of dark matter. There is also a discussion about possible extensions of the standard model of particle physics (which is outlined in appendix B), like heavy neutrinos and fermion constituents.

In appendix A a short introduction to cosmology is provided along with some common formulæ. For further details on symbols, constants, and abbreviations, see appendix C. Unless otherwise stated, I use natural units so that $c = \hbar = k_b = 1$. Technical words that appear *slanted* are explained in the glossary in the same appendix.

Chapter 2

History of the universe

Our understanding of the evolution of the universe is far from complete, but the picture is getting clearer by the day with the advent of new detectors and new experimental and theoretical results. We have entered an era of high-precision cosmology, where conjectures are replaced by detailed measurements, and slowly a "standard model" of cosmology is emerging. There are still many question marks and much to explore, but the main picture seems pretty clear by now. This section contains a description of the evolution of the universe as we understand it today, illustrated by table 2.1. These results are fairly robust unless otherwise specified. This description of the evolution of the universe is called Λ-Cold Dark Matter (or ΛCDM for short) and has recently become predominant due to good experimental support. In this chapter, the evolution of this ΛCDM universe is described. Some of the technical details of this model are explored in chapter 3.

2.1 The big bang

The universe started out some 14 billion years ago by being extremely dense and hot. Note, however, that we do not know what happened at the actual beginning, but we can extrapolate the current expansion of the universe back *towards* that time, $t = 0$. According to recent measurements, Spergel et al. (2007), this was $13.73^{+0.16}_{-0.15}$ billion years ago.

Contrary to common belief, there was no "explosion", but merely a rapid expansion of the fabric of the universe, like the rubber of a balloon stretches when you inflate it. The expansion of the universe still continues today and there is no indication that the expansion has a center. In an infinite universe, the big bang occurred everywhere at once. How we can conceive an infinite energy density at $t = 0$, or for that matter an infinite universe, is a philosophical question. Physicists generally content themselves with starting the exploration a fraction of time after $t = 0$.

During this first (and extremely brief) period of the universe, all forces are believed to have been just one and the same. However, as the universe cooled off, the forces separated into the electric, magnetic, gravitational, and the weak and strong nuclear force. An analogy with this separation would be the melting of ice cubes in a glass, being separate objects below freezing but melting into one homogeneous water mass at higher temperatures.

Note that this unification of forces is a theory without direct experimental support. Fortunately, the subsequent evolution of the universe does not hinge on this unification.

Table 2.1: History of the universe.

Time after BB	Events	Illustration
$\sim 10^{-43}$ s	• Unification of forces?	?
$\gtrsim 10^{-34}$ s	• Inflation • Exponential expansion	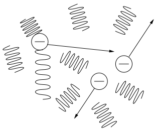
$\gtrsim 10^{-10}$ s	• Radiation domination • Protons and neutrons are stable • Antimatter disappears	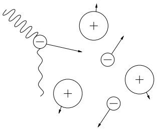
$\gtrsim 10^{2}$ s	• Matter domination • Hydrogen becomes stable • Nucleosynthesis	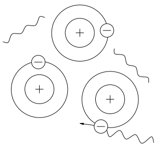
$\gtrsim 3 \times 10^{5}$ yrs	• Decoupling of matter • Transparent universe • The CMB is released	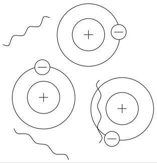
$\sim 10^{9}$ yrs	• Structure formation • The first stars and galaxies	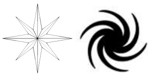

2.2 Inflation

When the universe was roughly 10^{-34} seconds old, a period of intensive expansion occurred and the universe became $\sim 10^{50}$ times bigger in a fraction of a second. This expansion is called inflation.

This theory has some more experimental support than that of the unification of forces. In fact, it was introduced to alleviate three serious deficits of the big bang theory: the horizon, the flatness and the monopole problem. Here comes a brief explanation of them. For more detail, I suggest the book by Peacock (1998). The horizon problem stems from the measured correlation between parts of the universe that never have been in contact (due to the finite speed of light). The flatness problem is that the universe can be measured to be nearly flat, as far as we can see, and this is unlikely from a theoretical point of view. The monopole problem is about the absence of so-called magnetic monopoles, which are theoretically predicted as a consequence of the unification of forces.

Furthermore, inflation also provides natural seeds for star and galaxy formation, through the growth of tiny quantum fluctuations into macroscopic fluctuations.

Although inflation has many attractive features, it is not yet a complete theory because many of the details still do not work out right in realistic calculations without assumptions that are poorly justified. Probably, most cosmologists today believe inflation to be correct at least in its outlines, but further investigation will be required to establish whether this is indeed so.

2.3 Radiation dominated era

After approximately 10^{-10} seconds the inflation period was at an end. The subsequent epoch is called the radiation dominated era in which the principal component of the universe was radiation – photons.

During this era, the *antimatter* disappeared from the universe through contact with matter, which resulted in annihilation. However, due to a slight excess of matter over antimatter, the antimatter was all consumed and only the excess of ordinary matter remained.

The universe had also become cool enough to allow protons and neutrons to form and become stable. Before this time, the quarks and gluons possibly co-existed in some sort of plasma. The protons are nothing but ionized hydrogen, which was the first type of atoms to form.

This early formation of particles touches upon the subject of particle physics, in which the author has a particular interest. For more information about other possible types of particles, see section 5.3 and also Elfgren (2002*a*,*b*).

2.4 Matter dominated era

Around one minute after the big bang, the radiation had lost enough energy density due to the expansion to allow matter to start dominating. This, in turn, means that the expansion rate of the universe changed.

During the matter dominated era, the thermal energy became low enough to allow the ionized hydrogen atoms to capture and keep electrons, thus forming the first neutral atoms. Furthermore, protons and neutrons started to fuse to form helium and other heavier elements. This process is called the *big bang nucleosynthesis* (BBN) but did last for only about three minutes (Alpher, Herman and Gamow 1948). After that time, the density and the temperature of the universe dropped below what is required for nuclear fusion (neutron capture). The brevity of BBN is important because it prevented elements heavier than beryllium from forming, while allowing unburned light elements, such as deuterium, to exist. The result of the BBN is that the universe contains 75% hydrogen, 25% helium, 1% deuterium and small amounts of lithium and beryllium. This predicted distribution corresponds very well to the measured abundances. For more detail on the BBN, see, e. g., Burles et al. (2001).

The matter dominated era extended until the *dark energy* took over after roughly five billion years. The nature of this dark energy is not well known. It has negative pressure, so it is not ordinary matter. The experimental reasons to believe in dark energy are the observations of the CMB (Spergel et al. 2007) and supernovæ type Ia (Perlmutter et al. 1999).

2.5 Decoupling of matter

When the temperature of the universe dropped below $T \sim 0.25$ eV ~ 3000 K the photons no longer had enough energy to ionize or excite the atoms. This means that the photons could neither loose, nor gain energy. Thus, the universe became transparent and the photons kept their energy indefinitely (unless otherwise perturbed). These photons constitue the CMB and their properties will be described in more detail in chapter 4.

In order to estimate this transition temperature, one can calculate the temperature at which there is one exciting photon per proton. For a photon to excite a hydrogen atom, it needs at least $E = 10.2$ eV, which corresponds to a transition from the ground state to the first excited state. This means that one requires:

$$n_p = n_\gamma(E_\gamma > 10.2\,\mathrm{eV}) = n_\gamma \cdot \frac{1}{e^{10.2\,\mathrm{eV}/k_B T} - 1}, \tag{2.1}$$

where n_p and n_γ are the number densities of protons and photons respectively, k_B is Boltzmann's constant and T is the temperature of the photons. Using $n_\gamma \sim 10^9\ n_p$, the temperature can be calculated to $T \approx 5700$ K. If a more detailed calculation is made, the temperature is found to be approximately 3000 K, which corresponds to $t \approx 400,000$ years after the big bang (and a *redshift*, $z \sim 1100$). As the universe expands, this temperature decreases as $1/a$, where $a = 1/(1+z)$ is the expansion factor. Since the universe has expanded by a factor of 1100 since decoupling, the temperature of the CMB has now dropped to 2.725 K (Mather et al. 1999).

This transition did not happen at one single time, but rather took something like 50,000 years ($\Delta z \approx 100$).

2.6 Structure formation

After the decoupling, the universe went through a period called the dark ages, which lasted until the onset of star formation about a billion years later. During this epoch the only thing that happened is that the CMB propagated and the matter slowly contracted due to gravity. Regions in space with an initial over-density (created by the inflation) attracted more matter, and eventually the matter density became high enough to sustain fusion, and thus the first generation of stars formed.

During the dark ages, dark matter played a key roll in shepherding matter into dense regions, thus allowing star formation. The dark matter is described briefly in section 5.2.

2.7 The first generation of stars

The first stars are called population III stars (see, e. g., Shioya et al. 2002) due to properties that are rather different from those of the stars today (see, e. g., Gahm 1990). The first stars were born in loosely bound gravitational structures defined by high *baryon* densities and a surrounding dark matter halo.

The source material of these stars is the matter that was created during the big bang nucleosynthesis, see section 2.4. This means that there is basically only hydrogen and helium in these stars.

As time passed by, the source material for new stars had more and more heavy elements since those were produced by the stars. The mass fraction of elements heavier than helium is called *metallicity*.

It is also believed that these first stars would have been rather heavy, see Cen (2003) and Fang and Cen (2004). The mass of the stars is characterized by the initial mass function (IMF). With a low metallicity and a high mass, the stars are short-lived and hot (Shioya et al. 2002). If the stars were not heavy, they would live longer and take more time to produce dust, thereby delaying the reionization to an improbable period. No population III stars have been observed.

2.8 Reionization

From decoupling until the reionization, the universe was made up of neutral atoms (along with photons, dark matter and dark energy). Today, however, the universe is largly ionized and it has been so for that last couple of billion years. The transition between the neutral and the ionized universe is called the reionization period. A recent review of this can be found in Choudhury and Ferrara (2006). For a more complete picture, involving star formation, reionization, and chemical evolution, see Daigne et al. (2004).

At the onset of the first generation of stars, energetic photons were produced. This happened when $z \sim 10$ and thus the CMB temperature was only $T_{CMB} \sim 30$ K, while the star temperature could be over 80,000 K (Shioya et al. 2002). At this temperature, the maximum emitted energy was at $E_\gamma \sim 21$ eV, which was more than enough to ionize hydrogen ($E_{H,ion} = 13.61$ eV).

The reionization process can be divided into three phases. In the pre-overlap phase, bulbs around stars were ionized, and slowly expanded into the neutral intergalactic medium (IGM). This effect was partly cancelled due to the natural tendency of hydrogen to capture an electron, thereby returning to a neutral state. In the overlap phase, the ionized regions started to overlap and subsequently ionize the whole of the IGM, except some high-density regions. At this stage the universe became largly transparent to ultraviolet (UV) radiation. In the post-overlap phase, in which we still are today, the ionization fronts propagates into the neutral high density regions, while recombination tends to resist this effect.

In the presence of free electrons, photons scatter through a process known as Thomson scattering. However, as the universe expands, the density of free electrons decreases, and so will the scattering frequency. In the period during and after reionization, but before significant expansion had occurred to sufficiently lower the electron density, the light that composes the CMB experienced observable Thomson scattering. This is characterized by the opacity, τ_e, which is defined through

$$e^{-\tau_e} = \text{probability of a photon to pass without being scattered.} \tag{2.2}$$

The effect of the reionization on the properties of the CMB is important and will be discussed in more detail in section 4.3.

Chapter 3

Cosmology

3.1 Introduction

Modern cosmology is based on two cornerstones: that the universe is homogeneous and isotropic. Together they are called the cosmological principle. By homogeneous we mean that, on a very large scale, the universe is the same everywhere. By isotropic we mean that there is no special direction in the universe. Obviously, what we see when we look out at the nearby universe is something far from homogeneous. There is the sun and the moon and further away the galactic center with a much higher star density, and then there is a vast expanse of void until the next galaxy, the Andromeda galaxy. The nearby universe is not isotropic either – if you try staring into the sun, the effect will be quite different from staring at a distant star. And further out, in the direction of the the Andromeda galaxy, there is light that can be seen with the naked eye while in other directions the sky is black. This means that the universe, *locally*, is both inhomogenous and anisotropic.

However, as we expand our view to look, not at our solar system, our galaxy or even our galaxy cluster, the universe looks more and more homogeneous and isotropic, as can be seen in figure 3.1. There are, however, those who challenge the cosmological principle, e. g., Barrett and Clarkson (2000), who claim that a class of inhomogeneous perfect fluid cosmologies could also be a possible alternative. Another possibility would be a different geometry of the universe. In Campanelli et al. (2006), an ellipsoidal universe is proposed as a solution to the quadrupole problem of the WMAP-data. This quadrupole can also be explained by a huge void (Martínez-González et al. 2006; Inoue and Silk 2007) with a diameter of $\sim 1 \times 10^9$ light years. A hole of this size is difficult to accomodate within the standard cosmology.

3.2 General relativity

This section is rather mathematical and requires some knowledge of tensor analysis. A classical overview of general relativity and tensor analysis can be found in Misner et al. (1973). We recall that when two indices are found in an equation, summation is implicitely assumed, $x^\mu x_\mu = \sum_\mu x^\mu x_\mu$, and greek indices $(\mu, \nu, \alpha, \beta, ...)$ go from 0 to 3 and roman indices $(i, j, k, ...)$ go from 1 to 3. The coordinates are $x^\mu = (t, \vec{x}) = (t, x, y, z)$.

3.2.1 The equivalence principle

The equivalence principle says that the gravitational effects are identical to those experienced through acceleration.

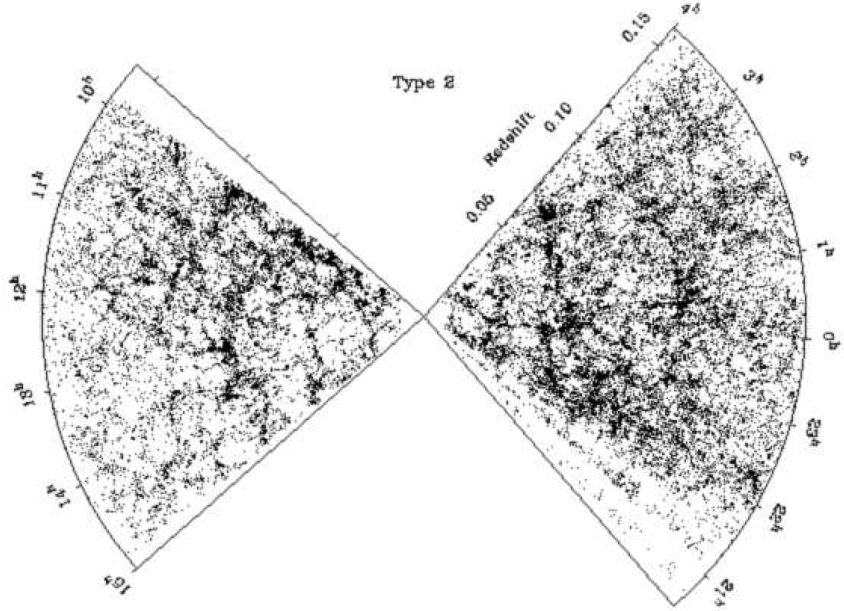

Figure 3.1: Distribution of galaxies within $\sim 2 \times 10^9$ light years. On these scales the universe looks rather homogeneous and isotropic, as postulated by the cosmological principle. The radial axis represents distance from the earth in terms of redshift ($z = 0 - 0.15$), and the angular axis represents the projected angular distribution (anti-clockwise from $21^h - 04^h$ and $10^h - 15^h$). Each dot is a galaxy. The figure is from Colless et al. (2001).

The weak equivalence principle states that in any gravitational field a freely falling observer experiences no gravitational effect, except tidal forces in the case of non-uniform gravitational fields. The spacetime is described by the Minkowski metric, see below.

The strong equivalence principle postulates that all the laws of physics take the same form in a freely falling frame in a gravitational field as they would in the absence of gravity.

3.2.2 The metric

In special relativity, the metric is given by

$$g_{\mu\nu} = \begin{pmatrix} 1 & 0 & 0 & 0 \\ 0 & -1 & 0 & 0 \\ 0 & 0 & -1 & 0 \\ 0 & 0 & 0 & -1 \end{pmatrix}, \tag{3.1}$$

which is called the Minkowski metric.

Mathematically, the metric is a covariant, second-rank, symmetric tensor in space time. It can be thought of as a local measure of length in non-euclidian space. Both the measure, called the line element,

$$ds^2 = g_{\mu\nu} dx^\mu dx^\nu \tag{3.2}$$

and the metric tensor, $g_{\mu\nu}$, are often referred to as 'the metric' in relativity.

If the cosmological principle (homogeneous and isotropic) holds, the metric can be written as

$$g_{\mu\nu} = \begin{pmatrix} 1 & 0 & 0 & 0 \\ 0 & -a^2(t)/(1-kr^2) & 0 & 0 \\ 0 & 0 & -a^2(t)r^2 & 0 \\ 0 & 0 & 0 & -a^2(t)r^2\sin^2\theta \end{pmatrix} \tag{3.3}$$

and the line element as

$$ds^2 = dt^2 - a^2(t)\left(\frac{dr^2}{1-kr^2} + r^2 d\theta^2 + r^2\sin^2\theta d\phi^2\right). \tag{3.4}$$

Here, the parameter $a(t)$ represents the global scaling of the universe, t is the time, and r, θ and ϕ are the coordinates in a spherical coordinate system. The geometry of the universe is given by k and if $k > 0$ the universe is open, if $k < 0$ it is closed and if $k = 0$ it is flat. Today, the evidence points towards $k = 0$.

We also notice that there are several other useful metrics in general relativity. For black holes, for example, there is the stationary Schwarzschild metrics and the rotating Kerr metric. For rotating fluid bodies, the Wahlqvist metric is appropriate even though it can not be smoothly joined to an exterior asymptotically flat vacuum region (Bradley et al. 2000).

3.2.3 The Einstein equations

The full Einstein equations, including a cosmological constant, are

$$R_{\mu\nu} - \frac{1}{2}g_{\mu\nu}R - \Lambda g_{\mu\nu} = 8\pi G_N T_{\mu\nu}, \tag{3.5}$$

where Newton's constant of gravitation is $G_N = 6.6742(10) \times 10^{-11}$ m^3/kg·s^2 and the other terms will be described below, from right to left.

The stress-energy tensor, $T_{\mu\nu}$, describes the density and flux of energy and momentum in spacetime, generalizing the stress tensor of newtonian physics. If there are many particles, the stress-energy tensor can be treated as a fluid. For a perfect fluid with pressure p, density ρ and velocity u^μ,

$$\begin{aligned} T^{\mu\nu} &= (p+\rho)u^\mu u^\nu - pg^{\mu\nu} && (3.6) \\ T^{\mu\nu}_{;\nu} &\equiv \partial_\nu T^{\mu\nu} + \Gamma^\nu_{\nu\alpha}T^{\alpha\mu} = 0. && (3.7) \end{aligned}$$

The metric, $g^{\mu\nu}$, captures the geometric and causal structure of spacetime, and it is used to define distance, volume, curvature, angle, future and past. The metric was introduced earlier in section 3.2.2.

The cosmological constant, Λ, is a rather mysterious entity. There is nothing in the derivation of the Einstein field equation that excludes a term proportional to the metric $g_{\mu\nu}$. Einstein introduced the cosmological constant in order to stop the universe from collapsing under the force of gravity, since the universe, at this time, was believed to be static. After the discovery by Edwin Hubble that there was a relationship between redshift and distance, thus indicating at dynamic universe, Einstein declared this formulation to be his "biggest blunder". However, cosmic acceleration (Perlmutter et al. 1999) along with the results of the Wilkinson microwave anisotropy Probe, WMAP (Spergel et al. 2003, 2007) has renewed the interest in a cosmological constant. Physically, it can be seen as a negative pressure, but its actual origin is still unknown. There are, however, also other possible causes for the observed data, like a local void (Alexander et al. 2007).

The Ricci scalar, R, is the contraction of the Ricci tensor,

$$R = g^{\mu\nu} R_{\mu\nu}. \tag{3.8}$$

The Ricci tensor, $R_{\mu\nu}$, is a symmetrical 4-dimensional tensor. It can be calculated from the Riemann tensor, $R_{\alpha\mu\beta\nu}$:

$$R_{\mu\nu} = g^{\alpha\beta} R_{\alpha\mu\beta\nu}. \tag{3.9}$$

The Riemann tensor, which has only 20 independent terms due to symmetries, is defined as

$$R_{\alpha\mu\beta\nu} = g_{\alpha\gamma} R^{\gamma}_{\mu\beta\nu} = g_{\alpha\gamma}\left[\Gamma^{\gamma}_{\mu\nu,\beta} - \Gamma^{\gamma}_{\mu\beta,\nu} + \Gamma^{\gamma}_{\sigma\beta}\Gamma^{\sigma}_{\nu\mu} - \Gamma^{\gamma}_{\sigma\nu}\Gamma^{\sigma}_{\beta\mu}\right], \tag{3.10}$$

where the (non-tensor) Christoffel symbols (also known as affine connections) $\Gamma^{\alpha}_{\mu\nu}$ are defined from the metric as

$$\Gamma^{\alpha}_{\mu\nu} = \frac{1}{2} g^{\alpha\beta}\left(\frac{\partial g_{\nu\beta}}{\partial x^{\mu}} + \frac{\partial g_{\mu\beta}}{\partial x^{\nu}} - \frac{\partial g_{\nu\mu}}{\partial x^{\beta}}\right) \tag{3.11}$$

3.3 Standard cosmology

The observational foundations for the standard model of cosmology are the expansion of the universe (Hubble 1929; Jackson 2007), the fossil record of light elements (Alpher, Bethe and Gamow 1948; Gamow 1948; Coc et al. 2004) that formed during the first minutes after the big bang, and the remnant of the intense thermal radiation field, the CMB (Penzias and Wilson 1965; Boggess et al. 1992; Fixsen et al. 1994; Dwek et al. 1998) that was released when the universe became transparent to radiation around 400,000 years after the big bang (see chapter 4). Among the early proponents of the standard cosmology were Efstathiou et al. (1990).

A homogeneous and isotropic universe with radiation, matter and vacuum energy is called a Friedmann-Lemaître-Robertson-Walker (FLRW) universe. The four diagonal terms of the left hand side of the Einstein equations can be evaulated for a homogeneous and isotropic universe (with the metric in equation (3.3))

$$00: \quad 3\left(\frac{\dot{a}}{a}\right)^2 + \frac{3k}{a^2} - \Lambda \tag{3.12}$$

$$ii: \quad \left(2\frac{\ddot{a}}{a} + \left(\frac{\dot{a}}{a}\right)^2 + \frac{k}{a^2} - \Lambda\right) g_{ii} \tag{3.13}$$

for the components $00, 11, 22$ and 33. Along with the right hand side of the Einstein equations (the stress-energy tensor for a perfect fluid, equation (3.7)), the resulting relations can be calculated. They are known as the Friedmann equations:

$$\left(\frac{\dot{a}}{a}\right)^2 = \frac{8\pi G_N}{3}\rho_{tot} \tag{3.14}$$

$$2\frac{\ddot{a}}{a} + \left(\frac{\dot{a}}{a}\right)^2 + \frac{k}{a^2} = -8\pi G_N p. \tag{3.15}$$

Here

$$\rho_{tot} = \rho_r + \rho_m + \rho_k + \rho_\Lambda, \tag{3.16}$$

with ρ_m being the matter density, ρ_r the radiation density, $\rho_k = -k/a^2 \cdot 3/8\pi G_N$, and $\rho_\Lambda = \Lambda/8\pi G_N$ being the vacuum energy density caused by the cosmological constant.

We also note that by using the second Friedmann equation along with the vanishing covariant divergence $T^{\mu\nu}_{;\mu} = 0$ it can be shown that

$$\frac{d}{dt}(\rho a^3) = -p\frac{d}{dt}a^3. \tag{3.17}$$

The equation of state for radiation is $p = \rho/3$, for matter $p = 0$ and for the cosmological constant $p = -\rho$. This gives the relation beween ρ_{tot} and a:

$$\rho_{tot} = \rho^*_{r0}\left(\frac{a_0}{a}\right)^4 + \rho_{m0}\left(\frac{a_0}{a}\right)^3 + \rho_{k0}\left(\frac{a_0}{a}\right)^2 + \rho_\Lambda, \tag{3.18}$$

where the zeroes indicate present-day values. Note that the radiation density has to be modified, $\rho^*_{r0} = \rho_{r0} \cdot g_*(a)/g_*(a_0)$, due to the reheating by particles falling out of equilibrium. This is treated in section 3.4.2. The densities can now be recast in relation to the critical density, $\rho_c = \frac{3H_0}{8\pi G_N}$:

$$\Omega = \frac{\rho_{tot}}{\rho_c} = \Omega_r \frac{g_*(a)}{g_*(a_0)}\left(\frac{a_0}{a}\right)^4 + \Omega_m\left(\frac{a_0}{a}\right)^3 + \Omega_k\left(\frac{a_0}{a}\right)^2 + \Omega_\Lambda. \tag{3.19}$$

The expansion rate of the universe, $\dot{a}/a = \sqrt{\rho_{tot} \cdot 8\pi G_N/3}$, is known as the Hubble parameter. In terms of the relative energy density of the universe, the Hubble parameter can be written as

$$H \equiv \frac{\dot{a}}{a} = H_0\sqrt{\Omega}, \tag{3.20}$$

where H_0 is the present day value of the Hubble parameter.

3.4 Thermodynamics of the early universe

The physics of the early universe is treated in great detail in the book by Kolb and Turner (1990) from which much of the material in this section is derived.

3.4.1 Thermal equilibrium

In the early universe (but after inflation), when the reaction rates $\Gamma \sim n\sigma|v|$ for particle-antiparticle annihilation were still much higher than the expansion of the universe, $H(t) = \dot{a}/a$, particles were in thermal equilibrium.

If the forces between the particles are weak and short-ranged, their distribution can be approximated by an ideal homogeneous gas. In such a gas, a particle with mass m and chemical potential μ at a temperature T has a number density given by

$$n = \frac{g_s}{(2\pi)^3}\int f(\vec{p})d^3|\vec{p}|, \tag{3.21}$$

where $E^2 = m^2 + |\vec{p}|^2$ and the occupancy function, $f(\vec{p})$, for a species in kinetic equilibrium is given by

$$f(\vec{p}) = \frac{1}{e^{(E-\mu)/T} \pm 1}. \tag{3.22}$$

The plus sign applies for fermions, which obey Fermi-Dirac statistics, and the minus sign applies for bosons, which follow Bose-Einstein statistics. The number of internal degrees of freedom (= spin states), g_s is 2 for most particles, though not for left-handed neutrinos, which have only one spin state and therefore $g_s = 1$.

In the relativistic limit, $T \gg m$, the integral can be evaluated if $T \gg \mu$:

$$n_{bosons} = g_s(\zeta(3)/\pi^2)T^3 \tag{3.23}$$

$$n_{fermions} = n_{bosons} \cdot 3/4, \tag{3.24}$$

where ζ is the Riemann zeta function and $\zeta(3) \approx 1.2020569032$.

In the non-relativistic limit, $m \gg T$, the integral is the same for bosons and fermions:

$$n = g_s \left(\frac{mT}{2\pi}\right)^{3/2} e^{-(m-\mu)/T}. \tag{3.25}$$

If a particle possesses a conserved charge, it may have an equilibrium chemical potential with a corresponding charge density. Astronomical observations indicate that the cosmological densities of all charges that can be measured are very small. Hence, we will assume that $\mu = 0$ in the following treatment.

3.4.2 Radiation

Photons are relativistic bosons and as such they have a number density of $n_\gamma = (2\zeta(3)/\pi^2) \cdot T^3$. The radiation density,

$$\rho = \frac{g_s}{(2\pi)^3} \int E(\vec{p}) f(\vec{p}) d^3|\vec{p}|, \tag{3.26}$$

can be calculated for a relativistic particle with $\mu \ll T$ and the result is

$$\rho = g_s(\pi^2/30) \cdot T^4. \tag{3.27}$$

Since the photon number density is not conserved ($\Rightarrow \mu_\gamma = 0$) this expression is therefore also valid for photons. However, in the early universe there are several particles that are in thermal equilibrium with the photons, thus contributing to the total radiation energy density

$$\rho_R = \frac{\pi^2}{30} g_*(T) T^4, \tag{3.28}$$

where g_* is the number of degrees of freedom of all particles in thermal equilibrium with the photons. This is the reason for the modification of equation (3.19). The number of relativistic degrees of freedom can be calculated as

$$g_* = \sum_{i=bosons} g_i \left(\frac{T_i}{T}\right) + \frac{7}{8} \sum_{i=fermions} g_i \left(\frac{T_i}{T}\right), \tag{3.29}$$

where g_i is the internal degrees of freedom of the particle (g_s above), and T_i is the temperature of the particle (which can be different from the photon temperature T). The factor 7/8 acounts for the difference between Bose and Fermi statistics. Unfortunately, the actual values of the T_i and the transitions are not trivial to calculate and we therefore refer the reader to Coleman and Roos (2003) for this calculation. The resulting $g_*(T)$ is shown in figure 3.2. In much the same manner, the number of relativistic degrees of freedom for the entropy, g_{*S}, can be found. The entropy is

$$s = \frac{2\pi^2}{45} g_{*S}(T) T^3. \tag{3.30}$$

And since it can be shown that the total entropy $S = g_{*S} T^3 a^3$ is constant, the relation between photon temperature and expansion becomes

$$\frac{T}{T_0} = g_{*S}^{-1/3} \frac{a_0}{a}. \tag{3.31}$$

This equation can then be used in conjunction with equations (3.19) and (3.20) to calculate the evolution of the universe as a function of temperature.

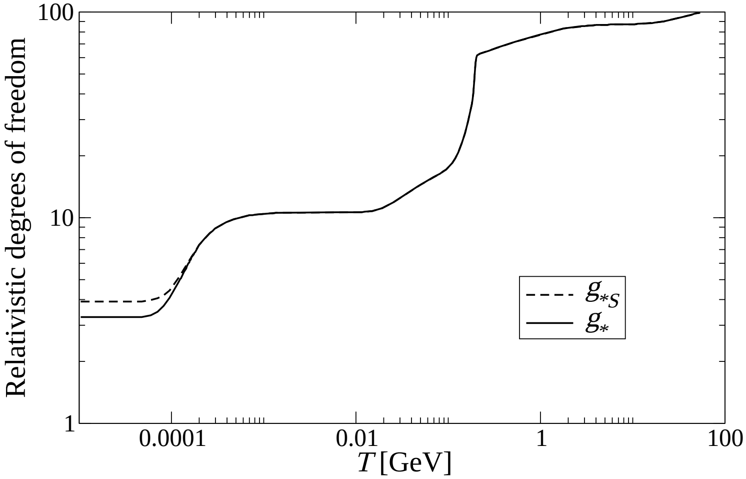

Figure 3.2: The number of relativistic degrees of freedom as a function of temperature (in GeV). The figure is from Coleman and Roos (2003).

The relation between time and temperature can now be calculated[1] as

$$\begin{aligned} H &= \frac{\dot{a}}{a} = \frac{d}{dt}\left(\frac{T_0 a_0}{T g_{*S}^{1/3}}\right)\frac{T g_{*S}^{1/3}}{T_0 a_0} = \frac{d}{dt}\left(\frac{1}{T g_{*S}^{1/3}}\right) T g_{*S}^{1/3} = \frac{-dg_{*S}/dt}{3g_{*S}} + \frac{-dT/dt}{T} \\ &= \frac{-dg_{*S}/dT}{3g_{*S}}\frac{dT}{dt} + \frac{-dT/dt}{T} = -\frac{dT}{dt}\left(\frac{dg_{*S}/dT}{3g_{*S}} + \frac{1}{T}\right), \end{aligned} \tag{3.32}$$

and we finally arrive at

$$\frac{dt}{dT} = -\frac{1}{H(T)}\left(\frac{dg_{*S}/dT}{3g_{*S}} + \frac{1}{T}\right) = -\frac{1}{H(T)}\left(\frac{d(\ln(g_{*S}^{1/3})}{dT} + \frac{1}{T}\right), \tag{3.33}$$

where dg_{*S}/dT can be obtained from figure 3.2.

3.5 Decoupling

The Boltzmann (transport) equation describes the statistical distribution of particles in a fluid (= a plasma, gas or liquid). The Boltzmann equation is used to study how a fluid transports physical quantities such as heat and charge, and thus to derive transport properties such as electrical conductivity, Hall conductivity, viscosity, and thermal conductivity. The Boltzmann equation is an equation for the time evolution of the distribution (in fact density) function $f(x, p, t)$ in one-particle phase space. It is particularly useful when the system is not in thermodynamic equilibrium, such as when the reaction rates, Γ, fall below the expansion rate of the universe, H.

In Hamiltonian mechanics, the Boltzmann equation can be written on the general form

$$\hat{L}(f) = C(f), \tag{3.34}$$

where the Liouville operator, $\hat{L}$, describes the evolution of a phase space volume and C is the collision operator. In general relativity, the Liouville operator can be written as

$$\hat{L} = p^\mu \partial x_\mu - \Gamma^\mu_{\alpha\beta} p^\alpha p^\beta \partial x_\mu. \tag{3.35}$$

---

[1] Since I have not seen this calculation before, I derive it in more detail than the previous parts of this chapter.

For the Robertson-Walker metric (homogeneous and isotropic), the Liouville operator is

$$\hat{L} = E\frac{df}{dt} - \frac{\dot{a}}{a}|\vec{p}|^2\frac{df}{dE}. \tag{3.36}$$

Using equation (3.21) with a time dependent $f = f(E, t)$ and integrating by parts we obtain

$$\dot{n} + 3Hn = \frac{g_s}{(2\pi)^3}\int C(f)\frac{d^3|\vec{p}|}{E}. \tag{3.37}$$

The complete expression for the integral on the right hand side is rather lenghty, involving all the interactions between the particle of interest and all other particles with which it interacts, as well as the corresponding matrix elements and phase space factors. This expression is given by Kolb and Turner (1990).

Using several (reasonable) assumptions, a simplified expresstion can be obtained for the evolution of the number density n of a particle:

$$\dot{n} + 3Hn = -\langle\sigma_A|v|\rangle\,(n^2 - n_{eq}^2), \tag{3.38}$$

where $\langle\sigma_A|v|\rangle$ is the sum of the thermally averaged cross sections times velocity. The assumptions are:

- No Bose condensation or Fermi degeneracy
- The particle is stable
- No asymmetry between the particle and its antiparticle
- All particles with which the particle interacts have a thermal distribution with zero chemical potential
- The evolution is done in the co-moving frame

Now the number density of the particle can be described in terms of the temperature

$$\frac{dn}{dT} = -\frac{dt}{dT}\left[3H(T)n(T) + \langle\sigma_A|v|\rangle\left(n(T)^2 - n_{eq}(T)^2\right)\right]. \tag{3.39}$$

Here dt/dT is given by equation (3.33) and the equilibrium number density n_{eq} is

$$n_{eq} = g_s\left(\frac{mT}{2\pi}\right)^{3/2} e^{-m/T} \tag{3.40}$$

for a non-relativistic particle with mass m, zero chemical potential and g_s internal degrees of freedom at a temperature T.

Chapter 4

The cosmic microwave background

As described in section 2.5 the cosmic microwave background (CMB) is simply radiation – light – with a blackbody spectrum of temperature $T_{CMB} = 2.725$ K (presently).

There are several aspects of the CMB that make it a most important cosmological tool. Back in 1992, the English physicist Stephen Hawking said that the COBE results on the CMB were "the greatest discovery of the century, if not of all times". It is currently the only experimental tool that allows us to probe anything further away than distant quasars, which are $\sim$ 12.7 billion light years away. The reionization was at its end by then and the first star generation had also passed, as well as the first structures in the universe. But the CMB has passed all this and been slightly affected by these events, which have left imprints in the spectral and spatial signature of the CMB.

Looking at the CMB, we see the universe largely as it was in its infancy, when it was merely 400,000 years old (and we can even see some traces from beyond that time).

From the CMB we can determine the age of the universe and its expansion rate; how much of the total energy content that is made out of ordinary matter (*baryons*), dark matter and dark energy; what the matter distribution was 400,000 years after the big bang and also, approximately, the subsequent formation of structures, such as clusters of galaxies.

The CMB was first discovered by Penzias and Wilson (1965) and the first precision measurements were done by COBE (Boggess et al. 1992; Fixsen et al. 1994; Dwek et al. 1998), and later improved by WMAP (Spergel et al. 2003, 2007).

The CMB has an almost perfect blackbody spectrum. There are, however, small perturbations in the spectrum, called *anisotropies*. These have characteristic length scales that correspond to angular scales for the measurements, and depend on what causes the anisotropy.

The anisotropies can be divided into two categories; primary and secondary. The primary anisotropies occur at, or just before, decoupling, while the secondary anisotropies occur after this event. For a more exhaustive treatment of these anisotropies, the reader is referred to Tegmark (1996).

The measured brightness can be divided into several components:

$$B(\hat{r}, \nu) = B_{CMB} + B_{SZ} + B_{dust} + B_{free-free} + ..., \tag{4.1}$$

where B_{CMB} is the intensity of the initial blackbody spectrum plus the primary anisotropies, B_{SZ} is the intensity due to the Sunyaev-Zel'dovich effect, B_{dust} is due to the dust contribution and $B_{free-free}$ is the intensity due to the thermal *bremsstrahlung* from within our galaxy. In sections 4.2 and 4.3 we will return to these and other effects and foregrounds and describe them in more detail. Now the CMB-part can be Taylor-expanded around its blackbody temperature:

$$T(\hat{r}) = T_0 + \Delta T_{CMB}(\hat{r}). \tag{4.2}$$

This gives

$$B_{CMB}(\hat{r},\nu) \approx B_{T_0}(\nu) + \Delta T_{CMB}(\hat{r}) \left.\frac{dB(\nu)}{dT}\right|_{T=T_0}. \tag{4.3}$$

The quantity to be measured by the Planck satellite and many other instruments is only the relative excess over B_{T_0}, i. e.,

$$\begin{aligned} \frac{B - B_{T_0}}{T_0(dB/dT)_{T_0}} &= \frac{\Delta T_{CMB}}{T_0} + \frac{B_{CMB} + B_{SZ} + B_{dust} + B_{free-free} + ...}{T_0(dB/dT)_{T_0}} \\ &\equiv \frac{\Delta T_{CMB}(\nu) + \Delta T_{SZ}(\nu,\hat{r}) + \Delta T_{dust}(\nu,\hat{r}) + ...}{T_0}. \end{aligned} \tag{4.4}$$

The measured anisotropies consist of the $\Delta T_X(\nu,\hat{r})/T_0$ terms in the expression above.

4.1 Primary anisotropies

The primary anisotropies can be divided into three main categories: gravitational, adiabatic and doppler. Other anisotropies, like topological defects, could also exist, but these are not considered to be very important and are beyond the scope of this introduction. The gravitational and adiabatic terms are combined on large angular scales ($\gg$ 1 degree) and are then called the Sachs-Wolf effect (Sachs and Wolfe 1967).

Furthermore, since the decoupling is not instantaneous, what we observe is a weighted average over the thickness of the decoupling surface (also called the last scattering surface, LSS). This means that primary anisotropies smaller than this thickness ($\Leftrightarrow \theta \sim 0.1^\circ$) are washed out.

Another effect is the so-called Silk damping (Silk 1968*a*), which means that small matter perturbations do not survive. The reason for this damping is the fact that in small structures the photons have time to diffuse out of the dense region (and drag the baryons with them) before the end of decoupling. The typical mass scale of this effect is $10^{11}\ M_\odot$, the mass of an ordinary galaxy.

4.1.1 Gravitational anisotropies

As the CMB photons climb out of a gravitational potential, they are redshifted by gravity. In terms of an equivalent temperature this is given by

$$\frac{\Delta T}{T} = -\Delta\Phi_e, \tag{4.5}$$

where $\Delta\Phi_e$ is the gravitational potential in excess of the background.

4.1.2 Adiabatic anisotropies

In a gravitational potential the number of photons is expected to be larger than normal and their temperature higher. At large angular scales ($\gg$ 1 degree), the induced anisotropies are

$$\frac{\Delta T}{T} = \frac{2}{3}\Delta\Phi_e, \tag{4.6}$$

but on small scales this is no longer the case due to *acoustic oscillations*.

This means that the Sachs-Wolf effect, which on large scales is the gravitational term plus the adiabatic term, can be written as

$$\frac{\Delta T}{T} = -\frac{1}{3}\Delta\Phi_e, \tag{4.7}$$

i. e., the photons are effectively redshifted by the gravitational potential. By measuring the size of these anisotropies and their relative strength one can estimate the matter distribution at the time of decoupling.

4.1.3 Doppler anisotropies

Due to local movement of the plasma at the time of decoupling, there is a kinetic doppler shift

$$\frac{\Delta T}{T} = \vec{v}(\vec{r}) \cdot \hat{r}, \tag{4.8}$$

where $\vec{v}(\vec{r})$ is the local velocity vector of the plasma at the point $\vec{r}$. This effect generally occurs at rather small scales compared to the Sachs-Wolf effect.

4.2 Secondary anisotropies

The secondary anisotropies are effects that changed the CMB photons between decoupling and now. They can be divided into three types; gravitational effects, local ionization and global ionization. These will be described one by one below.

4.2.1 Gravitational effects

There are three types of gravitational effects on the CMB; the early and the late integrated Sachs-Wolf effects (Sachs and Wolfe 1967), the Rees-Sciama effect (Rees and Sciama 1968) and gravitational lensing.

The integrated Sachs-Wolf (ISW) effect comes into action when there is a change in a gravitational potential as a function of time:

$$\frac{\Delta T}{T} = \int \Delta\dot{\Phi}\left(\vec{r}(t), t\right), \tag{4.9}$$

where $\Delta\dot{\Phi}$ is the time derivative of the gravitational potential in excess of the background potential.

The *early ISW effect* is due to the photon contribution to the gravitational potential. Since the photon energy decreases with time, this induces an integrated Sachs-Wolf effect.

The *late ISW effect* comes from the dark energy term that will become more and more important as time passes. This increase in energy also leads to an integrated Sachs-Wolf effect.

The Rees-Sciama effect is also called local ISW. It consists of galaxy clusters and other structures that evolve during the passage of the photons.

Gravitational lensing is an ISW effect perpendicular to the line of sight, affecting the angular distribution of the CMB and smearing it somewhat.

4.2.2 Local reionization

The local reionization effect occurs when the reionization affects the CMB through the presence of ionized gas through which the CMB photons must pass. This effect comes about when energetic electrons hit the photons and transfer energy to them, a phenomenon known as inverse Compton scattering. The impact on the CMB of the inverse Compton scattering is called the Sunyaev-Zel'dovich (SZ) effect (Sunyaev and Zel'dovich 1970, 1980; Rephaeli 1995). There are two types of the Sunyaev-Zel'dovich effect, thermal and kinetic, see figure 4.1.

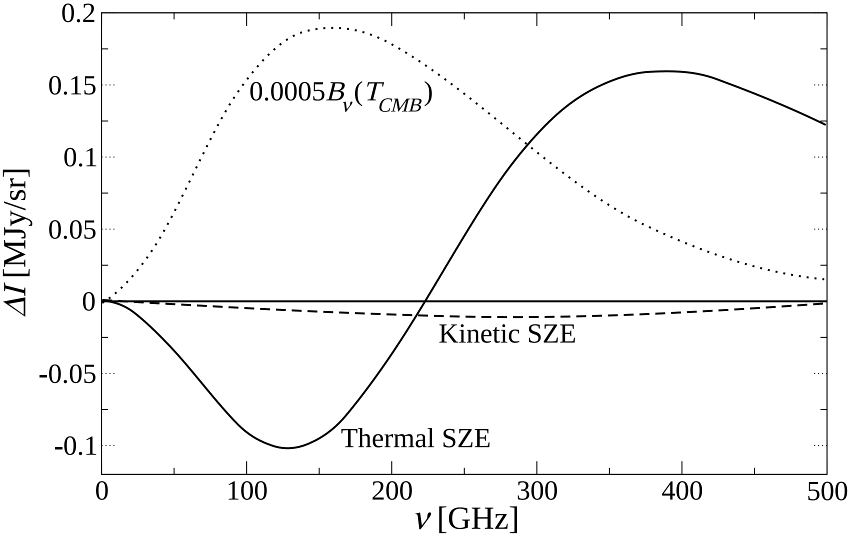

Figure 4.1: Illustration of the thermal and kinetic Sunyaev-Zel'dovich effect (SZE). The graph shows the intensity (in units of MJy/sr = MWm^{-2}Hz^{-1}sr^{-1}) as a function of frequency (in GHz). The thermal SZ effect increases the photons frequencies, through thermal excitation. The kinetic SZ effect decreases the intensity of the photons in this case because the gas cloud is moving away from us. For comparison, the shape of a blackbody spectrum with $T = T_{CMB}$ is also shown.

The thermal SZ effect is due to energetic free electrons and will have the effect of shifting the CMB spectrum towards higher frequencies since each photon subject to the inverse Compton scattering gains energy, but not in any particular direction.

The kinetic SZ effect is due to the global motion of a galaxy cluster or other large structures. Since there is a favored direction (in the direction of the velocity of the cluster), this causes a doppler shift of the CMB spectrum.

4.2.3 Global reionization

There are three types of global reionization: suppression of small scales, new doppler effect and the Vishniac effect.

The suppression of small scales is due to the fact that the photons that scatter during reionization loose their original direction. The amplitude of this effect depends on the time when the reionization occurred, the later time the higher amplitude, see figure 4.2. It also depends on the degree of reionization, in other words, on the *optical depth*. In fact, this effect suppresses all scales smaller than

$$\theta \leq \sqrt{\frac{\Omega_0}{z_i}}, \tag{4.10}$$

where Ω_0 is the total relative energy density of the universe, and z_i is the *redshift* at reionization. The suppression of the *power spectrum* on these scales is $e^{-2\tau}$, where τ is the opacity.

The new doppler effect is due to local velocity and density perturbations, and the Vishniac effect is caused by electrons falling in gravitational potential wells, but it is only active on scales $\theta \sim 0.02^\circ$ and even then it is quite feeble.

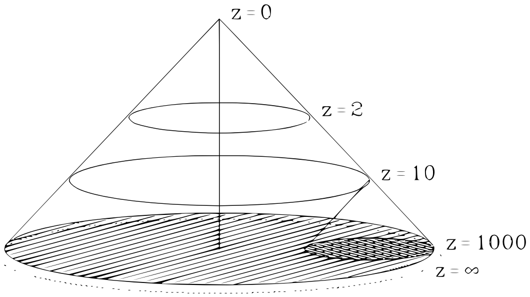

Figure 4.2: Illustration of the suppression of small scales due to the reionization. If photons scatter at reionization, they could come from anywhere within the lightcone projection at $z = 1000$. Through the finite speed of light, we know that they can not have come from anywhere outside of this projection, which corresponds to an angle $\sqrt{\Omega_0/z_i}$.

4.3 Foregrounds

Foregrounds are light sources in the universe emitting in the same frequency range as the CMB. There are three basic types of foregrounds; extragalactic, galactic and local.

4.3.1 Extragalactic foregrounds

The extragalactic foregrounds are point sources having an origin outside our galaxy. A point source has a very small angular extension. However, their total integrated effect can still be considerable. There are point sources that are active mostly in the radio domain, like, e. g., radio galaxies, but there are also sources active mostly in the infrared (IR) domain, like dusty galaxies.

As is shown in Paper II, there is also a kind of continuous IR source all over the sky with a bias for mass concentrations – the emission from the early dust.

4.3.2 Galactic foregrounds

The galactic foregrounds are all diffuse, meaning that they have a certain angular extension. The principal galactic foregrounds are emission from dust, free-free emission and synchrotron radiation. The angular correlations, described in section 4.4, of these foregrounds are all roughly $\propto \theta^3$.

The dust in our galaxy has been shown to have a Planck spectrum of temperature ~ 17 K, Boulanger et al. (1996).

The free-free emission comes from free electrons that are accelerated, thus emitting thermal *bremsstrahlung*. The free-free emission is almost independent of frequency.

The synchrotron radiation is due to acceleration of plasmas and is a sort of global bremsstrahlung. The synchrotron radiation is most effective for frequencies below 70 GHz.

4.3.3 Local foregrounds

Local foregrounds are perturbations from the solar system, like the planets, the moon, the sun, the atmosphere and instrumental noise. The solar system perturbations are well known, and the instrumental noise is instrument specific.

4.4 Power spectrum

In the previous section we saw that the measured anisotropies can be separated into several components, equation (4.4), each anisotropy with its specific spectral and spatial signature. In this section we will explore the *power spectrum*, which is a powerful tool to quantify the spatial signature of the signal.

The spatial signature is often expressed in terms of the Legendre spherical harmonics

$$\Delta T_X(\vec{r}, \nu) = \sum_{\ell=0}^{\infty} \sum_{m=-\ell}^{\ell} Y_{\ell m}(\vec{r}) a_{\ell m}^X(\nu), \tag{4.11}$$

where the spherical harmonics $Y_{\ell m}$ are the basis functions and $a_{\ell m}$ are their components. In order to determine correlations on different angular scales, the correlation functions are used:

$$C_\ell^X(\nu) = \frac{1}{2\ell + 1} \sum_{m=-\ell}^{\ell} \left\langle \left| a_{\ell m}^X(\nu) \right| \right\rangle. \tag{4.12}$$

This is also called the (angular) power spectrum. In the case of isotropic fluctuations the above equation simplifies to $\langle a_{\ell m}(\nu)^* a_{\ell' m'}(\nu) \rangle = \delta_{\ell\ell'} \delta_{mm'} C_\ell$. In order to convert from ℓ to θ a good rule of thumb is $\theta \approx 180^\circ/\ell$.

It is customary to plot the quantity $\ell(\ell+1)C_\ell/2\pi$ in units of $\mu\mathrm{K}^2$, cf figure 4.3. The reason for this choice is that it enables the root-mean-square (rms) of the temperature variations to become visually apparent:

$$\left\langle \Delta T(\nu)^2 \right\rangle = \sum_{\ell=0}^{\infty} \left(\frac{2\ell + 1}{4\pi} \right) \approx \int_1^{\infty} \left(\frac{\ell(\ell + 1)}{2\pi} \right) C_\ell d(\ln \ell), \tag{4.13}$$

where one has used $\frac{l(2\ell+1)}{4\pi} \approx \frac{\ell(\ell+1)}{2\pi}$ for $\ell \gg 1$. This means that in order to estimate the $(\mathrm{rms})^2$ of the anisotropies in the range $\ell_1 < \ell < \ell_2$ one needs to take only the rms height of the curve times $\ln(\ell_2/\ell_1)$.

4.4.1 Acoustic oscillations

Prior to decoupling, the matter and the photons were tightly coupled and effectively formed a baryon-photon fluid. Because of the density perturbations, this fluid started to oscillate. These oscillations are called acoustic (Silk 1967, 1968*a*,*b*). Each mode in those give rise to a correlation at a given angular scale in the power spectrum. The acoustic oscillations are a natural consequence of inflation and thus serves to corroborate the inflation theory.

4.4.2 Simulations of the cosmic microwave background

A program named CMB-fast, developed at Harvard, is used to estimate the CMB from theory (see, e. g., Seljak and Zaldarriaga 1996). The program is versatile, allowing the user to test different scenarios with different types of cosmologies and see what the expected power spectrum would be. Figure 4.4 shows the different components of the CMB and how they are affected by some cosmological parameters.

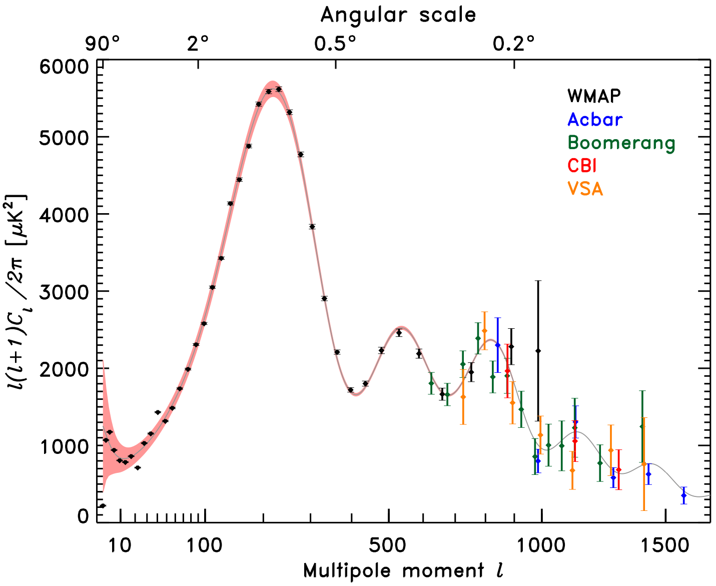

Figure 4.3: The power spectrum as measured by WMAP, CBI and ACBAR. The *x*-axis shows the inverse angular scale and the *y*-axis the correlation on that scale. The dots are data points, and the curve is the theoretical. Reprinted from Spergel et al. (2007).

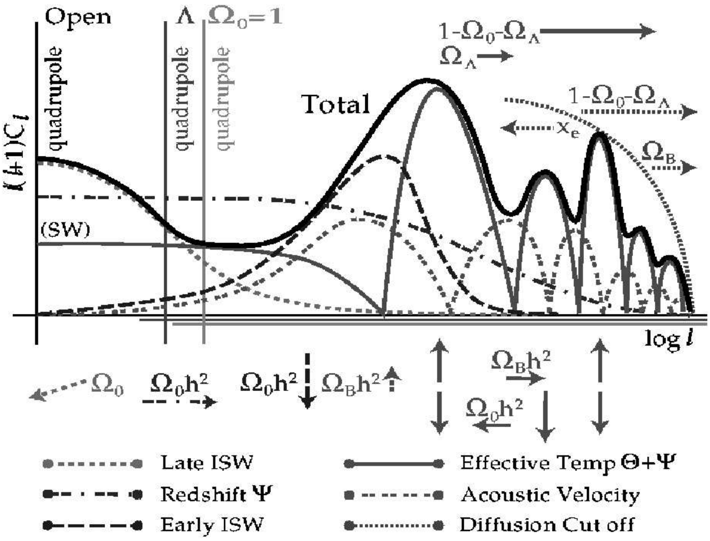
Open
Λ
$\Omega_0=1$
$l(l+1)C_l$
quadrupole
quadrupole
quadrupole
(SW)
Total
$1-\Omega_0-\Omega_\Lambda$
Ω_Λ
$1-\Omega_0-\Omega_\Lambda$
x_e
Ω_B
log l
Ω_0
Ω_0h^2
Ω_0h^2
Ω_Bh^2
Ω_Bh^2
Ω_0h^2
Late ISW
Redshift Ψ
Early ISW
Effective Temp Θ+Ψ
Acoustic Velocity
Diffusion Cut off

Figure 4.4: The power spectrum as calculated by CMB-fast. Reprinted from Tegmark (1996), originally from Hu (1995). The contribution from different types of anisotropies (see sections 4.1 and 4.2) is shown. The *x*-axis shows the inverse angular scale, log ℓ, and the *y*-axis the correlation on that scale, $\ell(\ell + 1)C_\ell$. We see the characteristic plateau of the Sachs-Wolf effect at large angles (small ℓ values) and the acoustic oscillations at small angles (large ℓ values). We can also see the impact of different cosmological parameters on the power spectrum.

Chapter 5

Introduction to the papers

This chapter is included in order to give the reader some background information that may be useful for the understanding of the particularities of the appended papers. Section 5.1 describes the dust, with its properties and production/desctruction mechanisms. Section 5.2 introduces dark matter, which is important for Paper II. Since the topic of heavy neutrinos (section 5.3) and preons (section 5.4) are more controversial than dust and dark matter, a motivation is provided for these subjects, as well as an introduction.

5.1 Dust

The abundance of dust in the universe can be calculated by estimating its production and destruction rate. These figures are not well known even for the nearby universe and even less so for the early universe. In this section the properties of this early dust are briefly discussed along with some general properties of the nearby dust. The section is included as a complement to Paper I, where the specifics of early dust are used. For a more complete review of dust in general, see Draine (2003).

5.1.1 Production

In section 2.4 the formation of light elements through the nucleosynthesis was treated, but most of the terrestrial material is made of heavier elements. The only known sources of such heavy elements are *supernovæ*. During its life, a star fuses hydrogen into helium and then into carbon, nitrogen and other heavy elements. If the star finishes as a supernova, these elements are released into the interstellar medium (ISM), and then serve to form new planets and stars.

On their way out, many of these elements are ionized by the surrounding plasma. When the ions meet they tend to form ionic bonds, and in this way tiny crystals are formed. These form what we call cosmic dust.

For an overview of dust production in the early universe, the reader is referred to Todini and Ferrara (2001).

5.1.2 Properties

The composition of interstellar dust grains is still largely unknown. Meteorites provide us with genuine specimens of interstellar grains for examination. However, these are subject to severe selection effects, and can not be considered representative of interstellar grains. Our only direct information about the composition of interstellar dust comes from spectral features of extinction, scattering, or emission.

By means of spectral measurements and stellar nucleosynthesis it is found that dust grains are composed mainly of elements like silicon, oxygen, nitrogen, carbon and iron. Dust grains are formed of molecules like CO, SiO_2, Al_2O_3, Fe, Fe_3O_4, $MgSiO_3$, Mg_2SiO_4 and amorphous carbon. These grains form at different temperatures. CO form at ~ 2500 K (Fischer 2003), amorphous carbon at ~ 1800 K, Al_2O_3 at ~ 1600 K and the other grain types at ~ 1100 K (Todini and Ferrara 2001).

The polarization of starlight was discovered more than 50 years ago, and was immediately recognized as being due to aligned dust grains. Two separate alignments are involved: (1) alignment of the grains' principal axis of largest moment of inertia with its angular momentum J, and (2) alignment of J, with the galactic magnetic field.

Woosley and Weaver (1995) calculate the chemical composition of different types of supernovæ with masses of $11 - 40\ M_\odot$ and metallicities $Z/Z_\odot = 0$, 10^{-4}, 0.01, 0.1 and 1. Galactic dust is found mostly in nebulæ, where it is an important factor in the star formation process.

5.1.3 Destruction

The destruction of dust particles is not very well understood, due to the fact that the dust is found in a variety of environments of rather complex nature. In this section, some important mechanisms for dust destruction are touched upon. Their exact impact, especially at the time of the early dust, remains unclear (Draine 1990).

There are a number of phenomena that destroy dust (or rather erode it into negligible pieces). The destruction mechanisms include *sputtering* and grain-grain collisions in interstellar shocks, *sublimation* during supernova radiation pulses, sputtering and sublimation regions with ionized hydrogen, photodesorption by UV light and sputtering by cosmic rays. A classic paper on dust destruction is Draine and Salpeter (1979).

This plethora of processes makes it difficult to calculate the life time of the dust. For a hot ionized medium the life time can be estimated to 10^8 years, in a cold neutral medium to 10^9 years and in a molecular cloud to 10^{10} years (Draine 1990). The actual environment of the dust from the first stars is largely unknown. What we do know, however, is that the universe was denser at that time than it is today, but also less clumped. There were no real galaxies, and in the beginning no ionized gas either.

5.2 Dark matter

Dark matter (DM) is not very well understood, but there are several properties that are known. There is also a multitude of particles that could possibly constitute this mysterious DM. It has not yet been directly seen, neither in astronomical telescopes, nor in particle accelerators. A review on DM can be found in Bergström (2000) and more recently in Bertone et al. (2005).

The DM was originally conceived to explain the velocities of stars in galaxies as a function of their distance from the center. For each of the stellar, galactic, and galaxy cluster/supercluster observation the basic principle is as follows. If we measure velocities in a certain region, there has to be enough mass present for gravity to stop all the objects flying apart. When such velocity measurements are made on large scales, it turns out that the amount of inferred mass is much higher than can be explained by the luminous matter we can observe. Hence we infer that there is DM in the universe.

The DM concept can also explain the gravity required for the creation of large-scale structures that we see in the universe today. This is mentioned in section 2.6.

DM candidates usually fall into two broad categories, with the second category being further sub-divided:

- Baryonic
- Non-Baryonic
  - Hot dark matter (HDM)
  - Cold dark matter (CDM),

depending on their respective masses and speeds. CDM candidates travel at slow speeds (hence "cold") or have little pressure, while HDM candidates move rapidly (hence "hot"). The CDM is currently the most likely candidate to be the dominant component of DM.

Since the DM has yet eluded detection, it is supposed that it only interacts very weakly with ordinary matter. This means that simulations of the structure evolution of the universe can be greatly simplified. Since we know that the gravitationally dominant form of matter in the early universe was DM, and its only interaction is gravitation, the equations of evolution are rather simple to solve. This means that huge simulations can be made, including millions of DM particles and covering hundreds of Mpc (mega parsecs). In simulations covering a significant part of the universe, each "particle" weighs in the order of 10^{10} solar masses.

5.3 Heavy neutrinos

5.3.1 Background

Ever since the discovery of the three families/generations of light leptons and quarks some striking similarites have intrigued physicists:

- Similarity between families
- Similar group structure of leptons and quarks
- Mass hierarchy
- Equal charge

The standard model of particle physics (Glashow 1961; Weinberg 1967; Salam 1968) postulates three families of leptons and quarks. However, there is no underlying theory predicting these families to be three or predicting the number to be the same for leptons and for quarks.[1] So far, it is only an experimental fact. Thus, a priori, there is no reason why this number should be restricted to three. In fact, the situation is rather the opposite: there is theoretical justification for *more* than three generations of leptons/quarks (cf. section 5.3.2).

Within the lepton family there is nothing to distinguish an electron from a muon or a tau, except their mass and life times. Furthermore, the symmetry of the group structure of leptons and quarks (cf. table 5.1) is a remarkable coincidence.

In the past, symmetries of this kind have been recognized as a sign of substructure. Also the remarkable mass distribution in figure 5.1 is an argument for either a substructure of fermions or for a classification as a representation of a larger group. If a substructure exists, then excited states ought to exist. If there is a larger group it might very well contain heavy leptons. A priori, there is no relation between heavy and excited leptons.

---

[1] In fact, in order for the standard model to be anomaly-free, the sum of the charge of all fermions must be zero, though this does not necessarily imply an equal number of leptons and quarks.

Table 5.1: The three families/generations of leptons (electrons, e, and electron neutrinos, ν_e; muons, μ, and muon neutrinos, ν_μ; taus, τ, and tau neutrinos, ν_τ) and quarks (up, u; down, d; charm, c; strange, s; top, t; and bottom, b) . The quarks d', s', b' are the weakly interacting mixed states of the mass eigenstates d, s, b. The indices L and R refer to left- and right-handed particles (for left-handed particles the spin is antiparallel with the direction of the particle, i. e., the spin points "backwards").

Leptons:	$\begin{pmatrix} \nu_e \\ e \end{pmatrix}_L$, e_R	$\begin{pmatrix} \nu_\mu \\ \mu \end{pmatrix}_L$, μ_R	$\begin{pmatrix} \nu_\tau \\ \tau \end{pmatrix}_L$, τ_R
Quarks:	$\begin{pmatrix} u \\ d' \end{pmatrix}_L$, u_R, d_R	$\begin{pmatrix} c \\ s' \end{pmatrix}_L$, c_R, s_R	$\begin{pmatrix} t \\ b' \end{pmatrix}_L$, t_R, b_R

The hierarchy of the masses suggests the possibility of a fourth, even heavier, generation of leptons. Its mass would be of the order of 100 GeV, which could be within the reach of the CERN LEP accelerator, where the sensitivity reaches up to $M \sim 200$ GeV in single production and up to $M \sim 100$ GeV in double production. The corresponding neutrino mass would, in principle, also have to be large ($\gtrsim M_Z/2$) in order to be in accord with the measured invisible width of the Z.

Besides the arguments in favor of heavy and excited fermions there are also several problems with the standard model.

- The standard model has more than 20 free parameters, which have to be determined experimentally (three lepton masses, six quark masses, W^+, W^-, Z^0 and *Higgs boson* masses, three coupling constants, four quark mixing angles, in addition to the masses and mixing angles of the neutrinos).
- The form of the Higgs potential is somewhat arbitrary. The Higgs particle has not yet been found and the stability of its mass against radiative corrections is fine-tuned.
- The nature and origin of the CP violation is introduced ad hoc as a complex phase in the CKM matrix.

5.3.2 Heavy fermions

Several theories predict the existence of new, heavy fermions. These extensions of the standard model generally have a mass scale at which a certain symmetry is restored. If we can obtain accelerator energies reaching this mass scale, we can directly probe the validity of the theory. However, these energies are generally far too high ($M \sim 10^{12}$ TeV) to be reached by present accelerators ($E \sim 1$ TeV).

The most ambitious of the theories is the superstring theory ($M \sim 10^{16}$ TeV), aiming at unifying all the known forces: electromagnetic, weak, strong and gravitational. It is currently the only viable theory to do so. The grand unified theories (unifications at $M \sim 10^{15}$ TeV) attempt all the above, except that they do not include gravity. Supersymmetry, which basically is a way of explaining the mass hierarchy discussed above, is an integral part of both the Superstring theory and most of the grand unified theories.

A characteristic property of these extended models is that they predict a zoo of new particles, which have to be detected in order to be validated. The experimental advantage is that they offer some concrete predictions.

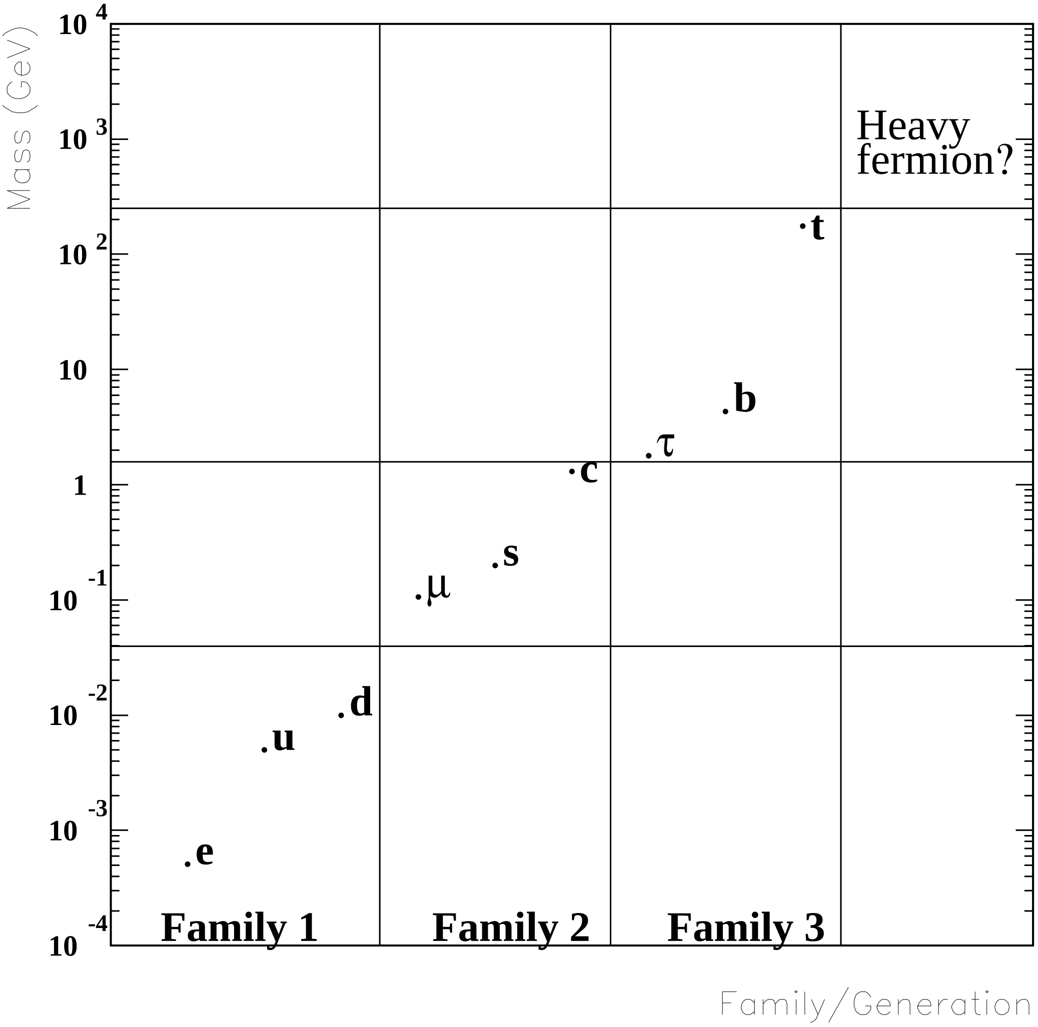

Figure 5.1: The mass hierarchy of the three fermion generations

The grand unified groups have fermion representations that contain the standard model quarks and leptons but often also additional fermions. The wide range of masses of the fermions suggests that some new leptons could have masses of about 100 GeV. There are three popular unifying groups, $SU(5)$, $SO(10)$ and E_6. The latter two contain new fermions. The group $SO(10)$ (Robinett and Rosner 1982; Barger et al. 1982) contains a right-handed *Majorana* neutrino and it is one of the simplest groups in which the standard model could be conveniently embedded ($SU(5)$ is the simplest). Majorana neutrinos are their own antiparticles. The exceptional group E6 (Hewett and Rizzo 1989) contains several singlet neutrinos as well as new charged leptons and quarks, and it is an acceptable four-dimensional field theoretical limit of superstring theory. There have also been several other propositions for heavy fermions, like in Tommasini et al. (1995).

There are four phenomenologically different types of heavy leptons (compare with table 5.1):

- **Sequential**
  A fourth generation of fermions with the same basic properties as the other three.
  $\begin{pmatrix} N \\ L^{\pm} \end{pmatrix}_L ;\ L^{\pm}_R$
  $\begin{pmatrix} U \\ D \end{pmatrix}_L ;\ U_R, D_R$
- **Mirror**
  Doublets have right chirality and singlets have left (opposite of the standard model).
  $\begin{pmatrix} N \\ L^{\pm} \end{pmatrix}_R ;\ L^{\pm}_L$
  $\begin{pmatrix} U \\ D \end{pmatrix}_R ;\ U_L, D_L$
  Mirror fermions occur in many extensions of the standard model trying to restore the left-right symmetry (Maalampi and Roos 1990) at the scale of the electroweak symmetry breaking.
- **Vectorial**
  Both the right and left chirality are doublets.
  $\begin{pmatrix} N \\ L^{\pm} \end{pmatrix}_L ; \begin{pmatrix} N \\ L^{\pm} \end{pmatrix}_R$
  $\begin{pmatrix} U \\ D \end{pmatrix}_L ; \begin{pmatrix} U \\ D \end{pmatrix}_R$
  Vector fermions occur, e. g., in the group E_6.
- **Singlet**
  Both the right and left chirality are singlets.
  $L^{\pm}_L,\ L^{\pm}_R\ ; N_L,\ N_R$
  $U_L,\ D_R\ ; U_R,\ D_L$
  Singlet fermions are found both in E_6 and in $SO(10)$.

In our Paper IV the focus is on sequential heavy leptons, also called fourth generation leptons. These new leptons are of the same character as the ones already known.

5.4 Preons

5.4.1 The standard model vs preons

The standard model (SM) of quarks and leptons serves as a background against which one might study new physics. One example is the speculations about the existence of heavy neutrinos, like in the previous chapter. A heavy neutrino would, however, make it quite logical to speculate also about new heavy charged leptons, as well as new heavy quarks, and maybe also new (super)heavy gauge bosons for the weak interaction.

Would such particles exist they might easily be included in a new version of the SM. The problem is rather that one might then doubt that quarks and leptons are truly fundamental. Why would nature be complicated enough to have more fundamental particles, when even the present 12 might seem too many? Such ideas call for a substructure of leptons and quarks in terms of *preons*.

Such preons are the subject of the fourth paper in this thesis, and I will therefore give a short introduction to preons here, as well as discuss why they might be needed. I will, in fact, argue that they are in a sense predicted by the SM.

To be more precise, I will discuss the following aspects of the SM and argue that they can all be qualitatively explained as a consequence of a preon substructure:

- There are many "fundamental" particles, arranged in a pattern (of three families)
- Almost all quarks and leptons are unstable
- There are many quantum numbers that are not understood from first principles
- Some quarks, leptons and gauge bosons mix/oscillate in a quantum-mechanical sense, but with no known reason
- The heavy vector bosons are massive and unstable, unlike other force particles (the photon and the gluon)
- There is a mixing of Z^0 with the photon, "explained" by the Higgs mechanism

The discussion will be rather general, although the fourth paper deals with a particular preon model (Dugne et al. 2002), discussed in the next subchapter.

5.4.2 A brief history of preon models

Preon models have their origin in the mid-1970s, and many preon, or "subquark", models developed between 1972 and the early 1980. Earlier Pati and Salam (1974) had tried to unify leptons and quarks by defining leptons as the "fourth color", with quarks having the normal three colors. In the early days Pati, Salam and Strathdee (1975) were instrumental for the development of preon models, and so were Japanese workers, like Terazawa (1980).

A comprehensive list of early references is given in Pati et al. (1981), as well as in the book by D'Souza and Kalman (1992).

From the subsequent development in the late 1970s and early 1980s, two models appear as particularly simple and elegant, namely the "rishon" model by Harari (1979) and Shupe (1979), and the "haplon" model by Fritzsch and Mandelbaum (1981).

In the rishon model there are only two preons, or rishons, T and V, and their anti-rishons. The T has charge $+e/3$, while V is neutral. Then the electron is $\bar{T}\bar{T}\bar{T}$ and the neutrino is VVV. The u quark is TTV and the d quark is $\bar{T}\bar{V}\bar{V}$. The $\bar{u}$ and the $\bar{d}$ are constructed in the same way from the corresponding anti-rishons. An interesting feature is that quark color can be seen as an ordering of the Ts and Vs of quarks, such that, e.g., TTV, TVT and VTT corresponding to u quarks with different colors. Hence only two rishons are needed to construct the four particles of the first family of quarks and leptons. Heavier families are supposed to be simple excitations of the first family, say radial ones. The gauge bosons γ, W and Z are assumed to be composite too, namely six-rishon states.

In the haplon model there are three preons, but with quite different properties. Two of them, α and β, have spin $1/2$ and charges $+e/2$ and $-e/2$, while another two, x and y, have spin $1/2$ and charges $e/6$ and $e/2$. Only x carries quark color and exists merely in quarks. Hence, $u = (\alpha x)$, $d = (\beta x)$, $e^- = (\beta y)$ and $\nu_e = (\alpha y)$. The heavy gauge bosons W and Z^0 are simple states of one α or β together with one of their anti-haplons $\bar{\alpha}$ or $\bar{\beta}$, in total spin 1. The authors mention that the weak interaction is not fundamental, and that the $\gamma - Z$ mixing in the "unified" electroweak interaction is similar to the $\gamma - \rho$ "mixing" of the so-called Vector Dominance Model for gamma interaction with hadrons and nuclei. Also in the haplon model, the two heavier families are considered to be excitations of the first one.

Table 5.2: A "supersymmetric" scheme of spin-1/2 preons and spin-0 anti-dipreons.

charge	$+e/3$	$-2e/3$	$+e/3$
spin-1/2 preons	α	β	δ
spin-0 (anti-)dipreons	$(\bar{\beta}\bar{\delta})$	$(\bar{\alpha}\bar{\delta})$	$(\bar{\alpha}\bar{\beta})$

Table 5.3: The composite states in the preon-trinity model; leptons with one preon and one dipreon, quarks with one preon and one anti-dipreon, and heavy vector bosons with one preon and one antipreon.

	$(\beta\delta)$	$(\alpha\delta)$	$(\alpha\beta)$	$(\bar{\beta}\bar{\delta})$	$(\bar{\alpha}\bar{\delta})$	$(\bar{\alpha}\bar{\beta})$	$\bar{\alpha}$	$\bar{\beta}$	$\bar{\delta}$	
α	ν_e	μ^+	ν_τ	u	s	c	Z^0, Z'	W^+	Z^*	α
β	e^-	$\bar{\nu}_\mu$	τ^-	d	X	b	W^-	Z', Z^0	W'^-	β
δ	$\nu_{\kappa 1}$	κ^+	$\nu_{\kappa 2}$	h	g	t	$\bar{Z}^*$	W'^+	Z'', Z'	δ

So the conclusion is that the rishon model has few different preons (two), while the haplon model has more preons, but fewer inside quarks and leptons (two).

These two models, and the original quark model (Gell-Mann 1964; Zweig 1964), inspired Dugne et al. (2002) to a model for *all* quarks and leptons. With three preons inside each, the minimal number of different preons is three. This would predict many new quarks and leptons. However, it is prescribed that preons bind each other pairwise into spin-0 "dipreons", and that quarks are preon–antidipreon combinations, while leptons are preon–dipreons. Heavy vector bosons are preon–antipreon states. There are only three different dipreons allowed by the Pauli principle. The preons and dipreons are given in table 5.2, and the composite states are shown in table 5.3.

This model is the most detailed one on the preon market, and hence suitable for analyzing such entities as the decay modes of the predicted new and heavy leptons and quarks. Such a study is the main ingredient of Paper IV. Many other details are discussed in the original paper Dugne et al. (2002).

Finally it should be mentioned that Hansson and Sandin (2005) and Sandin and Hansson (2007) recently analyzed the possibility of "preon stars", i. e., bodies in space consisting of preons only, and weighing, typically, about an earth mass.

Below we give more specific arguments why preons should exist, as "predicted" by some unexplained properties of the standard model.

5.4.3 Some general arguments

History tells that "there is always a deeper layer of compositeness". Earlier layers have normally been suggested and/or discovered when the model in fashion became too complex, or when there were too many different models for the "fundamental" particles. Nevertheless, compositeness has never been a main trend of high-energy research. Rather, a majority of theorists has regarded the "current" elementary particles as *the* fundamental ones.

The first theories of compositeness have, normally, faded away after some time, if not supported by observations. Examples are the quark model by Gell-Mann (1964); Zweig (1964) and the early preon models by Harari (1979) and Shupe (1979) ("rishons") and by Fritzsch and Mandelbaum (1981) ("haplons").

The quark model gained a wider acceptance only after the pioneering deep-inelastic scattering data of the late 1960s and the early 1970s, and their interpretation in terms of partons. There are no such supporting data for preons, and the interest in the first preon models was therefore gone a long ago, except among some enthusiasts.

Compositeness still appears as a word now and then in experimental work, but mostly in searches for deviations from the SM predictions in events with large transferred momenta. The lack of signals are normally quoted as a minimal preon energy scale of a few TeV (Yao et al. 2006).

Still, it is logically impossible to prove, by theoretical or experimental means, that a certain entity is *not* composite. This makes a preon model doubtful as a true theory, in the popperian sense, unless it has some precise predictions that can be tested in experiment.

Now I will go through a few arguments that build on ad hoc features in the SM, similar to earlier findings on a less fundamental level, and where the solutions turned out to be compositeness.

5.4.4 There are too many quarks and leptons

The most common argument in favour of preons (D'Souza and Kalman 1992) is that there are too many quarks and leptons to be understood from first principles. There is no obvious logical reason why there would be (at least) twelve fundamental particles. The case for preons is strengthened by the fact that these particles fall into a nice pattern of three "families".

Throughout history, the finding of "too many" fundamental particles preceded the discovery of yet smaller and fewer building blocks. Examples are:

- The existence of too many elements was explained by atoms with electrons and nuclei
- The existence of isotopes was explained by nuclei with protons and neutrons
- The existence of hundreds of hadrons was explained by just three quarks, with a flavour $SU(3)$ symmetry

A first guess is therefore that the many quarks and leptons reflect a preon substructure, and that the pattern of three families comes from the existence of three preons, with a preon-flavour $SU(3)$ symmetry. It is noteworthy that the early preon models did not, in general, provide a more rational explanation of the quarks and leptons of those days. Typically, four different preons were used to explain the existence of the four particles of the lightest quark/lepton family, while the heavier ones were not properly understood. A good preon model should hence explain *all* quarks and leptons.

5.4.5 Unstable fundamental particles?

Most quarks and leptons are unstable, decaying into lighter ones, and there is a logical problem with unstable fundamental particles: How can the most fundamental objects decay into equally fundamental objects? This logical problem is rarely addressed in the literature.

Throughout history all decays of "fundamental" particles have mirrored their compositeness. Examples are:

- The decays of atoms were found to come from the decays of their nuclei,
- which are caused by the decays of their nucleons,
- which are caused by the decays of their quarks.

Where will these explanations end? Not until we find a level with *stable* constituents. A preon model must therefore either have absolutely stable preons, or rely on yet composite preons ("pre-preons"). If preons are stable, all quark and lepton decays are just a regrouping of preons into systems with lighter quarks and leptons. This limits the number of preon models. The pioneering preon models did not have this property. The heavier two families remained unexplained, or were seen as internal excitations of the lightest one.

Summing up, one can predict the existence of three absolutely stable preons. This makes *net preon flavour* a conserved quantity. A by-product is that if two quarks or leptons would have identical net preon flavours, they will (must) mix into new mass eigenstates. This would be equivalent to, e. g., η/η'-mixing in the quark model. Hence such a preon model provides a possibility to understand the various mixings of quarks, neutrinos and weak isospin eigenstates in the SM. These will be discussed later.

5.4.6 Ad hoc quantum numbers

The SM contains a few quantum numbers that have been put in by hand, without a deeper understanding, and just in order to describe that some quark and lepton quantities are conserved or partially conserved.

These are quantum numbers that either seem absolutely conserved, such as baryon number, or are known to be conserved only in some reactions, e. g., weak isospin. Lepton numbers form a grey-zone. They seemed to be absolutely conserved until quite recently, when neutrino oscillations were discovered.

History again gives some clues. A long time ago, the "isotopic numbers" were understood only after the discovery of the neutron and the compositeness of atomic nuclei. In the 1950s hadronic isospin and strangeness/hypercharge were introduced to describe the observed approximate symmetries of hadronic decays and interactions. These three quantum numbers turned out to come from three quark flavours.

Since the number three appears also in the SM, one might guess that lepton number conservation has to do with preon number conservation, i. e., preon-flavour $SU(3)$ symmetry. The disturbing neutrino oscillations/mixings can then be understood if two or more neutrinos have identical net preon flavour. This will be discussed in the next section. The connection between weak isospin and the number of preons is not as obvious, but will also be discussed below.

5.4.7 Mixings of fundamental particles?

The SM prescribes that certain quarks, leptons and gauge bosons mix into new eigenstates before decaying or influencing other particles. Whenever simular situations have appeared in the past, the solution turns out to be in terms of compositeness.

A classical example is that different isotopes, created in nuclear reactions, mix in certain proportions in nature, and are inseparable in normal chemical reactions. Chemical isotope mixing hence has its root in the compositeness of atomic nuclei.

A more modern case is the mixing/oscillation of the two neutral kaons K^0 and $\bar{K}^0$ into the mass eigenstates K_L and K_S. This has to do with quark reactions inside kaons, i. e., with the compositeness of hadrons.

Both cases are examples of what happens when virtually different states have identical net quantum numbers relative the particular interaction used to "detect" them. I will now discuss three similar mixings of "fundamental" particles in the SM, and their possible compositeness.

The Cabibbo mixing of d and s

The d and s quarks might mix into the weak-interaction ("mass") eigenstates d' and s' because they have identical net preon contents. The problem is to arrange this in detail. One possibility is that the two quarks have identical preon contents, although with some internal differences between the detailed preon wave functions, e. g., with two different internal spin structures. The other one is to

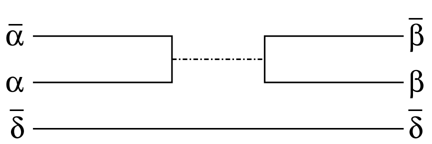

Figure 5.2: One way for two composite quarks to mix quantum-mechanically. A preon-antipreon pair annihilates and turns into another pair.

focus on the word "net", meaning that some preon flavours cancel inside either quark, e. g., because they contain preon-antipreon pairs.

The first alternative fits the neutrino sector better (see below). Instead quarks might be a preon-antipreon pair plus an additional preon. Consider a situation where the two quarks have the following compositions: $d = \beta\bar{\beta}\bar{\delta}$ and $d = \alpha\bar{\alpha}\bar{\delta}$, i. e., with the net flavour of the $\bar{\delta}$ preon. Hence the d and s quarks that are produced subsequently mix into mass eigenstates before they decay, or take part in a weak process. As an oscillation, the mixing can be illustrated with the Feynman-like diagram of figure 5.2. A preon-antipreon pair inside annihilates and produces another pair, resulting in another quark.

The intermediate system can be one or more photons, one or more gluons, or maybe new gauge bosons ("hypergluons"), which are assumed to exist in some preon models.

It is not realistic that this phenomenon can explain *all* quark mixings of the so-called CKM matrix (Cabibbo 1963; Kobayashi and Maskawa 1973). There is no third state made up of these three preons that can oscillate in a similar way to a d or an s. The smaller CKM matrix elements differ by an order of magnitude from the Cabibbo one, which means that the detailed mechanism for other quarks might be different from the one of section 5.4.2. A more detailed discussion of quark mixings can be found in Dugne et al. (2002).

The preon charges can easily be chosen as to fit the charge of the d and s quarks. Obviously, δ must have charge $+e/3$, while the other two can be "anything". It is wise to choose the charges $+e/3$ also for α and $-2e/3$ for β. This will be obvious from the discussion in the following subsection, although it seems attractive on general grounds to adopt the three charges of the original flavour-$SU(3)$ quark model.

Neutrino mixing

If we choose preon charges as multiples of $e/3$, and if a quark contains three entities, it will be almost necessary to make the charged leptons three-preon states. With the charges defined as above there are just three ways to make neutrinos: $\alpha\beta\delta$, $\alpha\alpha\beta$ and $\delta\delta\beta$.

There are several possible spin combinations if we want to build neutrinos. For simplicity, let us assume that two unequal preons prefer to form a total spin-0 "dipreon" pair, in the same way as quarks tend to form "diquarks" in many situations (Anselmino et al. 1993). The introduction of spin-0 dipreons results in the following *five* neutrinos: $\nu_1 = \alpha(\beta\delta)_{S=0}$, $\nu_2 = \beta(\alpha\delta)_{S=0}$, $\nu_3 = \delta(\beta\alpha)_{S=0}$. $\nu_4 = \alpha(\beta\alpha)_{S=0}$, $\nu_5 = \delta(\beta\delta)_{S=0}$. Note the similarity with the five neutral baryons in the spin-$1/2$ nonet (octet + singlet) of the original quark model.

It can be seen that the three neutrinos ν_1, ν_2 and ν_3 indeed have identical net preon flavours, and hence can mix/oscillate into three new mass eigenstates. Figure 5.3 shows the situation for an oscillation between ν_1 and ν_2. At this stage (of the discussion) it is not possible to tell which neutrinos that correspond to the different preon states. Three of the five states must naturally be connected to the three known neutrinos, while the other two must have masses in excess of half the Z^0 mass.

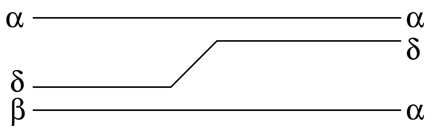

Figure 5.3: One way for two composite neutrinos to mix/oscillate. A preon oscillates in and out of two different “dipreon” (spin-0) pairs.

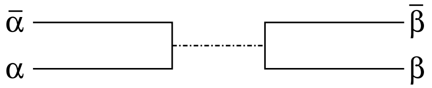

Figure 5.4: One way for two composite neutral vector bosons to mix. A preon-antipreon pair annihilates and turns into another pair.

It can be observed that with these preons it is impossible to construct *charged* leptons that oscillate or mix in the same way. Neither can there be decays of the type $\mu \rightarrow e\gamma$.

Electroweak mixing of W^0 and B^0

In many preon models (D’Souza and Kalman 1992) the weak gauge bosons are supposed to be built up by preon-antipreon pairs in total spin 1. With the preons described earlier, it is tempting to define $W^+ = (\alpha\bar{\beta})$ and $W^- = (\beta\bar{\alpha})$. The neutral sector is more complicated. There are five neutral combinations of the three preons, and three of these have identical net preon numbers: $\alpha\bar{\alpha}$, $\beta\bar{\beta}$ and $\delta\bar{\delta}$. They resemble the ρ^0, ω and ϕ of the vector meson nonet, and are expected to mix. It seems as if some combinations correspond to the two neutral weak-isospin eigenstates: $W^0 = (\alpha\bar{\alpha} - \beta\bar{\beta})/\sqrt{2}$ and $B^0 = (\alpha\bar{\alpha} + \beta\bar{\beta})/\sqrt{2}$. These two mix into two mass eigenstates, Z^0 and Z' (a new and even heavier boson). The partner of the Z is *not* the photon, like in the SM, because the weak interaction is not fundamental in models with composite Zs and Ws. There can hence not be an electroweak unification (and no Higgs). It should be added that most preon models, but not all, lack a Higgs mechanism.

The mixing of $(\alpha\bar{\alpha})$ with $(\beta\bar{\beta})$ can again can be illustrated in the fashion of a Feynman diagram, as in figure 5.4.

The intermediate state must be neutral in both charge and colour, as well as have spin 1, i. e., it could be one or more photons, two or three gluons, or a number of hypothetical “hypergluons”.

An interesting relation

The action in figure 5.2 and 5.4 takes place through similar preon subprocesses, as shown again in figure 5.5.

If the mixing fraction of the $(\alpha\bar{\alpha})$ and $(\beta\bar{\beta})$ pairs depends *only* on the masses and/or electric charges of α and β, and not on, e. g., the systems they are in, then one can show that there is a relation between the Cabibbo and Weinberg angles (Dugne et al. 2002):

$$\cos\theta_W - \sin\theta_W = \sqrt{2}\sin\theta_C. \tag{5.1}$$

With $\sin^2\theta_W = 0.23117 \pm 0.00016$ and $\sin\theta_C = 0.2225 \pm 0.0035$ (Yao et al. 2006) the *lhs* = 0.396 ± 0.001 and the *rhs* = 0.315 ± 0.005. This is a fair agreement. In addition, if we simplify the

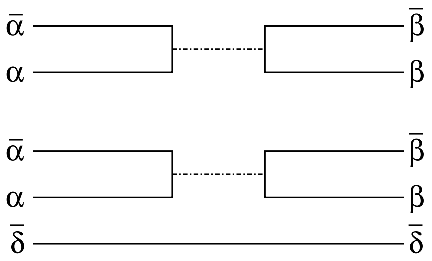

Figure 5.5: The Weinberg mixing of W^0 and B^0, in the upper part of the figure, and the Cabibbo mixing of d and s, in the lower part, come from the same basic preon processes, and are hence related.

situation again and assume that all such mixings occur through one-photon intermediate states, then the preon-antipreon pairs occur in proportion to their squared charges, and we expect:

$$\sin\theta_C = q_\alpha^2/(q_\alpha^2 + q_\beta^2) = 1/5, \tag{5.2}$$

which again is not far from reality.

Massive, charged and unstable weak gauge bosons

Most SM ingredients that lack a deeper understanding have to do with the fact that the weak interaction has massive gauge bosons. The situation with massive and unstable "gauge bosons" is, however, not new in high-energy physics. In nuclear physics it is often productive to regard the vector mesons, ρ, ω, ϕ etc, as gauge bosons of the nuclear forces that keep nucleons in place. They are supposed to close the gap between QCD and nuclear physics, by leaking colour-neutral quark-antiquark pairs between nucleons. It seems as if spin-1 particles are better than scalar ones in mimicing true (massless) gauge bosons.

History therefore warns us that massive gauge bosons might not be fundamental, but some kind of "neutral" leakage of more basic forces. Hence W and Z might well be false gauge bosons that just leak the basic preon forces. This implies that there are *nine* different heavy vector bosons (if we believe in preon-flavour $SU(3)$). Hence six very heavy ones have not yet been discovered. Five of the bosons are neutral (Zs) and four charged (Ws). Three of the Zs have identical net preon flavour and would mix, since they are built up by $\alpha\bar{\alpha}$, $\beta\bar{\beta}$ and $\delta\bar{\delta}$.

5.4.8 γ/Z mixing

Why does the Z^0 seem to mix with the photon, in a way that is well described by the electroweak sector of the SM and parametrized by the Weinberg angle?

This situation is not new. In the 1960s it was acknowledged that the photon sometimes behaves like a hadron in interactions with nucleons. It was suggested that its wave function has a hadronic component, consisting mainly of the ρ meson, but with some fraction also of more massive spin-1 mesons at higher Q^2 values. This idea was named Vector Meson Dominance, VMD (Schildknecht 1972). It was developed in detail and used to describe a wealth of data. It is still a good model for the behaviour of virtual photons in medium-Q^2 reactions with hadrons. Hence a photon is believed to couple via a ρ, like in figure 5.6, when interacting with a hadron.

At an early stage this was taken as a fact, and the origin of the coupling remained unknown for a while. A physicist could then have come up with a radical idea: The photon and the ρ are one and

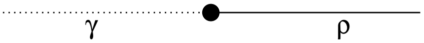

Figure 5.6: The photon mixes with ρ according to the Vector Meson Dominance model.

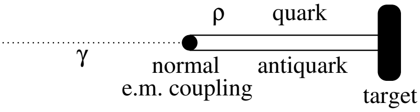

Figure 5.7: The γ/ρ mixing comes about because ρ is composite.

the same particle! This would open up for a new theory of *electrostrong unification*, where the γ/ρ mixing is parametrized by an electrostrong mixing angle. The difference in mass between the two particles could have been explained by an *electrostrong Higgs boson*, or rather a whole set of mixing angles and Higgs bosons, because the photon couples also to other vector mesons in the VDM.

Why was this model never invented (except here)? Because soon after the invention of VMD, the quark model came. Then it became evident that any spin-1 neutral meson couples to ("mixes" with) the photon just because its quarks are electrically charged. At high-enough Q^2 the photon sees the constituents, instead of the (invisible) neutral hadron. The true explanation of the γ/ρ mixing is hence *compositeness*, as illustrated by figure 5.7.

The conclusion for the Z^0 is then obvious. It contains charged preons, and is hence doomed to couple to a high-Q^2 photon, as in figure 5.8.

Qualitatively, the electroweak formalism is very similar to the old parametrization of the VDM model, i. e., the propagators in a Feynman-graph formalism look the same. The Z and Ws are just very good at mimicing true gauge bosons. One can even understand why one and the same Weinberg angle describes not only the γ/Z mixing in the SM but also the Z/Z' mixing in a preon model. This would come about if the preon-antipreon states inside the various Zs mix via virtual photons, rather than gluons or hypergluons.

However, the electroweak and "electrostrong" situation differ quantitatively, since no heavier (Z') boson has been found, in the meaning of deviations from the SM predictions, e. g., at the CERN LEP machine. But most searches for new gauge bosons are built on the assumption that they are just heavier versions of the normal ones, with the same effect when they are exchanged, and with similar decay modes (except for the higher masses). This need not be true if they are built of preons, which means that experiments have so far missed them.

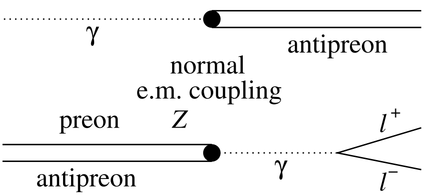

Figure 5.8: The γ/Z mixing comes about because Z is composite.

5.4.9 What next?

This discussion of crucial ad hoc features of the standard model has, step-by-step, led to strict and rather detailed requirements of a hypothetical preon model for quarks, leptons and heavy vector bosons. As one might guess, they are all in line with the “preon-trinity” model presented earlier by Dugne, Fredriksson and Hansson (2002).

This is the reason that we have started a more detailed search for signatures of quarks with the help of current data. Harari (1979) looks into the situation with data from the (closed) CERN LEP accelerator. In future projects we will also take a closer look at data from production of top quarks. At Fermilab there is not yet data enough to test the finer details of the model, so we would rather wait for the CERN LHC to look for the expected new and heavy particles predicted by the model, where the top is just one example.

Also, neutrino oscillations is on the list of possible future studies within this model.

Chapter 6

Discussion and conclusions

The universe truly is a marvelous place, and it is astonishing how much we can learn about its history and evolution just by observing some light that happens to reach the earth. The evolution of the universe has been treated in chapter 2 in order to set the stage for the dust and heavy neutrinos in the history of the universe.

6.1 Imprint of dust on the CMB

One of the things we might learn in the near future is the impact of dust from the first generation of stars. Since the dust has a particular spatial and spectral signature it might be detected by the Planck satellite, planned to be launched in 2008. This dust could help us to better understand two important things in the universe: the cosmic microwave background (CMB) and the formation of structures, like galaxies and stars in the early universe.

Chapter 2 dealt with two points pertaining particularly to dust: (1) The decoupling of matter from radiation (section 3.5), leaving the universe with an omnipresent radiation with an imprint of the properties of the universe when it was 400,000 years old; (2) The first generation of stars (section 2.7), which exploded as supernovæ and sprayed out heavy materials that condensed to form dust.

In chapter 4 followed a description of the properties and benefits of the CMB. The CMB radiation contains a wealth of cosmological information, which can be extracted with the help of the power spectrum (section 4.4).

Chapter 5 contained a description of our current knowledge of interstellar dust (section 5.1) and gave an introduction to dark matter (section 5.2). Neither of these subjects is particularly well known to us today, but there is a lot of circumstantial evidence helping us to understand the basics.

In my thesis I have sought to answer the following questions:

1. **How did the dust density evolve in the early universe?**
   The amount of dust produced by the first generation of stars (population III stars) was estimated in Paper I. Using the star formation model of Cen (2002), which explains the reionization of the universe through star formation, the dust production is simply taken as being proportional to this star formation rate. The results are then parametrized in terms of the fraction of fusioned atoms that became interstellar dust, f_d.

   The dust destruction rate in the early universe is not well known. Therefore the results are evaluated for three different dust life times, $\Delta t = 0.1$, 1 and 10 Giga years. The extrema are not very realistic but they give a span of the possible dust destruction rates. The relative dust

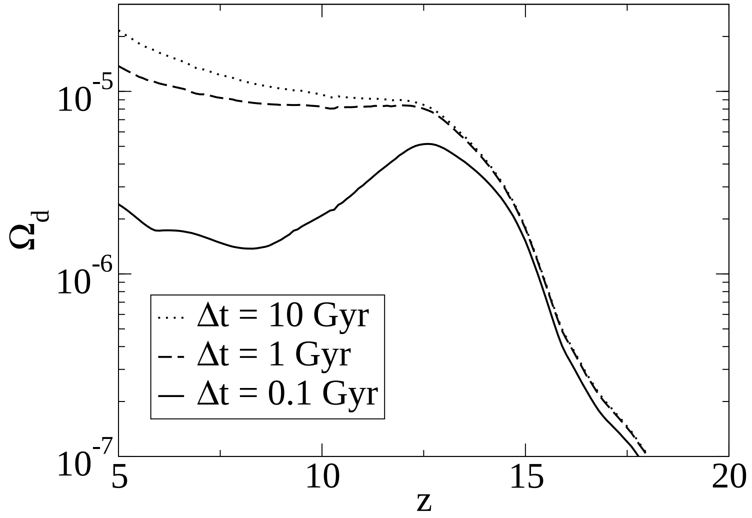

Figure 6.1: The co-moving relative dust density evolution $\Omega_d = \rho_{dust}/\rho_c$, for $f_d = 1$. The minima at $z = 6$ and 9 for $\Delta t \leq 0.1$ Gyr is due to the fact that $\Delta z = 1$ is not a constant time interval.

density is of the order of $\Omega_{Dust} \sim 10^{-6}$ for $\Delta t = 0.1$ Giga years and $\Omega_{Dust} \sim 10^{-5}$ for $\Delta t = 1$ and 10 Giga years, see figure 6.1.

2. **What is the spectrum of the thermal emission of dust from population III stars?**
   As was explored in Paper I, the dust from the first stars was heated by the CMB as well as by the stars themselves. This means that the dust has a modified blackbody spectrum with a temperature slightly above the CMB. The spectrum from this early dust as measured here on earth is a blackbody spectrum with $T = 2.725$ K multiplied by the square of the frequency, see figure 6.2. Unfortunately, this thermal dust emission is not high enough to be directly detected.

3. **What was the spatial distribution of the dust from population III stars?**
   In Paper II two different models were tested in order to study the dust distribution. The corresponding power spectrum of the dust emission was then calculated and compared with sensitivities of different detectors.

   If the dust is supposed to follow a smoothed DM distribution, a rather low power spectrum is found. A higher power spectrum is found if we assume that the dust simply is proportional to the DM distribution in the universe, as calculated by the GalICS simulation program.

   In figure 6.3 we see that for angular scales $\ell \sim 2000$ there is a small region where the dust could dominate over other sources of sub-millimeter emission, depending on f_d and Δt as stated above.

6.2 Implications and possible origin of hypothetical heavy neutrinos

The interest in heavy neutrinos has waned in the last decade or two since it was shown that they can not be a dominant component of the DM of the universe (Mori et al. 1992). As we have shown in

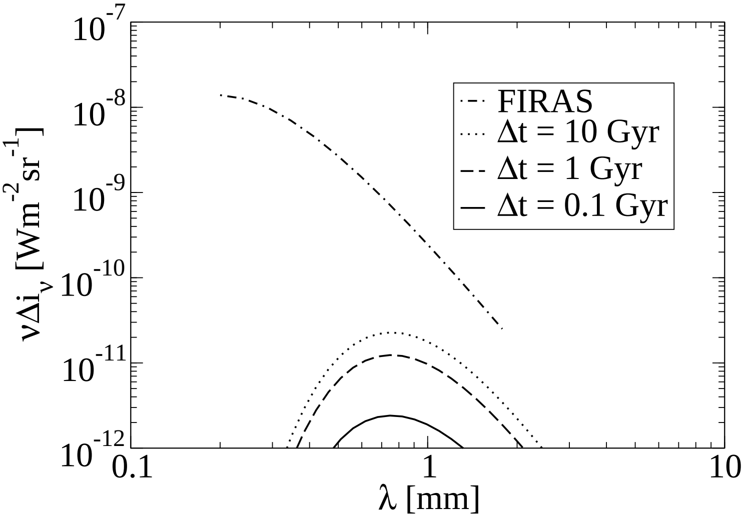

Figure 6.2: Comparison of the modeled intensity for the early dust emission in excess of the CMB with the observed FIRAS (Puget et al. 1996; Fixsen et al. 1998; Lagache et al. 1999) spectrum (dot-dashed curve) of the cosmic far IR background as detailed by Lagache et al. (1999).

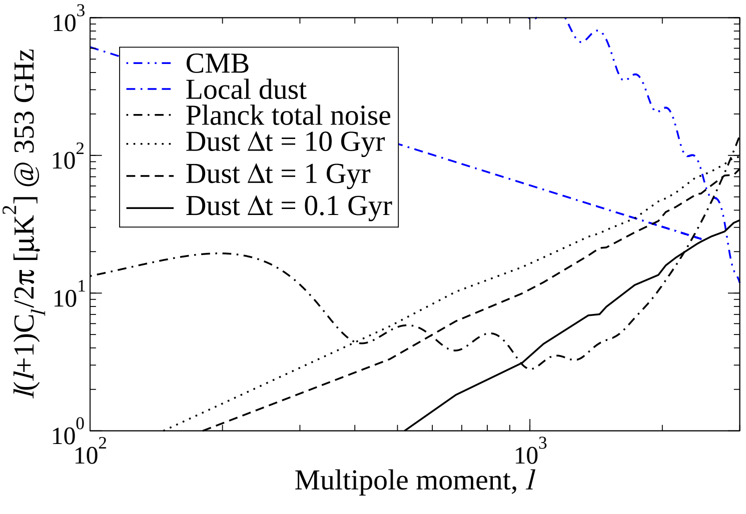

Figure 6.3: Comparison between dust power spectrum and Planck error limits at 353 GHz with binning 500. The error limits (total noise) consist of two parts; the CMB cosmic variance, which dominates for small ℓ and the instrument noise, which dominates for high ℓ.

our Paper III, though, this does not mean that they can not exist. If they exist, and if their mass is right, they would produce a small bump in the gamma-ray spectrum at $E_\gamma \sim 1$ GeV.

In order to evaluate the neutrino density evolution, we first need to study some cosmology and thermodynamics in the early universe. This was treated in chapter 3 along with the decoupling of non-relativistic particles from the radiation. The correct formulation for the evolution of the particle number density was derived, including the change in temperature due to freeze-out of (lighter) particles. This led to a somewhat higher estimation of the heavy neutrino number density than previous results (e. g., Fargion et al. 1995).

4. **How does the neutrino density evolve with time?**
   The neutrino density has been calculated in several papers in the past, most of them using the freeze-out temperature and then solving the problem analytically. One of the last contributions in this field is done by Fargion et al. (1995). In Paper III these results were first reproduced without our being certain about their approximations, but we found essentially the same relic neutrino density.

   Then a numerical calculation was made of the evolution of the neutrino density with the reheating from entropy conservation properly taken into account. The resulting neutrino density proved to be higher than the analytical result by a factor of ~ 2, see figure 6.4. It can be seen that the maximum value of the numerical simulation gives $\Omega_N \approx 0.04$ for $M_N = 140$ GeV which is about 15% of the dark matter content ($\Omega_{DM} = 0.24$) of the universe (dotted line).

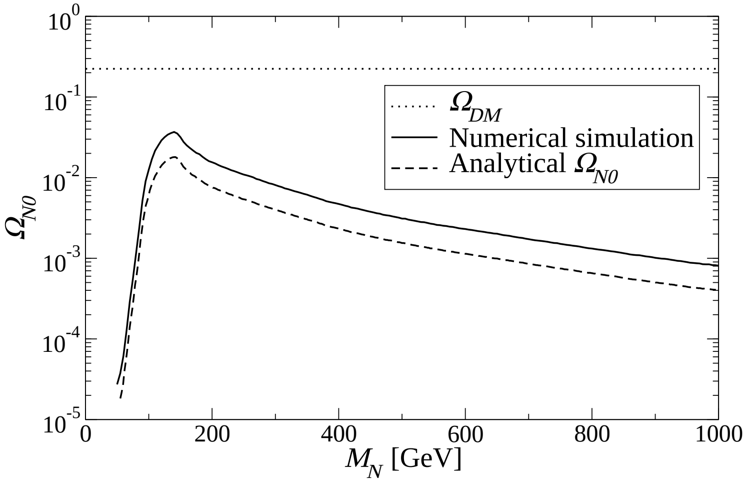

Figure 6.4: The relic relative density of heavy neutrinos as a function of their mass (in GeV).

5. **How large is the clumping enhancement for the neutrino-antineutrino signal?**
   Since the neutrino-antineutrino annihilation is proportional to the square of the neutrino density, structures with higher density, such as galactic clusters and galaxies, will have a positive net effect on the annihilation rate.

   This enhancement (the “clumping factor”) is estimated in Paper III, using a conservative DM halo radius equal to the virial radius of the DM halo. The DM simulations are the same as in Paper II.

   The signal from neutrino-antineutrino annihilation is thereby enhanced by a factor of ~ 30. The clumping factor as a function of time can be seen in figure 6.5.

6. **How much would heavy neutrinos contribute to the diffuse gamma-ray background?**
   The gamma-ray spectrum from distant neutrino-antineutrino annihilation is calculated in Paper III. Using the neutrino density and the clumping factor, the gamma-ray spectrum near earth was calculated.

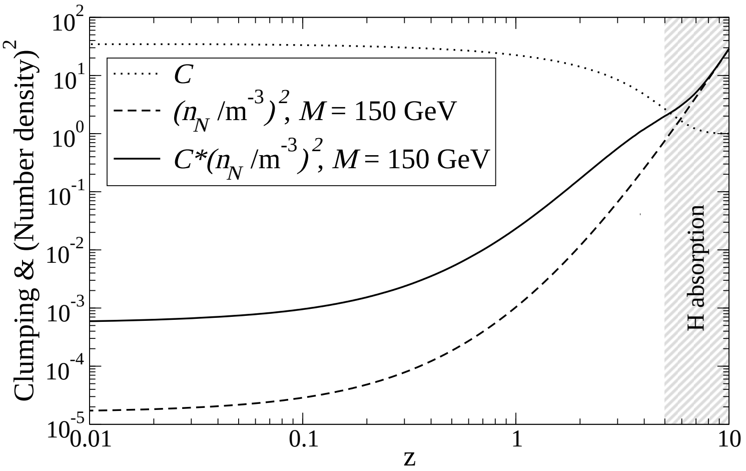

Figure 6.5: The clumping factor (C, dotted line) compared to the competing effect of the decreasing heavy neutrino number density squared (n_N^2, dashed line) for $M_N = 150$ GeV and the product of the two (solid line).

For neutrino masses of ~ 100 – 200 GeV, the signal was found to surpass the diffuse gamma-ray spectrum measured by the satellite-born EGRET telescope, see figure 6.6. If the neutrino mass would be on the boundaries of this exclusion region, the heavy neutrinos would give a small bump in the gamma-ray spectrum at ~ 1 GeV, as can be seen in figure 6.7.

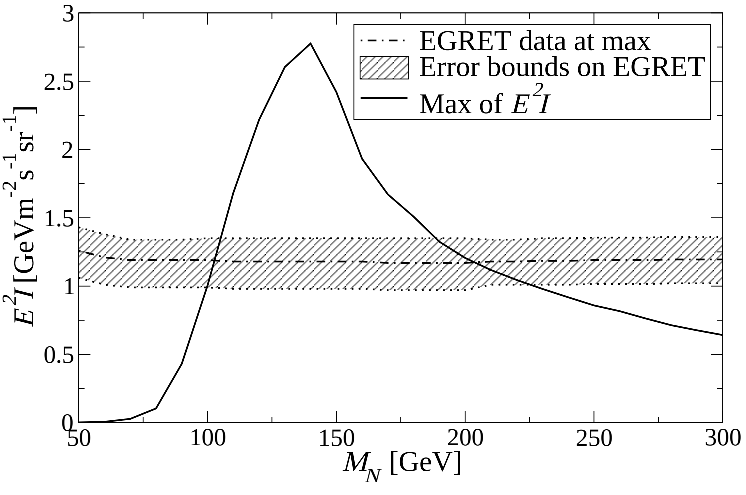

Figure 6.6: Maximum cosmic gamma radiation from photons produced in $N\bar{N}$-collisions as a function of neutrino mass (in GeV). The marked region is excluded since $\Omega_N > \Omega_{DM}$ within. The data are taken at the energy corresponding to the maxima in figure 6.7 with error bars.

7. **How would composite leptons and quarks reveal themselves in existing data?**
If the heavy leptons and quarks of the preon-trinity model exist, and if they are lighter than the top quark, as indicated by the model, then several of them are expected to be produced

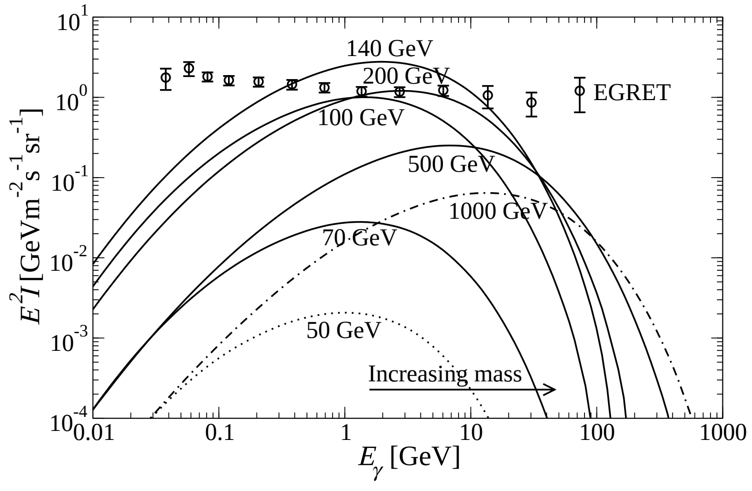

Figure 6.7: Cosmic gamma radiation from photons produced in $N\bar{N}$-collisions as a function of photon energy for neutrino masses $M_N = 50, 70, 100, 140, 200, 500, 1000$ GeV. The dotted line represents $M_N = 50$ GeV and the dot-dashed $M_N = 1000$ GeV. The solid lines are the masses in between. The circles represent data from EGRET (Sreekumar et al. 1998), with error bar, as derived for extragalactic sources.

at CERN LEP energies in e^+e^- annihilations. Most notably, a heavy neutrino is expected to decay into a light neutrino and a photon, but also through other decay modes. We predict also the decay modes of the heavy quarks of the model that we use. It is obvious in the model that single-top production is forbidden in e^+e^- annihilations at LEP energies. Since the model has no dynamics it is not possible to predict branching ratios and life times, only decay modes and very approximate masses.

6.3 Conclusions

The objectives of this doctoral thesis, as presented in chapter 1, were to investigate (1) the imprint of early dust on the CMB and (2) the implications and possible origin of hypothetical heavy neutrinos. These objectives have now been accomplished by the answers to the research questions in sections 6.1.1 and 6.1.2 above. There is some imprint of the dust although it is small. Heavy neutrinos might produce a gamma-ray signal under certain conditions. If they exist, they might be composite particles.

Chapter 7

Outlook

There are still numerous exciting problems to be solved in order to consolidate our understanding of the universe, in particular, regarding early dust, heavy neutrinos and preons.

The impact of dust on the history of the universe is still an open question. It would be interesting to see some detailed simulations of the evolution of the first galaxies, with dust production as well as dust destruction taken into account. This dust has important implications for the spectra emitted by these galaxies, which eventually could be detected. The Hubble ultra deep field (Beckwith et al. 2006) shows us the universe at an age of $\sim 0.7 - 2$ billion years. Even more interesting is the James Webb Space Telescope, the successor to the Hubble Space Telescope, which is planned to be launched in 2013. It will be almost three times the size of Hubble and it has been designed to work best at infrared wavelengths. This will allow it to study the very distant universe, looking for the first stars and galaxies that ever emerged.

The true nature of DM is still an unresolved question. Heavy neutrinos can not constitute a major part of the DM but they might contribute. The results of the GLAST satellite might give some evidence of this.

The truth behind the symmetries in the SM can also be further explored, especially in prospect of the CERN LHC that will come online in 2008. The preon model presented here have several attractive features that can give measureable predictions. In the end of the next decade, there will also be the International Linear Collider, for precision measurements at an initial energy of 500 GeV.

Another interesting path is to study the large scale structure of the universe. The "cold spot" in the CMB gives evidence of that the universe might not be as isotropic and homogeneous as has previously been presumed.

New instruments are continously being developed and our understanding of the universe is growing rapidly. All in all, the prospects of astrophysics are excellent in the future, and I look forward to take part in the coming exploration of the conditions for mankind to survive and prosper in the universe.

Bibliography

Alexander, S., Biswas, T., Notari, A. and Vaid, D. (2007), 'Local Void vs Dark Energy: Confrontation with WMAP and Type Ia Supernovae', *ArXiv e-prints, astroph/0712.0370,* pp. 1–26.

Alpher, R. A., Bethe, H. and Gamow, G. (1948), 'The Origin of Chemical Elements', *Physical Review* **73**, 803–804.

Alpher, R. A., Herman, R. and Gamow, G. A. (1948), 'Thermonuclear Reactions in the Expanding Universe', *Physical Review* **74**, 1198–1199.

Anselmino, M., Predazzi, E., Ekelin, S., Fredriksson, S. and Lichtenberg, D. B. (1993), 'Diquarks', *Reviews of Modern Physics* **65**, 1199–1233.

Ball, P. (2007), 'Splitting the quark'. Nature New, November 30.
URL: *http://www.nature.com/news/2007/071130/full/news.2007.292.html*

Barger, V., Ma, E., Whisnant, K., Deshpande, N. G. and Johnson, R. J. (1982), 'General constraints on neutral-current couplings from SO(10) grand unification', *Physics Letters B* **118**, 68–72.

Barrett, R. K. and Clarkson, C. A. (2000), 'Undermining the cosmological principle: almost isotropic observations in inhomogeneous cosmologies', *Classical and Quantum Gravity* **17**, 5047–5078.

Beckwith, S. V. W., Stiavelli, M., Koekemoer, A. M., Caldwell, J. A. R., Ferguson, H. C., Hook, R., Lucas, R. A., Bergeron, L. E., Corbin, M., Jogee, S., Panagia, N., Robberto, M., Royle, P., Somerville, R. S. and Sosey, M. (2006), 'The Hubble Ultra Deep Field', *Astronomical Journal* **132**, 1729–1755.

Bergström, L. (2000), 'Non-baryonic dark matter: observational evidence and detection methods.', *Reports of Progress in Physics* **63**, 793–841.

Bertone, G., Hooper, D. and Silk, J. (2005), 'Particle dark matter: evidence, candidates and constraints', *Physics Reports* **405**, 279–390.

Boggess, N. W., Mather, J. C., Weiss, R., Bennett, C. L., Cheng, E. S., Dwek, E., Gulkis, S., Hauser, M. G., Janssen, M. A., Kelsall, T., Meyer, S. S., Moseley, S. H., Murdock, T. L., Shafer, R. A., Silverberg, R. F., Smoot, G. F., Wilkinson, D. T. and Wright, E. L. (1992), 'The COBE mission - Its design and performance two years after launch', *Astrophysical Journal* **397**, 420–429.

Boulanger, F., Abergel, A., Bernard, J.-P., Burton, W. B., Desert, F.-X., Hartmann, D., Lagache, G. and Puget, J.-L. (1996), 'The dust/gas correlation at high Galactic latitude.', *Astronomy and Astrophysics* **312**, 256–262.

Bradley, M., Fodor, G., Marklund, M. and Perjes, Z. (2000), ‘The Wahlquist metric cannot describe an isolated rotating body’, *Classical and Quantum Gravity* **17**, 351–364.
URL: *http://arxiv.org/abs/gr-qc/9910001*

Burles, S., Nollett, K. M. and Turner, M. S. (2001), ‘What is the big-bang-nucleosynthesis prediction for the baryon density and how reliable is it?’, *Physical Review D* **63**(6), 512–519.

Cabibbo, N. (1963), ‘Unitary Symmetry and Leptonic Decays’, *Physical Review Letters* **10**, 531–533.

Campanelli, L., Cea, P. and Tedesco, L. (2006), ‘Ellipsoidal Universe Can Solve the Cosmic Microwave Background Quadrupole Problem’, *Physical Review Letters* **97**(13), 131302–+.

Cen, R. (2002), ‘The universe was reionized twice’, *Astrophysical Journal* **591**, 12–37.

Cen, R. (2003), ‘The Implications of Wilkinson Microwave Anisotropy Probe Observations for Population III Star Formation Processes’, *Astrophysical Journal, Letters* **591**, L5–L8.

Choudhury, T. R. and Ferrara, A. (2006), ‘Physics of Cosmic Reionization’, *ArXiv Astrophysics e-prints, astro-ph/0603149,* pp. 1–40.

Coc, A., Vangioni-Flam, E., Descouvemont, P., Adahchour, A. and Angulo, C. (2004), ‘Updated Big Bang Nucleosynthesis Compared with Wilkinson Microwave Anisotropy Probe Observations and the Abundance of Light Elements’, *Astrophysical Journal* **600**, 544–552.

Coleman, T. S. and Roos, M. (2003), ‘Effective degrees of freedom during the radiation era’, *Physical Review D* **68**(2), 027702–+.

Colless, M., Dalton, G., Maddox, S., Sutherland, W., Norberg, P., Cole, S., Bland-Hawthorn, J., Bridges, T., Cannon, R., Collins, C., Couch, W., Cross, N., Deeley, K., De Propris, R., Driver, S. P., Efstathiou, G., Ellis, R. S., Frenk, C. S., Glazebrook, K., Jackson, C., Lahav, O., Lewis, I., Lumsden, S., Madgwick, D., Peacock, J. A., Peterson, B. A., Price, I., Seaborne, M. and Taylor, K. (2001), ‘The 2dF Galaxy Redshift Survey: spectra and redshifts’, *Monthly Notices of the RAS* **328**, 1039–1063.

Daigne, F., Olive, K. A., Vangioni-Flam, E., Silk, J. and Audouze, J. (2004), ‘Cosmic Star Formation, Reionization, and Constraints on Global Chemical Evolution’, *Astrophysical Journal* **617**, 693–706.

Dirac, P. A. M. (1928), ‘The quantum theory of electron’, *Proc. Roy. Soc. Lond.* **A117**, 610–624.

Draine, B. T. (1990), ‘Evolution of interstellar dust’, *in* ‘ASP Conf. Ser. 12: The Evolution of the Interstellar Medium’, pp. 193–205.

Draine, B. T. (2003), ‘Astrophysics of Dust in Cold Clouds’, *ArXiv Astrophysics e-prints, astro-ph/0304488,* pp. 1–93.

Draine, B. T. and Salpeter, E. E. (1979), ‘Destruction mechanisms for interstellar dust’, *Astrophysical Journal* **231**, 438–455.

D’Souza, I. A. and Kalman, C. S. (1992), ‘Preons: Models of leptons, quarks and gauge bosons as composite objects’, p. 108. Singapore, Singapore: World Scientific (1992) 108 p.

Dugne, J.-J., Fredriksson, S. and Hansson, J. (2002), ‘Preon trinity – A schematic model of leptons, quarks and heavy vector bosons’, *Europhysics Letters* **60**, 188–194.

Dwek, E., Arendt, R. G., Hauser, M. G., Fixsen, D., Kelsall, T., Leisawitz, D., Pei, Y. C., Wright, E. L., Mather, J. C., Moseley, S. H., Odegard, N., Shafer, R., Silverberg, R. F. and Weiland, J. L. (1998), 'The COBE Diffuse Infrared Background Experiment Search for the Cosmic Infrared Background. IV. Cosmological Implications', *Astrophysical Journal* **508**, 106–122.

Efstathiou, G., Sutherland, W. J. and Maddox, S. J. (1990), 'The cosmological constant and cold dark matter', *Nature* **348**, 705–707.

Elfgren, E. (2002*a*), 'Detection of a Hypercharge Axion in ATLAS', *in* 'Fundamental Interactions, Proceedings of the Sixteenth Lake Louise Winter Institute, held 18-24 February, 2001. Edited by A. Astbury, B. A. Campbell, F. C. Khanna, and M. G. Vincter. World Scientific Publishing Company, 2002., p.185', pp. 185–192.

Elfgren, E. (2002*b*), Heavy and Excited Leptons in the OPAL Detector?, Master's thesis, Université de Montréal. (hep-ph/0209238).

Elfgren, E. (2007), 'Using Monte Carlo to optimize variable cuts'. Submitted to Physics Letters B (hep-ph/0712.3340).

Elfgren, E. and Désert, F.-X. (2004), 'Dust from reionization', *Astronomy and Astrophysics* **425**, 9–14.

Elfgren, E., Désert, F.-X. and Guiderdoni, B. (2007), 'Dust distribution during reionization', *Astronomy and Astrophysics* **476**, 1145–1150.

Elfgren, E. and Fredriksson, S. (2007*a*), 'Are there indications of compositeness of leptons and quarks in CERN LEP data?'. Submitted to Physical Review D (hep-ph/0712.3342).

Elfgren, E. and Fredriksson, S. (2007*b*), 'Mass limits for heavy neutrinos', *Astronomy and Astrophysics* **710**. Accepted for publication on December 10, 2007 (astro-ph/0710.3893).

Enqvist, K., Kainulainen, K. and Maalampi, J. (1989), 'Cosmic abundances of very heavy neutrinos', *Nuclear Physics B* **317**, 647–664.

Fang, T. and Cen, R. (2004), 'The Transition from Population III to Population II Stars', *Astrophysical Journal, Letters* **616**, L87–L90.

Fargion, D., Khlopov, M. Y., Konoplich, R. V. and Mignani, R. (1995), 'Bounds on very heavy relic neutrinos by their annihilation in the galactic halo', *Physical Review D* **52**(4), 1828–1836.

Fischer, E. (2003), 'Extinction by grey dust in the intergalactic medium', *ArXiv Astrophysics e-prints, astro-ph/0306459,* pp. 1–6.

Fixsen, D. J., Cheng, E. S., Cottingham, D. A., Eplee, Jr., R. E., Isaacman, R. B., Mather, J. C., Meyer, S. S., Noerdlinger, P. D., Shafer, R. A., Weiss, R., Wright, E. L., Bennett, C. L., Boggess, N. W., Kelsall, T., Moseley, S. H., Silverberg, R. F., Smoot, G. F. and Wilkinson, D. T. (1994), 'Cosmic microwave background dipole spectrum measured by the COBE FIRAS instrument', *Astrophysical Journal* **420**, 445–449.

Fixsen, D. J., Dwek, E., Mather, J. C., Bennett, C. L. and Shafer, R. A. (1998), 'The Spectrum of the Extragalactic Far-Infrared Background from the COBE FIRAS Observations', *Astrophysical Journal* **508**, 123–128.

Fritzsch, H. and Mandelbaum, G. (1981), 'Weak interactions as manifestations of the substructure of leptons and quarks', *Physics Letters B* **102**, 319–322.

Gahm, G. F. (1990), ‘Star formation after core collapse.’, *in* B. Battrick, ed., ‘Formation of Stars and Planets, and the Evolution of the Solar System’, pp. 43–51.

Gamow, G. (1948), ‘The Origin of Elements and the Separation of Galaxies’, *Physical Review* **74**, 505–506.

Gell-Mann, M. (1964), ‘A schematic model of baryons and mesons’, *Physics Letters* **8**, 214–215.

Glashow, S. L. (1961), ‘Partial symmetries of weak interactions’, *Nuclear Physics* **22**, 579–588.

Hansson, J. and Sandin, F. (2005), ‘Preon stars: A new class of cosmic compact objects’, *Physics Letters B* **616**, 1–7.

Harari, H. (1979), ‘A schematic model of quarks and leptons’, *Physics Letters B* **86**, 83–86.

Hewett, J. L. and Rizzo, T. G. (1989), ‘Low-energy phenomenology of superstring-inspired E6 models’, *Physics Reports* **183**, 193–381.

Hu, H. (1995), Wandering in the background: A Cosmic microwave background explorer, PhD thesis, UC Berkeley.

Hubble, E. (1929), ‘A Relation between Distance and Radial Velocity among Extra-Galactic Nebulae’, *Proceedings of the National Academy of Science* **15**, 168–173.

Inoue, K. T. and Silk, J. (2007), ‘Local Voids as the Origin of Large-Angle Cosmic Microwave Background Anomalies: The Effect of a Cosmological Constant’, *Astrophysical Journal* **664**, 650–659.

Jackson, N. (2007), ‘The Hubble Constant’, *Living Reviews in Relativity* **10**, 4–+.

Kobayashi, M. and Maskawa, T. (1973), ‘CP-Violation in the Renormalizable Theory of Weak Interaction’, *Progress of Theoretical Physics* **49**, 652–657.

Kolb, E. and Turner, M. (1990), *The Early Universe*, Westview Press, Oxford.

Lagache, G., Abergel, A., Boulanger, F., Désert, F. X. and Puget, J.-L. (1999), ‘First detection of the warm ionised medium dust emission. Implication for the cosmic far-infrared background’, *Astronomy and Astrophysics* **344**, 322–332.

Maalampi, J. and Roos, M. (1990), ‘Physics of mirror fermions’, *Physics Reports* **186**, 53–96.

Majorana, E. (1937), ‘Theory of the symmetry of electrons and positrons’, *Nuovo Cimento* **14**, 171–184.

Martínez-González, E., Cruz, M., Cayón, L. and Vielva, P. (2006), ‘The non-Gaussian cold spot in WMAP’, *New Astronomy Review* **50**, 875–879.

Mather, J. C., Fixsen, D. J., Shafer, R. A., Mosier, C. and Wilkinson, D. T. (1999), ‘Calibrator Design for the COBE Far-Infrared Absolute Spectrophotometer (FIRAS)’, *Astrophysical Journal* **512**, 511–520.

Misner, C. W., Thorne, K. and Wheeler, J. (1973), *Gravitation (Physics Series)*, W. H. Freeman, New York.

Mohr, P. J. and Taylor, B. N. (2000), ‘CODATA Recommended Values of the Fundamental Constants’, *in* ‘AIP Conf. Proc. 543: Atomic and Molecular Data and their Applications, ICAM-DATA’, pp. 1–333.

Mori, M., Hikasa, K., Nojiri, M. M., Oyama, Y., Suzuki, A., Takahashi, K., Yamada, M., Takei, H., Miyano, K., Miyata, H., Hirata, K. S., Inoue, K., Ishida, T., Kajita, T., Kihara, K., Nakahata, M., Nakamura, K., Sakai, A., Sato, N., Suzuki, Y., Totsuka, Y., Koshiba, M., Nishijima, K., Kajimura, T., Suda, T., Fukuda, Y., Kodera, E., Nagashima, Y., Takita, M., Yokoyama, H., Kaneyuki, K., Takeuchi, Y., Tanimori, T., Beier, E. W., Frank, E. D., Frati, W., Kim, S. B., Mann, A. K., Newcomer, F. M., van Berg, R. and Zhang, W. (1992), 'A limit on massive neutrino dark matter from Kamiokande', *Physics Letters B* **289**, 463–469.

Odom, B., Hanneke, D., D'Urso, B. and Gabrielse, G. (2006), 'New Measurement of the Electron Magnetic Moment Using a One-Electron Quantum Cyclotron', *Physical Review Letters* **97**(3), 030801–+.

Pati, J. C. and Salam, A. (1974), 'Lepton number as the fourth "color"', *Physical Review D* **10**, 275–289.

Pati, J. C., Salam, A. and Strathdee, J. (1975), 'Are quarks composite?', *Physics Letters B* **59**, 265–268.

Pati, J. C., Salam, A. and Strathdee, J. (1981), 'A preon model with hidden electric and magnetic type charges', *Nuclear Physics B* **185**, 416–428.

Peacock, J. (1998), *Cosmological Physics*, Cambridge University Press, Cambridge, U.K.; New York, U.S.A.

Penzias, A. A. and Wilson, R. W. (1965), 'A Measurement of Excess Antenna Temperature at 4080 Mc/s.', *Astrophysical Journal* **142**, 419–421.

Perlmutter, S., Aldering, G., Goldhaber, G., Knop, R. A., Nugent, P., Castro, P. G., Deustua, S., Fabbro, S., Goobar, A., Groom, D. E., Hook, I. M., Kim, A. G., Kim, M. Y., Lee, J. C., Nunes, N. J., Pain, R., Pennypacker, C. R., Quimby, R., Lidman, C., Ellis, R. S., Irwin, M., McMahon, R. G., Ruiz-Lapuente, P., Walton, N., Schaefer, B., Boyle, B. J., Filippenko, A. V., Matheson, T., Fruchter, A. S., Panagia, N., Newberg, H. J. M., Couch, W. J. and The Supernova Cosmology Project (1999), 'Measurements of Omega and Lambda from 42 High-Redshift Supernovae', *Astrophysical Journal* **517**, 565–586.

Peskin, M. E. and Schroeder, D. V. (1995), *An Introduction to Quantum Field Theory*, Perseus Books, Cambridge, Massachusetts.

Puget, J.-L., Abergel, A., Bernard, J.-P., Boulanger, F., Burton, W. B., Desert, F.-X. and Hartmann, D. (1996), 'Tentative detection of a cosmic far-infrared background with COBE.', *Astronomy and Astrophysics* **308**, L5+.

Rees, M. J. and Sciama, D. W. (1968), 'Larger scale Density Inhomogeneities in the Universe', *Nature* **217**, 511–+.

Rephaeli, Y. (1995), 'Comptonization Of The Cosmic Microwave Background: The Sunyaev-Zel'dovich Effect', *Annual Review of Astronomy and Astrophysics* **33**, 541–580.

Robinett, R. W. and Rosner, J. L. (1982), 'Prospects for a second neutral vector boson at low mass in SO(10)', *Physical Review D* **25**, 3036–3064.

Sachs, R. K. and Wolfe, A. M. (1967), 'Perturbations of a Cosmological Model and Angular Variations of the Microwave Background', *Astrophysical Journal* **147**, 73–90.

Salam, A. (1968), 'Weak and electromagnetic interactions', *in* N. Svartholm, ed., 'Elementary Particle Theory, Proceedings Of The Nobel Symposium Held 1968 in Lerum, Sweden', Almqvist and Wiksell, Stockholm, pp. 367–377.

Sandin, F. and Hansson, J. (2007), 'The observational legacy of preon stars - probing new physics beyond the LHC', *ArXiv Astrophysics e-prints, astro-ph/0701768* pp. 1–8.

Schaller, G., Schaerer, D., Meynet, G. and Maeder, A. (1992), 'New grids of stellar models from 0.8 to 120 solar masses at Z = 0.020 and Z = 0.001', *Astronomy and Astrophysics, Supplement* **96**, 269–331.

Schildknecht, D. (1972), 'Vector meson dominance, photo- and electroproduction from nucleons', *Springer Tracts Modern Physics* **63**, 57–97.

Seljak, U. and Zaldarriaga, M. (1996), 'A line of sight approach to cosmic microwave background anisotropies', *Astrophysical Journal* **469**, 437–444.

Shioya, Y., Taniguchi, Y., Murayama, T., Nishiura, S., Nagao, T. and Kakazu, Y. (2002), 'Effects of a Burst of Formation of First-Generation Stars on the Evolution of Galaxies', *Astrophysical Journal* **576**, 36–44.

Shupe, M. A. (1979), 'A composite model of leptons and quarks', *Physics Letters B* **86**, 87–92.

Silk, J. (1967), 'Fluctuations in the Primordial Fireball', *Nature* **215**, 1155–+.

Silk, J. (1968*a*), 'Cosmic Black-Body Radiation and Galaxy Formation', *Astrophysical Journal* **151**, 459–471.

Silk, J. (1968*b*), 'When were Galaxies and Galaxy Clusters formed?', *Nature* **218**, 453–454.

Spergel, D. N., Bean, R., Doré, O., Nolta, M. R., Bennett, C. L., Dunkley, J., Hinshaw, G., Jarosik, N., Komatsu, E., Page, L., Peiris, H. V., Verde, L., Halpern, M., Hill, R. S., Kogut, A., Limon, M., Meyer, S. S., Odegard, N., Tucker, G. S., Weiland, J. L., Wollack, E. and Wright, E. L. (2007), 'Three-Year Wilkinson Microwave Anisotropy Probe (WMAP) Observations: Implications for Cosmology', *Astrophysical Journal, Supplement* **170**, 377–408.

Spergel, D. N., Verde, L., Peiris, H. V., Komatsu, E., Nolta, M. R., Bennett, C. L., Halpern, M., Hinshaw, G., Jarosik, N., Kogut, A., Limon, M., Meyer, S. S., Page, L., Tucker, G. S., Weiland, J. L., Wollack, E. and Wright, E. L. (2003), 'First-Year Wilkinson Microwave Anisotropy Probe (WMAP) Observations: Determination of Cosmological Parameters', *Astrophysical Journal, Supplement* **148**, 175–194.

Sreekumar, P., Bertsch, D. L., Dingus, B. L., Esposito, J. A., Fichtel, C. E., Hartman, R. C., Hunter, S. D., Kanbach, G., Kniffen, D. A., Lin, Y. C., Mayer-Hasselwander, H. A., Michelson, P. F., von Montigny, C., Muecke, A., Mukherjee, R., Nolan, P. L., Pohl, M., Reimer, O., Schneid, E., Stacy, J. G., Stecker, F. W., Thompson, D. J. and Willis, T. D. (1998), 'EGRET Observations of the Extragalactic Gamma-Ray Emission', *Astrophysical Journal* **494**, 523–+.

Sunyaev, R. A. and Zel'dovich, I. B. (1970), 'Small-Scale Fluctuations of Relic Radiation', *Astrophysics and Space Science* **7**, 3–19.

Sunyaev, R. A. and Zel'dovich, I. B. (1980), 'Microwave background radiation as a probe of the contemporary structure and history of the universe', *Annual Review of Astronomy and Astrophysics* **18**, 537–560.

Tegmark, M. (1996), 'Doppler Peaks and all that: CMB Anisotropies and What They Can Tell Us', *in* S. Bonometto, J. R. Primack and A. Provenzale, eds, 'Dark Matter in the Universe, Proc. of the Int. School of Physics Course CXXXII', Italian Physical Society, Oxford, GB: IOS Press, pp. 379–419.

Terazawa, H. (1980), 'Subquark model of leptons and quarks', *Physical Review D* **22**, 184–199.

Todini, P. and Ferrara, A. (2001), 'Dust formation in primordial Type II supernovae', *Monthly Notices of the RAS* **325**, 726–736.

Tommasini, D., Barenboim, G., Bernabeu, G. and Jarlskog, C. (1995), 'Non-decoupling of heavy neutrinos and lepton flavour violation', *Nuclear Physics B* **444**, 451.
URL: *http://www.citebase.org/abstract?id=oai:arXiv.org:hep-ph/9503228*

Weinberg, S. (1967), 'A model of leptons', *Physical Review Letters* **19**, 1264–1266.

Woosley, S. E. and Weaver, T. A. (1995), 'The Evolution and Explosion of Massive Stars. II. Explosive Hydrodynamics and Nucleosynthesis', *Astrophysical Journal, Supplement* **101**, 181–235.

Yao, W.-M., Amsler, C., Asner, D., Barnett, R., Beringer, J., Burchat, P., Carone, C., Caso, C., Dahl, O., D'Ambrosio, G., DeGouvea, A., Doser, M., Eidelman, S., Feng, J., Gherghetta, T., Goodman, M., Grab, C., Groom, D., Gurtu, A., Hagiwara, K., Hayes, K., Hernández-Rey, J., Hikasa, K., Jawahery, H., Kolda, C., Y., K., Mangano, M., Manohar, A., Masoni, A., Miquel, R., Mönig, K., Murayama, H., Nakamura, K., Navas, S., Olive, K., Pape, L., Patrignani, C., Piepke, A., Punzi, G., Raffelt, G., Smith, J., Tanabashi, M., Terning, J., Törnqvist, N., Trippe, T., Vogel, P., Watari, T., Wohl, C., Workman, R., Zyla, P., Armstrong, B., Harper, G., Lugovsky, V., Schaffner, P., Artuso, M., Babu, K., Band, H., Barberio, E., Battaglia, M., Bichsel, H., Biebel, O., Bloch, P., Blucher, E., Cahn, R., Casper, D., Cattai, A., Ceccucci, A., Chakraborty, D., Chivukula, R., Cowan, G., Damour, T., DeGrand, T., Desler, K., Dobbs, M., Drees, M., Edwards, A., Edwards, D., Elvira, V., Erler, J., Ezhela, V., Fetscher, W., Fields, B., Foster, B., Froidevaux, D., Gaisser, T., Garren, L., Gerber, H.-J., Gerbier, G., Gibbons, L., Gilman, F., Giudice, G., Gritsan, A., Grünewald, M., Haber, H., Hagmann, C., Hinchliffe, I., Höcker, A., Igo-Kemenes, P., Jackson, J., Johnson, K., Karlen, D., Kayser, B., Kirkby, D., Klein, S., Kleinknecht, K., Knowles, I., Kowalewski, R., Kreitz, P., Krusche, B., Kuyanov, Y., Lahav, O., Langacker, P., Liddle, A., Ligeti, Z., Liss, T., Littenberg, L., Liu, L., Lugovsky, K., Lugovsky, S., Mannel, T., Manley, D., Marciano, W., Martin, A., Milstead, D., Narain, M., Nason, P., Nir, Y., Peacock, J., Prell, S., Quadt, A., Raby, S., Ratcliff, B., Razuvaev, E., Renk, B., Richardson, P., Roesler, S., Rolandi, G., Ronan, M., Rosenberg, L., Sachrajda, C., Sarkar, S., Schmitt, M., Schneider, O., Scott, D., Sjöstrand, T., Smoot, G., Sokolsky, P., Spanier, S., Spieler, H., Stahl, A., Stanev, T., Streitmatter, R., Sumiyoshi, T., Tkachenko, N., Trilling, G., Valencia, G., van Bibber, K., Vincter, M., Ward, D., Webber, B., Wells, J., Whalley, M., Wolfenstein, L., Womersley, J., Woody, C., Yamamoto, A., Zenin, O., Zhang, J. and Zhu, R.-Y. (2006), 'Review of Particle Physics', *Journal of Physics G Nuclear Physics* **33**, 1–1232.

Zweig, G. (1964), 'An SU(3) model for strong interaction symmetry and its breaking'. CERN-TH-412 (unpublished).

Appendix A

Cosmology reference

A.1 Basic introduction

This appendix contains some explanations for those not so familiar with cosmology but with some knowledge of physics in general and also a short list of relevant equations. The symbols are explained in appendix C.

First, it is important to know that distance and time are used interchangeably. Since light moves with a constant speed, c, we know that the distance traveled is $c \cdot t$. So, if we say that something is 100 light years away we see it as it was 100 years ago.

Another important measure of distance is (cosmological) redshift, z. The relation between time, t, and redshift, z, is given in section A.2 and is also plotted in figure A.1. Astronomers and astrophysicists often mean distance when they speak about redshift, while cosmologists often mean time. In fact, the definition of redshift is:

$$z = \frac{\lambda_0 - \lambda_e}{\lambda_e}, \tag{A.1}$$

where λ_0 is the observed wavelength and λ_e is the emitted wavelength. The reason why $\lambda_0 \neq \lambda_e$ is the expansion of the universe – the light waves also expand and thus their wavelength increases. Consequently the redshift can also be expressed as $z + 1 = 1/R$, where R is the expansion of the universe. Note that light emitted nearby will not have been subject to any expansion of the universe and thus corresponds to $z = 0$.

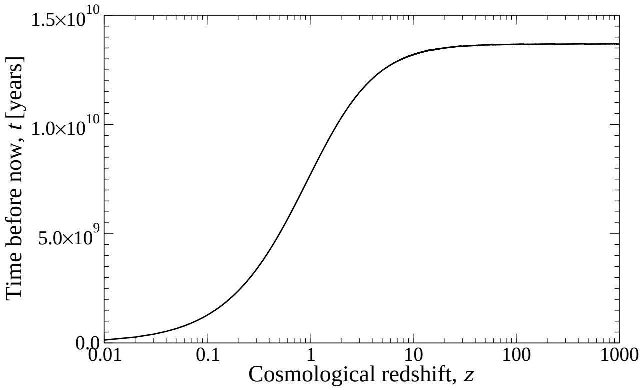

Figure A.1: Time versus redshift.

A.2 Cosmological equations

Relation between temperature, T, expansion of the universe R and time since the big bang, t:

Radiation dominated universe:

$$T \propto 1/R \propto 1/t^{1/2}. \tag{A.2}$$

Matter dominated universe:

$$T \propto 1/R \propto 1/t^{2/3}. \tag{A.3}$$

Evolution of matter and radiation density:

Matter density:

$$\rho_M \propto R^{-3}. \tag{A.4}$$

Radiation density:

$$\rho_R = \sigma T^4/c^2 \propto R^{-4}. \tag{A.5}$$

General:

Time/redshift (for $z < 1000$):

$$\frac{dz}{dt} = -H_0 \sqrt{(1+z)^2(1-\Omega_m+\Omega_m(1+z)^3)}. \tag{A.6}$$

Measured angles:

$$\frac{\pi}{\ell} \approx \theta[rad] = \frac{D_c}{L_c} = \frac{D_c}{c \cdot \int_{t_i}^{t_0}(1+z)dt} = \frac{D_c}{c\int_z^0 dz(1+z)\frac{dt}{dz}}, \tag{A.7}$$

where D_c denotes the co-moving distance and the other symbols are explained in appendix C.

Spectra:

Blackbody spectrum:

$$B_\nu = \frac{2h\nu^3}{c^2}(e^{h\nu/k_BT}-1)^{-1}. \tag{A.8}$$

Conversion $\nu \leftrightarrow \lambda$:

$$f(\nu)d\nu = f(\lambda)d\lambda, \quad \forall f. \tag{A.9}$$

Appendix B

Particle physics

B.1 The standard model of particle physics

The standard model (SM) of particle physics (Glashow 1961; Weinberg 1967; Salam 1968) is both one of the most successful theories of science and also one of the most frustrating. A theoretical prediction of the so-called anomalous magnetic dipole moment of the electron has been verified experimentally to more than 12 significant digits (Odom et al. 2006). This is unprecedented. At the same time, there are 29 ad hoc parameters in the model. There is also a beautiful unification of the electromagnetic and the weak force, but the force of gravity is not compatible.

In the SM there are twelve particles (six quarks and six leptons), five force carrying particles and the Higgs boson. The SM has withstood every test to which it has been submitted to, except one. The Higgs boson has not yet been detected. Groups at the Fermilab Tevatron accelerator search frenetically and when the Large Hadron Collider, which is scheduled to be turned on in 2008, the Higgs boson can not be missed. Eventually, it will be detected – if it exists.

The practical aim in particle physics is often to calculate the cross sections, life times and branching ratios for certain interactions in order to achieve a deeper understanding of the microcosmos.

B.2 Quantum field theory

Quantum field theory (QFT) is a quantum description of a field. It originated in the 1920s from the problem of creating a quantum mechanical theory of the electromagnetic field. QFT started with the Dirac equation (Dirac 1928), a single-particle equation obeying both relativity and quantum mechanics:

$$(\gamma^{\mu}\partial_{\mu} + im)\psi = 0. \tag{B.1}$$

Here

$$\gamma^0 = \begin{pmatrix} 1 & 0 & 0 & 0 \\ 0 & 1 & 0 & 0 \\ 0 & 0 & -1 & 0 \\ 0 & 0 & 0 & -1 \end{pmatrix}, \tag{B.2}$$

and

$$\gamma_i = \begin{pmatrix} 0 & \sigma_i \\ \sigma_i & 0 \end{pmatrix}, \tag{B.3}$$

where the Pauli matrices are given by

$$\sigma_i = \begin{pmatrix} 0 & 1 \\ 1 & 0 \end{pmatrix}, \begin{pmatrix} 0 & -i \\ i & 0 \end{pmatrix}, \begin{pmatrix} 1 & 0 \\ 0 & -1 \end{pmatrix}. \tag{B.4}$$

In the Dirac equation, $\gamma^\mu \partial_\mu$ corresponds to $\sqrt{E^2 - p^2}$, which in special relativity is the invariant mass, as is the case in the Dirac equation.

Adding a quantized electromagnetic field to this theory leads to the theory of quantum electrodynamics (QED). The Lagrangian of QED is

$$\mathcal{L} = i\bar{\psi}\gamma^\mu \partial_\mu \psi - e\bar{\psi}\gamma_\mu A^\mu \psi - m\bar{\psi}\psi - \frac{1}{4}F_{\mu\nu}F^{\mu\nu}, \tag{B.5}$$

where A^μ is the electromagnetic vector potential and $F_{\mu\nu} = \partial_\mu A_\nu - \partial_\nu A_\mu$ is the electromagnetic field tensor. The first and third terms are the same as in the Dirac equation above. The second term represents the coupling to the electromagnetic field and the fourth term the electromagnetic self-coupling.

The actual calculations of cross sections are made using perturbation theory, which have a simple pictorial representation as Feynman diagrams. In these diagrams, points where lines connect to other lines are called interaction vertices, or vertices for short. There are three types of lines: incoming, internal and external. Incoming lines represent the initial (noninteracting) state, outgoing lines the final (noninteracting) state and internal lines connect two vertices. The probability of each final state of an interaction is obtained by summing over all possible Feynman diagrams.

For a treatment of QFT, see the book by Peskin and Schroeder (1995).

B.3 Electroweak interactions

The electroweak theory is the part of the SM that treats the electromagnetic force and the weak force. There are three basic types of weak interaction vertices. Quarks and leptons can emit or absorb a *Z* boson. This is called a neutral current. A charged lepton can also emit or absorb a *W* boson and convert into a corresponding neutrino. A quark with charge -1/3 can emit or absorb a W boson and convert into a superposition of charge +2/3 quarks and conversely, a quark with charge +2/3 can emit or absorb a *W* boson and convert into a superposition of charge -1/3 quarks. The interactions involving the *W* boson are called charged current interactions.

The Lagrangian of the electroweak interaction has four parts:

$$\mathcal{L} = \mathcal{L}_i + \mathcal{L}_k + \mathcal{L}_H + \mathcal{L}_Y. \tag{B.6}$$

The first term, $\mathcal{L}_i$, is the electroweak interaction term corresponding to $-\frac{1}{4}F_{\mu\nu}F^{\mu\nu}$ above. The second term is the kinetic term corresponding to $i\bar{\psi}\gamma^\mu \partial_\mu \psi - e\bar{\psi}\gamma_\mu A^\mu \psi - m\bar{\psi}\psi$ above. The third term accounts for the Higgs particle and the fourth term is the Yukawa coupling, which couples the particle of interest to the Higgs particle.

B.4 Heavy neutrinos

There are two normal types of heavy neutrinos, Majorana and Dirac. A Majorana neutrino is its own antiparticle. A Dirac neutrino, on the other hand exists both as particle and antiparticle, N and $\bar{N}$.

The heavy neutrinos can annihilate into various other particles through Z^0 exchange. For $M_N \ll M_Z$, the (virtual) Z^0 then decays into two fermions, $f\bar{f}$, and the total cross sections for these processes are (Kolb and Turner 1990)

$$\langle \sigma_A |a| \rangle = \frac{G_F^2 m_N^2}{2\pi} \sum_{f \in \{m_f < m_N\}} \sqrt{1 - (m_f/m_N)^2} (C_{V_f}^2 + C_{A_f}^2)(1 + (m_f/m_N)^2/2) \tag{B.7}$$

for a Dirac neutrino, and

$$\langle \sigma_A |a| \rangle = \frac{G_F^2 m_N^2}{2\pi} \sum_{f \in \{m_f < m_N\}} \sqrt{1 - (m_f/m_N)^2} \left[(C_{V_f}^2 + C_{A_f}^2) 8\beta_f^2/3 + C_{A_i}^2 2(m_f/m_N)^2 \right] \tag{B.8}$$

for a *Majorana* neutrino. Here $G_F = 1.166 \times 10^{-5}$ GeV^{-2} is the Fermi constant, β_f is the relative velocity of fermion f and C_V and C_A are the neutral vector and axial vector couplings given in terms of the weak isospin, I_3, and the electric charge q of fermion f: $C_A = I_3$ and $C_V = I_3 - 2q \sin^2 \theta_W$, where $\theta_W \approx 0.24$ is the Weinberg angle.

For neutrinos heavier than Z^0 the expressions for the cross sections are more complicated, and the possibilities will only be outlined here: $\sigma_Z(N\bar{N} \to f\bar{f})$, $\sigma_H(N\bar{N} \to f\bar{f})$, $\sigma(N\bar{N} \to H^0\bar{H}^0)$ and $\sigma(N\bar{N} \to W^+\bar{W}^-)$. The index on σ denotes the interaction channel (H for Higgs particle and Z for the Z^0 boson). The complete expressions (for Dirac neutrinos) can be found in Enqvist et al. (1989).

Appendix C

Explanations

C.1 Glossary

For further descriptions of astronomical terms, the interested reader is referred to http://factguru.com/.

Acoustic oscillations The oscillations due to density variations in the photon-baryon fluid prior to decoupling.

Antimatter Antimatter is constituted of *antiparticles*.

Antiparticle An antiparticle is defined as having the opposite *quantum numbers* of the corresponding particle, while it has the same mass.

Boson A particle with an integer-valued spin, in contrast to fermions, which have half-integer spin. A photon is a boson, as are the other force carrying particles. Bosons obey Bose-Einstein statistics, named after the Indian physicist Satyendra Nath Bose and Albert Einstein.

Baryonic matter “Ordinary matter” consisting of baryons, i. e., protons and neutrons.

Big bang The origin of the universe some 14 billion (= 10^9) years ago - see section 2.1.

Bremsstrahlung Radiation emitted due to acceleration of charged particles.

CMB Cosmic microwave background. The fossil radiation left from the *decoupling* of radiation from matter, ~ 400,000 years after the *big bang*. The CMB radiation has a blackbody spectrum with a temperature of $T_{CMB} = 2.725 \pm 0.002$ K (Mather et al. 1999).

Dark energy Dark energy constitutes $\sim 70\%$ of the total energy content of the universe today but the exact nature of dark energy is unknown. It has a negative pressure and is represented by the Λ-term in the Einstein equations (3.5).

Dark matter Exotic dark matter is believed to constitute $\sim 25\%$ of the total energy of the universe. Ordinary (*baryonic*) matter only constitutes $\sim 5\%$ of the total energy of the universe. The domination of dark matter is inferred from the rotations of galaxies and the evolution of large scale structures (e. g., galaxy clusters) in the universe. Note, however, that ordinary matter invisible to us is also dark matter. It is still an unsettled question what dark matter actually is. For more information, see section 5.2.

Decoupling When the interaction rate of a particle is slower than the expansion of the universe, $\Gamma \lesssim H$. For a more detailed treatment, see section 3.5.

Decoupling (of photons) When there was not enough thermal energy to excite hydrogen, the energy of the photons did not change anymore and they continued virtually unhindered.

Dirac (particle) It has a distinct antiparticle, contrary to Majorana particles, which are identical to their antiparticles.

Early ISW effect This is due to the fact that the photons contribute to the gravitational potential. Since the photon energy decreases with time, this induces an integrated Sachs-Wolf effect.

Equilibrium, chemical The chemical activities or concentrations of the reactants and products have no net change over time.

Equilibrium, local kinetic In this case only the gas particle velocities are given by thermodynamic equilibrium.

Equilibrium, local thermodynamic In this case the excitation and ionization of the gas as well as the particle velocities are all the same as in thermodynamic equilibrium, but the radiation field is not.

Equilibrium, radiative The amount of energy radiated by a volume is the same as the amount absorbed.

Equilibrium, thermodynamic With this kind of equilibrium in a volume all parameters including all aspects of the radiation field are those given by the laws of thermodynamics.

Fermions Particle with a half-integer spin, in contrast to bosons, which have integer spin. Examples of fermions: electrons, protons, quarks and neutrinos. Fermions obey Fermi-Dirac statistics, named after the Italian physicist Enrico Fermi and the Brittish physicist Paul Dirac.

Foregrounds Other signals that (partly) hide the primordial CMB. Examples: Our galaxy and point sources like nearby planets and distant galaxies and dust, cf section 4.3.

GalICS A computer program, developed at the Centre de Recherche Astronomique de Lyon, used to simulate dark matter and the evolution of galaxies and their spectra.

Heavy neutrino Hypothetical neutrino with a substantial mass, higher than half the Z^0 mass. It appears in models with more than three generations (or families) of leptons. Some models predict several different heavy neutrinos.

Higgs boson The particle in the standard model of particle physics that gives mass to the other particles. It has not yet been found, see appendix B.

Integrated Sachs-Wolf effect (ISW) When a gravity potential changes over time. See section 4.2.

Late ISW effect This comes from the dark energy term that will become more and more important as time passes. This increase in energy also leads to an integrated Sachs-Wolf effect.

Majorana (particle) It is its own antiparticle (Majorana 1937) contrary to a Dirac particle, which has a distinct antiparticle.

Metallicity The mass proportion of elements heavier than helium, denoted Z. The sun has a metallicity of $Z_\odot \approx 0.02$ (Schaller et al. 1992).

Monte Carlo A Monte Carlo method is a computational algorithm that relies on repeated random sampling.

Optical depth, τ The probability of a photon passing through a medium without scattering is $e^{-\tau}$.

Planck A satellite that will be launched in 2008, planned to measure the CMB over the entire sky with unprecedented precision. It is named after the German physicist Max Planck.

Population III stars The first generation of stars with extremely low *metallicity* and probably a high mass and a short life.

Power spectrum A plot of the angular correlations of the measured CMB, cf section 4.4.

Preon Name of hypothetical constituents of leptons and quarks. Preon stands for “pre-quark”, sometimes also called “subquark”. There are many different, more or less detailed, preon models on the market.

Quantum numbers The numbers, which can be said to best describe the state of a particle. Examples: electric charge (Q), lepton number (L), baryon number (B), parity (P), spin (S), isospin (I), strangeness (S), and charge conjugation (C).

Quasar Extremely distant and luminous astronomical objects, which are much smaller than a galaxy and much more luminous. They are very young and very active galactic nuclei, most probably centered around a gigantic black hole.

Redshift, z Used to measure distance from us to a distant light-source, far outside our own galaxy. Equivalently, redshift measures time from now and backwards. Today the nearby universe has $z = 0$. A billion years ago correspond to $z \sim 0.1$, ten billion years ago to $z \sim 2$, and thirteen billion years ago to $z \sim 8$. The redshift is due to the expansion of the universe. Contrary to popular belief, this is not a doppler shift. Most galaxies move away from us, but this is not caused by their redshifts. Instead, as a light wave travels through the fabric of space, the universe expands and the light wave gets stretched and therefore redshifted. See also appendix A.

Reionization This happened when the first generation of stars formed, emitting high energy photons capable of ionizing the hydrogen and helium gas. The reionization lasted for some five billion years.

Sachs-Wolf effect When a photon has to climb out of a gravitational well and thereby gets redshifted.

Silk damping Damping of density perturbations up to $10^{11} M_\odot$ prior to *decoupling*, due to photon diffusion.

Sputtering Bombarding a target material with energetic (charged) atoms, which release atoms from the target, thus eroding it.

Sublimation The change of a solid substance directly into a vapor without first passing through the liquid state.

Sunyaev-Zel’dovich effect When an electron hits a photon and changes its energy. See section 4.2.

Supernova A gigantic stellar explosion in which the luminosity of the star suddenly increases as much as a billion times. Most of its substance is blown off, leaving behind at least in some cases, an extremely dense core, which may become a neutron star.

C.2 Abbreviations

BBN	Big Bang Nucleosynthesis
CDM	Cold Dark Matter
CMB	Cosmic Microwave Background
DM	Dark Matter
GalICS	Galaxies In Cosmological Simulations
HDM	Hot Dark Matter
IGM	InterGalactic Medium
ISM	InterStellar Medium
ISW	Integrated Sachs-Wolf effect
PAH	Polycyclic Aromatic Hydrocarbon
SM	Standard Model of particle physics
SN	SuperNova
SZ	Sunyaev-Zel'dovich effect
WMAP	Wilkinson's Microwave Anisotropy Probe

C.3 List of variables

$a_{\ell m}$	Component of $Y_{\ell m}$.
a	The expansion of the universe is $\propto a$, see z.
$B(\hat{r}, \nu)$	Measured intensity in W/m^2 in direction $\hat{r}$.
$B_X = B_X(\hat{r}, \nu)$	Intensity of component X.
C_ℓ	Angular correlation on scale ℓ.
$\Delta\Phi$	Gravitational potential excess over background.
ΔT_X	Anisotropy for component X.
E_γ	Energy of photons.
f_d	Fraction of baryons in stars the end up as dust.
$g_{\mu\nu}$	Metric of the space-time.
g_*	Number of relativistic degrees of freedom.
g_s	Number of internal degrees of freedom.
H	The Hubble parameter.
I	Intensity
ℓ	Inverse angle scale, $\theta \approx 180^\circ/\ell$.
λ	Wavelength.
M_N	Mass of heavy neutrino in GeV.
n_γ	Number density of photons.
n_p	Number density of protons.
Ω_X	Relative density of X in comparison the the critical density.
$\vec{r}$	Spatial coordinate vector.
ρ_c	Critical energy density of the universe.
ρ_k	Equivalent curvature density.
ρ_Λ	Equivalent vacuum energy density.
ρ_m	Matter density.
ρ_r	Radiation density.
s	Entropy.
σ	Cross section.

$\sqrt{\langle \Delta T(\nu)^2 \rangle}$	Root mean square of temperature differences.
θ	Angle on the sky.
t	Time in seconds.
T	Temperature in Kelvin.
$T_{\mu\nu}$	Stress-energy tensor.
$\vec{v}$	Velocity vector.
ν	Frequency in Hz.
$Y_{\ell m}(\theta, \phi)$	Basis functions of angular orbital momentum, called spherical harmonics.
z	The *redshift*, which is dimensionless, is often used to describe time or length through the intermediary of the expansion of the universe R. See also figure A.1.
z_i	Redshift of the reionization.

C.4 List of some cosmological constants

h_0	0.72±0.03	Hubble's relative constant (Spergel et al. 2003).
$H_0 = 100 \cdot h_0 \frac{\text{km/s}}{\text{Mpc}}$	2.33×10^{-18} s^{-1}	Hubble's constant.
$\rho_c = \frac{3H_0^2}{8\pi G}$	$(0.97 \pm 0.04) \times 10^{-26}$ kg/m^3	Critical density of the universe.
$\Omega_{tot} = \rho_{tot}/\rho_c$	1.02 ± 0.02	Total relative energy content of the universe (Spergel et al. 2003).
$\Omega_m = \rho_m/\rho_c$	$(0.133 \pm 0.006)/h^2$	Relative matter content of the universe (Spergel et al. 2003).
$\Omega_b = \rho_b/\rho_c$	$(0.0226 \pm 0.0008)/h^2$	Relative baryon content of the universe (Spergel et al. 2003).
$M_\odot$	1.99×10^{30} kg	Mass of the sun.

C.5 List of some physical constants and units

The values of these constants are cited from (Mohr and Taylor 2000):

c	299,792,458 m/s	Speed of light in vacuum, from Latin "celeritas" = speed.
G	$6.6742(10) \times 10^{-11}$ m^{3}kg^{-1}s^{-2}	Newton's constant of gravitation.
k_B	$1.3806505 \times 10^{-23}$ J/K	Boltzmann's constant.
$\hbar$	$1.05457168(18) \times 10^{-34}$ Js	The reduced Planck constant (Dirac's constant).

1 erg	10^{-7} J	Unit energy in the cgs (centimeter-gram-second) system of units, frequently used in astronomy.
1 eV	$1.60217653(14) \times 10^{-19}$ J	Electron volt, energy.
1 pc	$3.0856775807(4) \times 10^{16}$ m	A parsec is defined as the distance from the sun that would result in a parallax of 1 second of arc as seen from the earth.

Paper I

Dust from reionization

The production of dust in the early universe is estimated from the number of stars needed to achieve reionization. The spectral signature of the dust is calculated and compared to measurements. The contribution from the dust layer to the Cosmic microwave background is found to be small.

Elfgren, Erik and Désert, François-Xavier
Astronomy and Astrophysics 425, 9-14, 2004
(astro-ph/0310135)

A&A 425, 9–14 (2004)
DOI: 10.1051/0004-6361:20034448
© ESO 2004

Astronomy & Astrophysics

Dust from reionization

E. Elfgren[1] and F.-X. Désert[2]

[1] Department of Physics, Luleå University of Technology, 971 87 Luleå, Sweden
e-mail: `elf@ludd.luth.se`
[2] Laboratoire d'Astrophysique, Observatoire de Grenoble, BP 53, 414 rue de la piscine, 38041 Grenoble Cedex 9, France

Received 6 October 2003 / Accepted 13 May 2004

Abstract. The possibility that population III stars have reionized the Universe at redshifts greater than 6 has recently gained momentum with WMAP polarization results. Here we analyse the role of early dust produced by these stars and ejected into the intergalactic medium. We show that this dust, heated by the radiation from the same population III stars, produces a submillimetre excess. The electromagnetic spectrum of this excess could account for a significant fraction of the FIRAS (Far Infrared Absolute Spectrophotometer) cosmic far infrared background above 700 micron. This spectrum, a primary anisotropy (ΔT) spectrum times the ν^2 dust emissivity law, peaking in the submillimetre domain around 750 micron, is generic and does not depend on other detailed dust properties. Arcminute–scale anisotropies, coming from inhomogeneities in this early dust, could be detected by future submillimetre experiments such as Planck HFI.

Key words. cosmology: cosmic microwave background – cosmology: early Universe

1. Introduction

More accurate measurements of the cosmic microwave background (CMB) implies a need for a better understanding of the different foregrounds. We study the impact of dust in the very early universe $5 < z < 15$. WMAP data on the CMB polarization, Kogut et al. (2003) provides a strong evidence for a rather large Thomson opacity during the reionization of the Universe: $\tau_e = 0.17 \pm 0.04$ (68% *C.L.*). Although the mechanism of producing such an opacity is not fully understood, Cen (2002, 2003) has shown that early, massive population-III (Pop III) stars could ionize the Universe within $5 < z < 15$ (see Figs. 1 and 2). Adopting this hypothesis, we discuss the role and observability of the dust that is produced by the Pop III stars. As we can only conjecture about the physical properties and the abundance of this early dust, we adopt a simple dust grain model with parameters deduced from the Milky Way situation. The dust production is simply linked to the ionizing photon production by the stars through their thermal nuclear reactions. The low potential well of the small pre-galactic halos allows the ejected dust to be widely spread in the intergalactic medium. The ionizing and visible photons from the same Pop III stars heat this dust. There are no direct measurements of this dust, but by means of other results the amount of dust can be estimated. A similar study has been done for a later epoch of the universe, in which data are more readily available, Pei et al. (1999). We use a cosmology with $\Omega_{\rm tot} = \Omega_{\rm m} + \Omega_\Lambda = 1$, where $\Omega_{\rm m} = \Omega_{\rm b} + \Omega_{\rm DM} = 0.133/h^2$, $\Omega_{\rm b} = 0.0226/h^2$ and $h = 0.72$ as advocated by WMAP, Spergel et al. (2003), using WMAP data in combination with large scale structure observations (2dFGRS + Lyman α). Furthermore, since $z \gg 1$ the universe is matter-dominated. We relate all cosmological parameters to their measurement today so that they have their present-day values throughout our calculations.

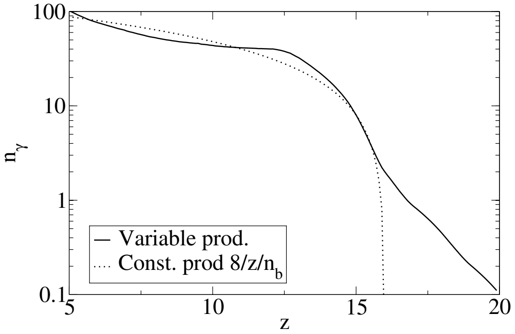

Fig. 1. Total number of ionizing photons produced from Pop III stars per baryon, cf. (Cen 2002, Fig. 14). The dotted line represents a simplified model with a constant photon production, from $z = 16$, of 8 per unit z per baryon. The results are similar.

We now proceed to compute the abundance and the temperature of this dust. Consequences on the CMB distortions are then to be discussed.

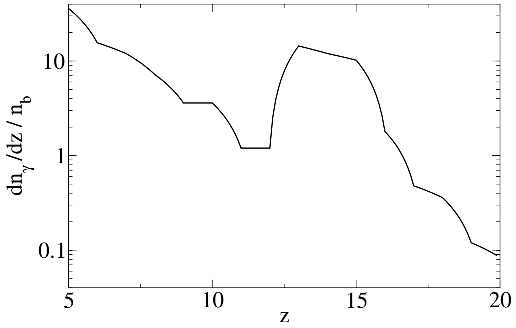

Fig. 2. Production rate of ionizing photons from Pop III stars per baryon, $\frac{dn_\gamma}{dz}/n_b$. The odd form between each integer z is not physical but are due to the fact that the redshift z is a nonlinear function of time.

2. Dust model

Here we assume the dust properties to be similar to what is observed in our galaxy. For simplicity, we suppose spherical dust grains with radius $a = 0.1\ \mu$m and density $\rho_g = 2.3 \times 10^3$ kg/m^3. The absorption cross section, σ_ν, between photons and dust can be written as

$$\sigma_\nu = Q_\nu \pi a^2, \tag{1}$$

where we parametrize the frequency dependency as

$$Q_\nu = \begin{cases} Q_0 \frac{a}{a_r} \left(\frac{\nu}{\nu_r}\right)^{\beta_\nu} & \text{submm and infra red (IR),} \\ 1 & \text{visible and ultra violet (UV),} \end{cases} \tag{2}$$

where ν_r, a_r and Q_0 are normalization constants. There is only one independent constant which means that we can fix $a_r = 0.1\,\mu$m. In (Desert et al. 1990, Fig. 3) the poorly known knee wavelength, $\lambda_r = c/\nu_r$ was set to 100 μm. Here, we choose 40 μm for simplicity, so that early dust radiates mostly in the ν^2 emissivity regime. Above the characteristic frequency ν_r the spectral index $\beta = 1$, below $\beta = 2$. The exact position of ν_r is not very important for our study because it is mainly above the interesting wave-length region ~0.3−3 mm and it will not change the magnitude of the signal.

In the submm and far IR range, the spectral index is constant, and with $Q_0 = 0.0088$ the assumed opacity agrees well with measurements by FIRAS on cirrus clouds in our galaxy, cf. Boulanger et al. (1996); Fixsen et al. (1998); Lagache et al. (1999). In the visible and UV region, the cross section is independent of the frequency because $\lambda < 2\pi a$. In the submm region, the cross section is proportional to the mass of the grain.

In order to evaluate the significance of the dust during the reionization, we calculate the amount of dust present in the universe at a given time. The co-moving relative dust density is $\Omega_{d,0} = \rho_d(z)/((1+z)^3\rho_c)$, where $\rho_d(z)$ is the dust density, z is the red-shift, $\rho_c = \frac{3H_0^2}{8\pi G}$ is the critical density (H_0 and G are Hubble's and Newton's constants, respectively). The co-moving relative dust density as measured today evolves as:

$$\frac{d\Omega_{d,0}}{dz} = J_+ - J_-, \tag{3}$$

where J_+ and J_- are the production and the destruction rate respectively.

The Pop III stars produce enough photons for the reionization while burning H and thus forming metals (Li and higher). These metals are released in supernovae explosions at the end of the stars short lives (~1 Myr), whereafter they clump together to form dust, Nozawa et al. (2003). Knowing the production rate of ionizing photons to be $\frac{dn_\gamma}{dz}/n_b$ (Fig. 2), we can calculate the total photon energy released from the Pop III stars. This can be done by supposing that each photon has an effective energy of $E_\gamma = c_\gamma \int_{\nu_{\rm ion}}^{\infty} d\nu\, h\nu B_\nu(T_*)/ \int_{\nu_{\rm ion}}^{\infty} d\nu\, B_\nu(T_*)$, where $h\nu_{\rm ion} =$ 13.6 eV and $B_\nu(T_*)$ is the spectrum of a star with temperature T_*. The energy of the non-ionizing photons is included through $c_\gamma = u_{\rm tot}/u_{\nu>\nu_{\rm ion}}$ (u is the energy from the star). A Pop III star has $T_* \sim 80\,000$ K (Shioya et al. 2002, p. 9) which gives $E_\gamma \approx 36$ eV. Note that for other reasonable star temperatures, E_γ does not vary significantly, $E_\gamma|_{60\times10^3\ \rm K} \approx 36$ eV and $E_\gamma|_{100\times10^3\ \rm K} \approx 40$ eV. Hence, the total Pop III photon energy production is $E_\gamma \frac{dn_\gamma}{dz}/n_b$ per baryon per unit z. For each consumed nucleon, we assume that a nuclear energy of $E_r =$ 7 MeV is released as radiation, which means that the nucleon consumption rate is $\frac{E_\gamma}{E_r}\frac{dn_\gamma}{dz}/n_b$ nucleons per baryon per unit z. If f_d is the fraction of the consumed baryon mass that becomes interstellar dust, (some of the metal atoms will remain with the core after the SN explosion, some will stay in the close vicinity of the SN and some will never clump together to form dust) the co-moving dust production rate will be

$$J_+ = f_d \frac{E_\gamma}{E_r} \Omega_b \frac{dn_\gamma}{dz}/n_b. \tag{4}$$

A dust grain will eventually be destroyed, e.g. by collision, by supernova shockwaves or by cosmic rays, see Draine & Salpeter (1979) for further discussion. If a dust grain has a lifetime of Δt we can write the dust destruction rate as

$$J_- = \frac{\Omega_{d,0}(z)}{\Delta t}\frac{dt}{dz} \approx -\frac{\Omega_{d,0}(z)}{\Delta t H_0 \Omega_m^{1/2}(1+z)^{5/2}}, \tag{5}$$

where Ω_m is the relative matter content today, because the universe is matter dominated for $5 < z < 15$.

Solving Eq. (3) gives the dust density evolution

$$\Omega_{d,0}(z) = \int_z^{z_i} J_+(z')\frac{Y(z')}{Y(z)}dz', \tag{6}$$

where $z_i = 20$ is the beginning of the dust formation (see Fig. 1) and

$$Y(z) = \exp\left(\frac{2}{3}\frac{(1+z)^{-3/2}}{\Omega_m^{1/2}\Delta t H_0}\right). \tag{7}$$

We note that the source term J_+ is modulated by the destruction term $\frac{Y(z')}{Y(z)}$. The dust density is plotted in Fig. 3 where we note a strong dependency on the dust lifetime. In local dust $\Delta t \sim$ 100 Myr, Draine & Salpeter (1979). However, the uncertainty is rather large, according to Draine (1990), $\Delta t = 30$ Myr−10 Gyr, depending on the environment. Note, however, that the density at the reionization red-shifts is much lower than in the interstellar medium in the Milky Way which implies a rather long dust life-time.

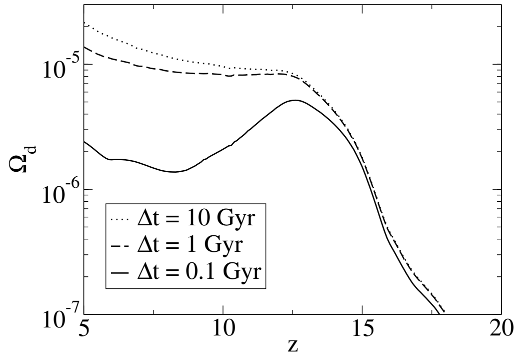

Fig. 3. The co-moving relative dust density evolution $\Omega_{d,0} = \rho_{dust}/\rho_c$, for $f_d = 1$. The minima at $z = 6$ and 9 for $\Delta t \leq 0.1$ Gyr is due to the fact that $\Delta z = 1$ is not a constant time interval.

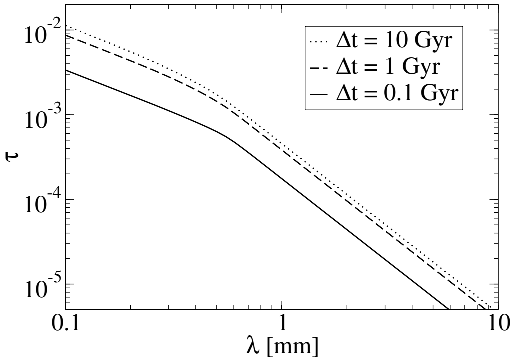

Fig. 4. Opacity τ with dust evolution taken into account.

3. Results and discussion

3.1. Metallicity

If we suppose that most of the metals were ejected as dust (not as gas) the metallicity comes from the dust grains. The metallicity is directly obtained through the produced dust. By letting $\Delta t \to \infty$ ($\Delta t = 10$ Gyr is good enough) we find the metallicity:

$$\frac{Z}{Z_\odot} = \frac{\Omega_{d,0}(\Delta t \to \infty)}{0.02 \cdot \Omega_b} \approx 1147 \cdot \Omega_{d,0}(\Delta t \to \infty) \tag{8}$$

or in absolute terms $Z \approx 22.9\Omega_{d,0}$. At $z = 5$ we have $\Omega_{d,0} = 2.3 \times 10^{-5} f_d$, which gives $Z \approx 5.2 \times 10^{-4} f_d = 0.026 f_d Z_\odot$.

There are not much metallicity data available for $z > 5$. Metal poor stars in our galaxy are one point of reference, absorption lines in the Lyα spectrum from quasars are another one. The lowest metallicities found in stars in the Milky Way are $Z/Z_\odot \sim 0.01$, Depagne et al. (2002). The Lyα forest suggests (Songaila & Cowie 2002, Fig. 13) that $Z/Z_\odot \sim 0.003$ for $z \sim 4.5$ assuming that [Fe/H] $\approx \log(Z/Z_\odot)$ as suggested by (VandenBerg et al. 2000, page 432). This indicates that $f_d \sim 0.1$. However, this might be lower than the actual value, cf. (Pettini et al. 1997, Fig. 4).

In heavy stars, virtually all the helium is consumed, producing metals. For simplicity (and lack of data), we assume that all the ejected metals clump to form dust, $f_d \approx f_{eject}$. This means that f_d will almost entirely depend on the dust ejection rate in the supernova explosion. In Iwamoto et al. (1998) a detected hypernova of mass $M \sim 14\ M_\odot$ seems to have $f_{eject} \gtrsim 0.7$. Furthermore, according to a dust production model by Nozawa et al. (2003), $f_d \approx 0.2$–0.3. At the same time, some of the stars will become black holes, not ejecting any metals, Heger & Woosley (2002), decreasing f_d. Currently this decrease is largely unknown.

In summary, the mass fraction of the produced metals in the Pop III stars, having become interstellar dust, should be around $f_d \sim 0.1$–0.3. In the following we use the more conservative $f_d = 0.1$, in agreement with the Lyα forest measurements, unless otherwise stated.

3.2. Dust opacity

With our model for the dust density evolution, we want to calculate the opacity of the dust, as seen by the CMB. This will tell us how much the CMB spectrum is altered by the passage through the dust.

The dust opacity is given by

$$\tau_\nu = c \int dz \frac{dt}{dz} \sigma_{\nu_e} n_d(z) \tag{9}$$

$$= \frac{Q_0 c}{\sqrt{\Omega_m} a_r H_0} \frac{3}{4} \frac{\rho_c}{\rho_g} \int dz \left(\frac{\nu}{\nu_r}\right)^{\beta_{\nu_e}} \Omega_{d,0}(z)(1+z)^{1/2+\beta_{\nu_e}}, \tag{10}$$

where ν (ν_e) is the observed (emitted) frequency and $\nu = \nu_e/(1+z)$. The dust number density is $n_d(z) = (1+z)^3 \times \rho_c \Omega_{d,0}(z)/m_g$ where $m_g = \frac{4\pi a^3}{3}\rho_g$ is the grain mass. We see (from $\tau \propto \Omega_{d,0}$) that τ is proportional to the parameter f_d.

The resulting opacity can be seen in Fig. 4. We note that the opacity is small, $\tau \ll 1$. The smooth knee is due to the change of β at the redshifted ν_r, see Sect. 2, but this is not in the spectral range of the CMB. The differential opacity $d\tau/dz$ is plotted in Fig. 5 for $\lambda = 1$ mm. We see that with a short dust lifetime, the dust differential opacity falls off almost immediately (in terms of z). However, for longer lifetimes, the early dust could still play a certain role for $z < 3$. This could eventually contribute to dimming of distant objects. We also note the impact of the expansion of the universe in decreasing the dust density and thus the opacity. This is why the increase in Fig. 1, at $z \sim 5$, is not apparent in the opacity, Fig. 4. Furthermore, the submillimetre effective dust opacity follows a ν^2 emissivity law.

3.3. Dust temperature

In order to deduce the equilibrium temperature of the dust, we write the balance between the absorbed CMB, the absorbed starlight and the emitted IR light from the dust:

$$P_d = P_* + P_{CMB}. \tag{11}$$

The powers P_d and P_{CMB} can be written as

$$P_X = 4\pi \int_0^\infty d\nu_e\, \sigma_{\nu_e} B_{\nu_e}(T_X), \tag{12}$$

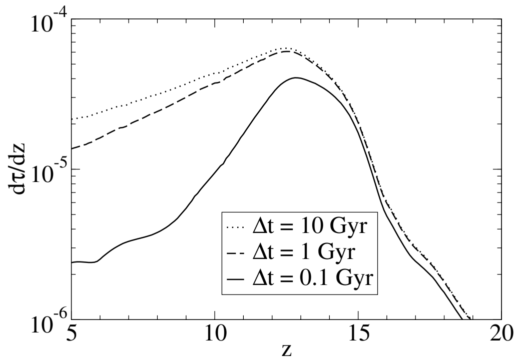

Fig. 5. The differential opacity $d\tau/dz$ at $\lambda = 1$ mm for different dust lifetimes.

where B_ν is a Planck blackbody spectrum and $X = \{\mathrm{CMB}, \mathrm{d}\}$. In the wave-length range considered, the spectral index $\beta = 2$. Supposing that β is constant, Eq. (11) can be solved for the dust temperature analytically in the submm range:

$$T_{\mathrm{d}}^{4+\beta} = T_{*\mathrm{eff}}^{4+\beta} + T_{\mathrm{CMB}}^{4+\beta}, \tag{13}$$

where the effective temperature is defined by

$$T_{*\mathrm{eff}}^{4+\beta} = \frac{P_*}{8\pi^2 hc^{-2}(Q_0 \cdot (a^3/a_r)\nu_r^{-\beta})(k_{\mathrm{B}}/h)^{4+\beta} C_\beta} \tag{14}$$

and $C_\beta = \int_0^\infty \mathrm{d}x x^{3+\beta}/(\mathrm{e}^x - 1) = (\beta + 3)! \sum_{k=1}^\infty k^{-(4+\beta)}$, such that $C_0 \approx 6.494$, $C_1 \approx 24.89$ and $C_2 \approx 122.1$.

However, in our calculations we use the exact Eqs. (11) and (12), while Eq. (14) can be used as a cross-check.

The absorbed power density, P_* from the radiation of Pop III stars peaks in the UV-region and can be approximated by

$$P_* = \sigma_{\mathrm{UV}} u_*(z) c, \tag{15}$$

where σ_{UV} is the dust-photon cross section in the UV region and the energy density is

$$u_*(z) = f_{\mathrm{esc}} \int_{z_i}^{z} \mathrm{d}z' \frac{\mathrm{d}n_\gamma}{\mathrm{d}z'} E_\gamma \left(\frac{1+z}{1+z'}\right)^4, \tag{16}$$

where f_{esc} is the escape fraction of photons from the star halos. We neglect the loss of photons due to the reionization itself. $E_\gamma \frac{1+z}{1+z'}$ is the effective energy of the photon emitted at z' and then redshifted to z. According to Cen (2003), $f_{\mathrm{esc}} = 0.3$ gives an electron opacity $\tau_{\mathrm{e}} \approx 0.13$ which is within one standard deviation of the results by WMAP. Hereafter, we adopt this value of f_{esc}.

The energy density of the ionizing photons are compared to the CMB in Fig. 6. The star energy density is much less than the CMB energy density at this epoch, and the curve resembles the accumulated photons in Fig. 1. Hence, the dust temperature closely follows the CMB temperature, see Fig. 7 and Eq. (12).

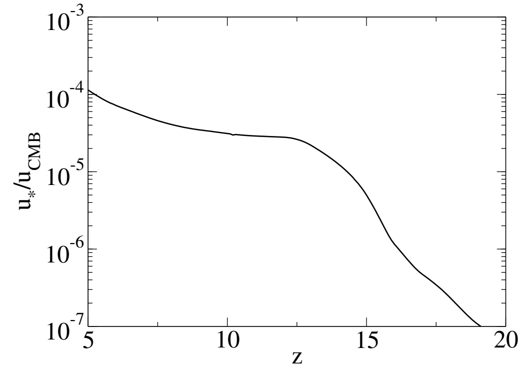

Fig. 6. Energy density of ionizing photons compared to $u_{\mathrm{CMB}} = 4\sigma_{\mathrm{S}} T_{\mathrm{CMB}}^4/c$, where σ_{S} is Stefan-Boltzmann's constant.

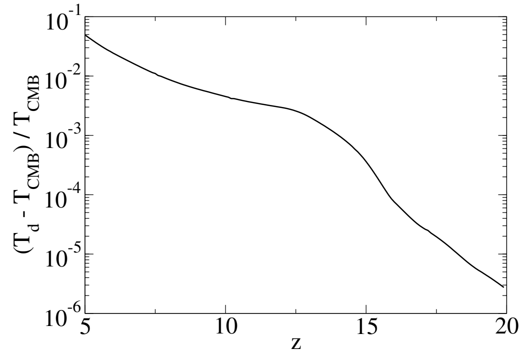

Fig. 7. The dust temperature is plotted against the CMB temperature with the relative quatity $(T_{\mathrm{d}} - T_{\mathrm{CMB}})/T_{\mathrm{CMB}}$.

3.4. Observed intensity

Now we proceed to compute the average intensity (monopole term) of the submm and microwave background which is made of the CMB and early dust emission. The simple radiative transfer of the CMB through the uniform dust screen yields the following observed intensity:

$$i_\nu = \mathrm{e}^{-\tau_\nu}\left[B_\nu(T_{\mathrm{CMB}}) + \int_0^{\tau_\nu} \mathrm{e}^{\tau_{\mathrm{e}}} \frac{B_{\nu_{\mathrm{e}}}(T_{\mathrm{d}}(z))}{(1+z)^3}\,\mathrm{d}\tau_{\mathrm{e}}\right]. \tag{17}$$

From Figs. 4 and 7, we see that the opacity is small, ($\tau \ll 1$) and the dust temperature is only slightly higher than the CMB temperature ($T_{\mathrm{d}} \gtrsim T_{\mathrm{CMB}}$). This gives the following formula for the excess intensity relative to the unperturbed CMB:

$$\begin{aligned}\Delta i_\nu &\equiv i_\nu - B_\nu(T_{\mathrm{CMB}}) \\ &\approx T_{\mathrm{CMB}} \left.\frac{\mathrm{d}B_\nu}{\mathrm{d}T}\right|_{T=T_{\mathrm{CMB}}} \int_0^{\tau_\nu} \frac{T_{\mathrm{d}}(z) - T_{\mathrm{CMB}}(z)}{T_{\mathrm{CMB}}(z)}\mathrm{d}\tau_{\mathrm{e}},\end{aligned} \tag{18}$$

where T_{CMB} is the CMB temperature today. The integrant is plotted in Fig. 7. We note that a new component is added to the primary CMB spectrum. Equation (18) tells us that it has a

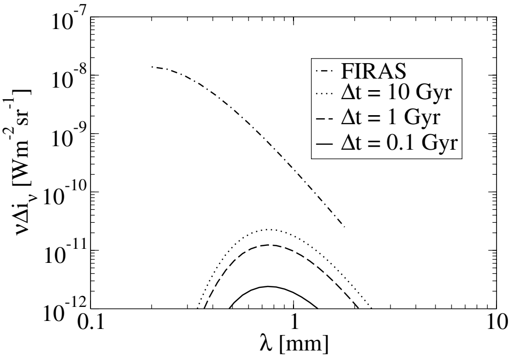

Fig. 8. Comparison of the modeled intensity for the early dust emission in excess of the CMB with the observed FIRAS spectrum (dashed red curve) of the cosmic far IR background as detailed by Lagache et al. (1999).

specific spectrum which is the product of a 2.725 K blackbody temperature fluctuation spectrum (like primary anisotropies) and a ν^2 power law (from $d\tau_e$). This effect is mostly visible in the submm range and has a minor contribution in the radio domain.

In Fig. 8, the excess intensity is plotted along with the extragalactic background measured by FIRAS, Puget et al. (1996); Fixsen et al. (1998); Lagache et al. (1999). Depending on the dust destruction rate (parametrized by the dust lifetime Δt), the computed early dust background can be an important part of the observed background from 400 μm up to the mm wave-length. The exact position of λ_r will only slightly displace the spectrum, leaving the magnitude unchanged. Most of the far IR background can now be explained by a population of $z = 0$ to $z = 3$ luminous IR galaxies, Gispert et al. (2000). A fraction of the submillimetre part of this background could arise from larger redshift dust emission as suggested by Fig. 8.

In order to check our results, we calculate the co-moving luminosity density of the dust in the submm region and compare it with (Gispert et al. 2000, Fig. 4). We find them compatible.

3.5. Discussion

Just like the Thomson scattering during reionization, early dust will also tend to erase the primordial anisotropies in the CMB. However, due to the much smaller dust opacity (compare $\tau_d(1\text{ mm}) \lesssim 10^{-3}$ and $\tau_e = 0.17$), this effect will be negligible.

The early dust will also introduce a new type of secondary anisotropies with a typical size of a dark matter filament. Here, we only estimate the order of magnitude of this effect. If the co-moving size of the dark matter filament is L, the angular size is $3 \cdot (L/5\text{ Mpc})$ arcminutes at $z = 10$ which corresponds to multipole number $\ell \sim 4000 \cdot (L/5\text{ Mpc})$. Fortunately, this region in ℓ-space does not contain any primordial fluctuations because of the Silk damping. However, there are other foregrounds in the same region, see Aghanim et al. (2000). If we suppose a contrast of 10% in the dust intensity between dark matter filaments and the void, we obtain values of $\Delta T/T \approx 3 \times 10^{-7}$ (for $\lambda = 1$ mm, $f_d = 0.1$ and $\Delta t = 1$ Gyr). These anisotropies, pending more accurate calculations, clearly are in the range of expected arcminute secondary anisotropies from other effects. They could be detected by Planck HFI (High Frequency Instrument), Lamarre et al. (2003) and FIRAS-II type of instrument, Fixsen & Mather (2002).

The results of these calculations depend only very weakly on the precise dust model assumptions. We have also tried a different (but similar) shape of the ionizing photon production, Fig. 1, and found that the results do not vary significantly.

Very little is known about the universe during the reionization epoch. Nevertheless, there are several parameters that could be calculated more accurately.

The two most important parameters in the present model are the dust lifetime, Δt and the mass fraction of the produced metals that are ejected as interstellar dust, f_d. The dust lifetime could be determined more precisely by making 3D simulations of the dust production in combination with structure formation. The simulations would also give the inhomogeneous dust density evolution. The result would be a better estimate of the aforementioned secondary anisotropies caused by the variations in the dust opacity. A more refined dust grain model, using e.g. a distribution of grain sizes would also be more realistic. If the dust is long-lived, it could also have a certain impact on measurements in the optical and UV region. Finally, we note that most of the results are proportional to the dust density and thus to f_d. To evaluate f_d more precisely, we need a better understanding of the typical properties of the first generation of stars, see Sect. 3.1, which is currently much debated.

4. Conclusions

We have shown that the radiation from early dust, produced and heated by Pop III stars, contributes to the extragalactic submillimetre background within the limits set by FIRAS. It may not be detected by the present generation of instruments but future experiments such as Planck HFI and FIRAS-II should be able to measure it, by using its specific predicted spectral signature. This high-redshift dust, contemporary to the reionization, should show up as small-scale anisotropies when observed by sensitive submillimetre instruments. These anisotropies are in the same range as other small-scale anisotropy effects.

References

Aghanim, N., Balland, C., & Silk, J. 2000, A&A, 357, 1
Boulanger, F., Abergel, A., Bernard, J.-P., et al. 1996, A&A, 312, 256
Cen, R. 2002, ApJ, 591, 12
Cen, R. 2003, ApJ, 591, L5
Depagne, E., Hill, V., Spite, M., et al. 2002, A&A, 390, 187
Desert, F.-X., Boulanger, F., & Puget, J. L. 1990, A&A, 237, 215
Draine, B. T. 1990, in The Evolution of the Interstellar Medium, ASP Conf. Ser., 12, 193
Draine, B. T., & Salpeter, E. E. 1979, ApJ, 231, 438

Fixsen, D. J., Dwek, E., Mather, J. C., Bennett, C. L., & Shafer, R. A. 1998, ApJ, 508, 123
Fixsen, D. J., & Mather, J. C. 2002, ApJ, 581, 817
Gispert, R., Lagache, G., & Puget, J. L. 2000, A&A, 360, 1
Heger, A., & Woosley, S. E. 2002, ApJ, 567, 532
Iwamoto, K., Mazzali, P. A., Nomoto, K., et al. 1998, Nature, 395, 672
Kogut, A., Spergel, D. N., Barnes, C., et al. 2003, ApJS, 148, 161
Lagache, G., Abergel, A., Boulanger, F., Désert, F. X., & Puget, J.-L. 1999, A&A, 344, 322
Lamarre, J. M., Puget, J. L., Bouchet, F., et al. 2003, [`arXiv:astro-ph/0308075`]
Nozawa, T., Kozasa, T., Umeda, H., Maeda, K., & Nomoto, K. 2003, [`arXiv:astro-ph/0307108`]
Pei, Y. C., Fall, S. M., & Hauser, M. G. 1999, ApJ, 522, 604
Pettini, M., Smith, L. J., King, D. L., & Hunstead, R. W. 1997, ApJ, 486, 665
Puget, J.-L., Abergel, A., Bernard, J.-P., et al. 1996, A&A, 308, L5
Shioya, Y., Taniguchi, Y., Murayama, T., et al. 2002, ApJ, 576, 36
Songaila, A., & Cowie, L. L. 2002, AJ, 123, 2183
Spergel, D. N., Verde, L., Peiris, H. V., et al. 2003, ApJS, 148, 175
VandenBerg, D. A., Swenson, F. J., Rogers, F. J., Iglesias, C. A., & Alexander, D. R. 2000, ApJ, 532, 430

Paper II

Dust distribution during reionization

The spatial distribution of the dust is estimated using simulations of dark matter density evolution. Combining the calculated intensity from Paper I with this density and integrating along the line of sight, the spatial signature of the dust is obtained. The distribution of the dust gives a detectable signal.

Elfgren, Erik, Désert, François-Xavier and Guiderdoni, Bruno
Astronomy and Astrophysics 476, 1145-1150, 2007
(astro-ph/0705.3403)

A&A 476, 1145–1150 (2007)
DOI: 10.1051/0004-6361:20053151
© ESO 2007

Astronomy & Astrophysics

Dust distribution during reionization

E. Elfgren[1], F.-X. Désert[2], and B. Guiderdoni[3]

[1] Department of Physics, Luleå University of Technology, 971 87 Luleå, Sweden
e-mail: `elf@ludd.luth.se`
[2] Laboratoire d'Astrophysique, Observatoire de Grenoble, BP 53, 414 rue de la piscine, 38041 Grenoble Cedex 9, France
[3] Université Lyon 1, Centre de Recherche Astrophysique de Lyon, Observatoire de Lyon, 9 avenue Charles André, 69230 Saint Genis Laval; CNRS, UMR 5574, France

Received 29 March 2005 / Accepted 8 October 2007

ABSTRACT

Context. The dust produced by the first generation of stars will be a foreground to cosmic microwave background.
Aims. In order to evaluate the effect of this early dust, we calculate the power spectrum of the dust emission anisotropies and compare it with the sensitivity limit of the Planck satellite.
Methods. The spatial distribution of the dust is estimated through the distribution of dark matter.
Results. At small angular scales ($\ell \gtrsim 1000$) the dust signal is found to be noticeable with the Planck detector for certain values of dust lifetime and production rates. The dust signal is also compared to sensitivities of other instruments. The early dust emission anisotropies are finally compared to those of local dust and they are found to be similar in magnitude at mm wavelengths.

Key words. cosmology: cosmic microwave background – cosmology: early Universe – infrared: general

1. Introduction

The importance of the cosmic microwave background (CMB) as a cosmological tool has been demonstrated thoroughly during the last few years. It has been used to evaluate the age, the Hubble parameter, the baryon content, the flatness and the optical depth of the reionization of the universe (Bennett et al. 2003). It has also been used to set upper limits on the non-Gaussianity of the primary fluctuations (Komatsu et al. 2003), the Sunyaev-Zeldovich fluctuations from the first stars (Oh et al. 2003), the primordial magnetic fields (Subramanian et al. 2003), the spatial curvature of the universe (Efstathiou 2003), the formation of population III stars (Cen 2003), and the neutrino masses using only WMAP data (Ichikawa et al. 2005) as well as combining them with other data (Hannestad 2003). However, in order to interpret the CMB signal correctly, its foregrounds must also be well known.

In this paper we focus on one particular aspect of the foreground of the CMB: the dust from the first generation of stars. It is here assumed that dust was created during the reionization period in the first generation of stars and was then ejected into the intergalactic medium (IGM). The dust is heated by the ionizing photons to a temperature slightly above T_{CMB}. The net effect on the CMB is a small monopole distortion of the CMB with a characteristic electromagnetic spectrum close to the CMB primary anisotropy (ΔT) spectrum times the frequency squared. This effect was studied in Elfgren & Désert (2004).

Moreover, the dust also has a characteristic spatial distribution, which could be used to identify its signal. The distribution gives rise to anisotropies in the dust emission, which can be measured with several current and future experiments. The objective of this paper is to determine this spatial distribution and its resulting anisotropies. Of particular interest is the Planck satellite mission, but other instruments are also useful, like ALMA (Wootten 2003), BLAST (Devlin 2001), BOLOCAM (LMT) and (CSO) (Mauskopf et al. 2000), MAMBO (Greve et al. 2004), SCUBA (Borys et al. 1999), and SCUBA2 (Audley et al. 2004).

The spatial distribution of the dust is estimated with the help of GalICS (Galaxies In Cosmological Simulations) N-body simulations of dark matter (DM) (Hatton et al. 2003), which are described in more detail in Sect. 2. The dust distribution is then combined with the intensity of the dust emission, and this is integrated along the line of sight. The resulting angular power spectrum is then computed as C_ℓ and compared with the detection limits of Planck.

In the following, we assume a ΛCDM universe with $\Omega_{\mathrm{tot}} = \Omega_{\mathrm{m}} + \Omega_\Lambda = 1$, where $\Omega_{\mathrm{m}} = \Omega_{\mathrm{b}} + \Omega_{\mathrm{DM}} = 0.133/h^2$, $\Omega_{\mathrm{b}} = 0.0226/h^2$, $h = 0.72$ and $\tau_{\mathrm{e}} = 0.12$, as advocated by WMAP (Spergel et al. 2003), using WMAP data in combination with other CMB datasets and large-scale structure observations (2dFGRS + Lyman α).

2. Dark matter simulation

The distribution of DM in the universe is calculated with the GalICS program. The cosmological N-body simulation we refer to throughout this paper is done with the parallel tree-code developed by Ninin (1999). The power spectrum is set in agreement with Eke et al. (1996): $\sigma_8 = 0.88$, and the DM-density field was calculated from $z = 35.59$ to $z = 0$, outputting 100 snapshots spaced logarithmically in the expansion factor.

The basic principle of the simulation is to randomly distribute a number of DM-particles N^3 with mass M_{DM} in a box of size L^3. Then, as time passes, the particles interact gravitationally, clumping together and forming structures. When there are at least 5 particles together, we call it a DM-clump. There are supposed to be no forces present other than gravitation, and the boundary conditions are assumed to be periodic.

In the simulation we set the side of the box of the simulation to $L = 100\,h^{-1}$ Mpc and the number of particles to 256^3, which

Article published by EDP Sciences and available at http://www.ata-journal.org or http://dx.doi.org/10.1051/0004-6361:20053151

implies a particle mass of $\sim 5.51 \times 10^9\ h^{-1}\ M_\odot$. Furthermore, for the simulation of DM, the cosmological parameters were $\Omega_\Lambda = 2/3$, $\Omega_\mathrm{m} = 1/3$ and $h = 2/3$. The simulation of the DM was done before the results from WMAP were published, which explains the difference between these parameters and the values used elsewhere in this paper, as stated in the introduction. Fortunately, the temporal distribution of the dust is independent of the value of h, which means that the impact of this small discrepancy is not important. Between the assumed initial dust formation at $z \sim 15$ and the end of this epoch in the universe at $z \sim 5$, there are 51 snapshots. In each snapshot a friend-of-friend algorithm was used to identify virialized groups of at least 5 DM-particles. For high resolutions, it is clear that the mass resolution is insufficient. Fortunately, the first 5-particle DM-clump appears at $z = 14.7$, while the bulk of the luminosity contribution comes from $z \lesssim 12.5$. At $z = 12.6$ there are 19 clumps and at $z = 12.2$ there are 45 clumps (and rapidly increasing in number) so it should be statistically sufficient.

In order to make a correct large-scale prediction of the distribution of the DM and therefore the dust, the size of the box would have to be of Hubble size, i.e., ~3000 h^{-1} Mpc. However, for a given simulation time, increasing the size of the box and maintaining the same number of particles would mean that we lose out in mass resolution, which is not acceptable if we want to reproduce a fairly realistic scenario of the evolution of the universe.

There is another way to achieve the desired size of the simulation without losing out in detail or making huge simulations. This method is called MoMaF (Mock Map Facility) and is described in detail in Blaizot et al. (2005). The basic principle is to use the same box, but at different stages in time and thus a cone of the line of sight can be established. In order to avoid replication effects, the periodic box is randomly rotated for each time-step. This means that there will be a loss of correlation information on the edges of the box, since these parts will be gravitationally disconnected from the adjacent box. Fortunately, this loss will only be of the order of 10%, as shown in Blaizot et al. (2005). For scales larger than the size of the box, there is obviously no information whatsoever on correlation from the simulation.

2.1. Validity of the simulation

GalICS is a hybrid model for hierarchical galaxy formation studies, combining the outputs of large cosmological N-body simulations with simple, semi-analytic recipes to describe the fate of the baryons within DM-halos. The simulations produce a detailed merging tree for the DM-halos, including complete knowledge of the statistical properties arising from the gravitational forces.

The distribution of galaxies resulting from this GalICS simulation has been compared with the 2dS (Colless et al. 2001) and the Sloan Digital Sky Survey (Szapudi et al. 2001) and found to be realistic on the angular scales of $3' \lesssim \theta \lesssim 30'$, see Blaizot et al. (2006). The discrepancy in the spatial correlation function for other values of θ can be explained by the limits of the numerical simulation. Obviously, any information on scales larger than the size of the box ($\sim 45'$) is not reliable. Fortunately, the dust correlations increase at smaller angles, while the CMB and many other signals decrease. This means that our lack of information on angular scales $\theta > 45'$ ($\ell \lesssim 250$) will not be important, as can be seen in Fig. 4. The model has also proven to give reasonable results for Lyman break galaxies at $z = 3$ (Blaizot et al. 2004). It is also possible to model active galactic nuclei using the same model (Cattaneo et al. 2005).

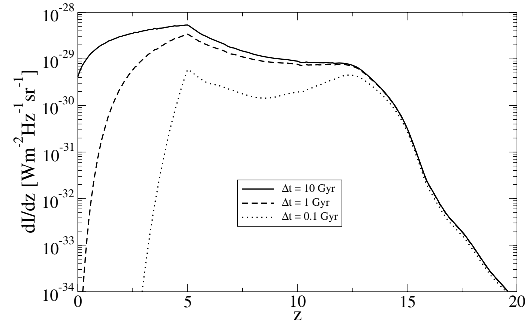

Fig. 1. Intensity contribution from the dust per time-step z integrated over all frequencies. This model assumes that the fraction of metals produced in stars that end up as dust is $f_\mathrm{d} = 0.3$. The mean dust lifetime is a largly unknown parameter, and therefore three different values are explored, $\Delta t = 0.1$, 1 and 10 Gyr.

Since it is possible to reproduce reasonable correlations from semi-analytic modeling of galaxy formation within this simulation at $z = 0$–3, we hereafter attempt to do so at higher z values, when the early dust is produced.

3. Model

Since very little is known about the actual distribution of the dust throughout the universe at this time, we simply assume that the dust distribution follows the DM-distribution. We propose and explore two different ways for the dust distribution to follow the DM-distribution. The first is to let the dust be proportional to the DM-clumps, the second is to make a hydrodynamical smoothing of the DM-density field and set the dust density proportional to this density. In both cases we assume that

$$\rho_\mathrm{dust}(\boldsymbol{r}, z) \propto \rho_\mathrm{DM}(\boldsymbol{r}, z), \tag{1}$$

where ρ_DM represents either the clump method or the smoothing method density. The stars that produce the dust are probably formed close to gravitational hot-spots in the universe and these spots are shaped by the DM. This means that the production of dust can be well approximated by the DM distribution. According to Venkatesan et al. (2006), the initial velocity of the dust is in the order of $10^5\ \mathrm{m\,s^{-1}}$ and the DM-simulations give halos with an escape velocity that is $v_\mathrm{e} \gtrsim 10^5\ \mathrm{m\,s^{-1}}$, given that their mass is $\gtrsim 4.1 \times 10^{10}\ M_\odot$. This means that most of the dust will stay near the halo and we will therefore focus on the clump method. The hydrodynamical smoothing case is included for reference only.

In order to estimate the measured intensity, we need to calculate this distribution in terms of the intensity from the dust emission. The early dust is optically thin, and its intensity as a function of redshift has been calculated in Elfgren & Désert (2004) and is shown in Fig. 1. This model assumes that the fraction of metals produced in stars that end up as dust is $f_\mathrm{d} = 0.3$. The mean dust lifetime is a largly unknown parameter and therefore three different values are explored, $\Delta t = 0.1$, 1, 10 Gyr.

In our present model, we put the spatial distribution of the dust intensity to

$$\frac{\mathrm{d}I}{\mathrm{d}z}(\boldsymbol{r}, z) = \frac{\mathrm{d}I(z)}{\mathrm{d}z} \cdot \frac{\rho_{\mathrm{DM}}(\boldsymbol{r}, z)}{\langle\rho_{\mathrm{DM}}\rangle(z)}, \tag{2}$$

where $\mathrm{d}I(z)/\mathrm{d}z$ is the dust intensity at redshift z as measured at $z = 0$ and $\langle\rho_{\mathrm{DM}}\rangle(z)$ is the mean DM-density at redshift z. The MoMaF method (see Sect. 2) is then used to project the emitted intensity from the dust on a $45' \times 45'$ patch along the line of sight. The contribution from each simulated box is added, and the integrated dust intensity is calculated.

For $z > 2.3$, the time-steps are smaller than the size of the box and each box overlaps with the next box along the line of sight. However, for $z < 2.3$ the time-steps were simulated too far apart and when we pile the boxes, there will be a small part of the line of sight that will not be covered. Fortunately, this is of little consequence since the dust intensity is low at this time, and the gap is small. Each box ($45' \times 45'$) is divided into a grid according to the resolution that we wish to test. For Planck this means a grid that is 18×18 pixels^2, for SCUBA 45×45 pixels^2.

To check the normalization of the resulting intensity image, we have calculated its $\sum \mathrm{d}I_{x,y}/N^2_{\mathrm{pix}}$, where $\mathrm{d}I_{x,y}$ is the observed intensity on pixel (x, y) and N^2_{pix} is the number of pixels^2, and found it to be equal to $\int \mathrm{d}I(z)\mathrm{d}z$ to within a few per cent.

4. Results and discussion

As described above, the MoMaF technique produces an image of the line of sight. This image represents the patch of the sky covered by the box, 150 co-moving Mpc^2, which translates to ~ 45 arcmin^2 at $z = 14.7$. In order to avoid artifacts at the edges, the image is apodized, whereafter it is Fourier transformed into frequency space P_k. In order to convert this spectrum into spherical-harmonics correlation functions we apply the following transformation:

$$\ell = k2\pi/\theta, \tag{3}$$

$$C_\ell = \theta^2 C_k, \tag{4}$$

where θ is the size in radians of the analyzed box. These C_ℓ are then calculated at a frequency $\nu = 353$ GHz, which is one of the nine Planck frequency channels. As found in Elfgren & Désert (2004), the intensity is proportional to the frequency squared, which means that the power spectrum from the dust at a frequency ν is

$$C_\ell(\nu) = C_\ell(353\mathrm{GHz}) \cdot \left(\frac{\nu}{353\mathrm{GHz}}\right)^4, \tag{5}$$

where C_ℓ is given in terms of $\mu\mathrm{K}^2_{\mathrm{CMB}}$. In order to estimate an average power spectrum, 400 such images were generated and the C_ℓ were averaged over these. For comparison, we also tried to paste all these images together and calculate the C_ℓ for this (180×180 pixels^2) image. The result was similar to the average C_ℓ. To validate our results, we also calculated the variance of the images and compared them with $\sum_\ell \frac{2\ell+1}{4\pi} C_\ell$, and found them to be compatible. The resulting power spectra can be seen in Fig. 2. The lifetime of these dust particles is a largely unknown factor, and we plot three different lifetimes, 0.1, 1 and 10 Gyr (for a more detailed discussion of dust lifetimes, see Draine 1990). Furthermore, the dust intensity is proportional to the fraction of the formed metals that actually end up as dust, which we have assumed to be $f_{\mathrm{d}} = 0.3$. This means that the dust power spectrum is

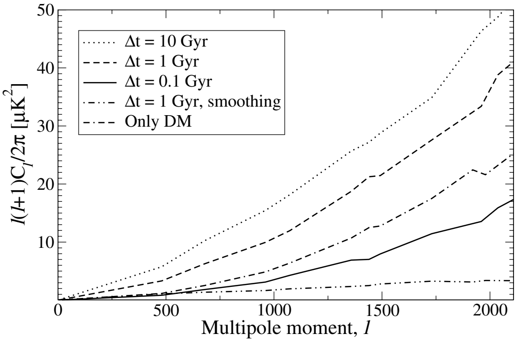

Fig. 2. Dust power spectrum in CMB thermodynamic units at 353 GHz for a map $45' \times 45'$ and Planck resolution $5'$ for three different lifetimes for the dust particles, 0.1, 1, and 10 Gyr, with a solid, dashed and dotted line, respectively. The DM smoothing method for a dust lifetime of 1 Gyr is the dot-dot-dash line.

$$C_\ell(f_{\mathrm{d}}) = C_\ell(f_{\mathrm{d}} = 0.3) \cdot (f_{\mathrm{d}}/0.3)^2. \tag{6}$$

We note that there is only a small difference between dust lifetimes of 10 Gyr and 1 Gyr, while the one at 0.1 Gyr is lower by a factor of four. The lowest curve in the figure represents the hydrodynamical smoothing method of distributing the dust for a dust lifetime of 1 Gyr. Naturally, it is lower than the corresponding C_ℓ for the clump method, since the DM-clumps are much more grainy (especially early in history) than the smoothed DM field. The power spectra of the two methods differ by a factor of ~10 but they do not have exactly the same form.

The dust frequency spectrum is distinctly different from that of other sources in the same frequency range. In Fig. 3, we compare this spectrum with that of the primordial CMB ΔT anisotropies and that of galactic dust, $T = 17$ K (Boulanger et al. 1996). In order to focus on the forms of the spectra, we normalize the three curves to one at $\nu = 353$ GHz. In case of a weak early dust signal, this frequency signature could help us identify the signal by component separation spectral methods.

4.1. Detectability with Planck

The Planck satellite[1], due for launch in 2007, will have an angular resolution of $30'-5'$ and will cover the whole sky. The Planck high frequency instrument (HFI) will measure the submillimeter sky at $\nu = 100$, 143, 217, 353, 545, and 857 GHz. We have chosen $\nu = 353$ GHz as our reference frequency. At higher frequencies, the galactic dust will become more of a problem, and at lower frequencies the CMB primary anisotropies will dominate.

In order to test the detectability of the dust with Planck, we evaluate the sensitivity,

$$\sigma = \sigma_\ell^{\mathrm{CMB}} + \sigma_\ell^{\mathrm{instr}} = \sqrt{\frac{2}{(2\ell+1)f_{\mathrm{cut}}L}} \times (E_{\mathrm{CMB}} + E_{\mathrm{instr}}) \tag{7}$$

---

[1] Homepage: `http://www.rssd.esa.int/index.php?project=Planck`

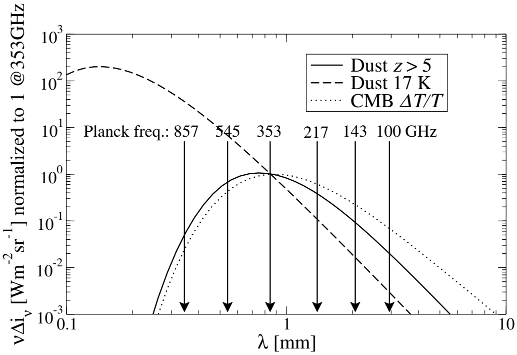

Fig. 3. The form of the early dust spectrum compared to the form of galactic dust (with a temperature of 17 K) and the CMB along with indicators of the Planck HFI frequencies. The curves have been normalized to unity at 353 GHz. We see that the early dust has a special spectral signature.

Table 1. Parameters of the PLANCK HFI detector properties (The Planck collaboration 2005).

Frequency [GHz]	100	143	217	353	545	857
FWHM [′]	9.5	7.1	5.0	5.0	5.0	5.0
s_X [μK s$^{1/2}$]	32.0	21.0	32.3	99.0	990	45 125

(Tegmark 1997) where $f_\mathrm{cut} = 0.8$ is the fraction of the sky used, L is the bin-size, $E_\mathrm{CMB} = \ell(\ell+1)C_\ell^\mathrm{CMB}/2\pi$ (Lambda web-site: `http://lambda.gsfc.nasa.gov` 1 March 2005) is the cosmic variance. The instrument error is

$$E_\mathrm{instr} = C_\ell^\mathrm{instr}\frac{\ell(\ell+1)}{2\pi} = f_\mathrm{sky}\frac{4\pi s_\mathrm{X}^2}{t_\mathrm{obs}} \cdot \mathrm{e}^{\ell^2\cdot\sigma_\mathrm{b}^2} \cdot \frac{\ell(\ell+1)}{2\pi}, \tag{8}$$

where $f_\mathrm{sky} = 1$ is the fraction of the sky covered, s_X is the noise [μK s$^{1/2}$], $t_\mathrm{obs} = 14 \cdot 30 \cdot 24 \cdot 3600$ s is the observation time (14 months), and $\sigma_\mathrm{b} = FWHM/2.35$ (*FWHM* is the full width at half maximum of the beam in radians). For Planck, the values of these parameters are given in Table 1.

The resulting errors for a binning of $L = 500$ along with the dust power spectrum is plotted in Figs. 4–5. In Fig. 4, the frequency $\nu = 353$ GHz is fixed, while ℓ is varied. We note that $\ell \sim 1000$ seems to be a good value to search for dust. At low ℓ, the error due to the cosmic variance dominates, whereas at high ℓ the instrument noise dominates.

In Fig. 5, the ℓ multipole binning center is fixed, and we show the electromagnetic spectrum of the primordial anisotropies and the early dust emission. The fourth point from the left in the figures corresponds to $\nu = 353$ GHz and gives the best signal over noise ratio. At low ℓ the cosmic variance is important, at high ℓ, the instrument noise dominates.

Early dust may therefore produce a measurable disturbance in the primordial anisotropy angular power spectrum at high multipoles (in the Silk's damping wing). Although the primary contaminant to the CMB in the submillimeter domain is the interstellar dust emission, this new component vindicates the use of more than two frequencies to disentangle CMB anisotropies from submillimeter foregrounds.

Component separation methods for the full range of Planck frequencies should be able to disentangle the CMB anisotropies from early dust, far-infrared background fluctuations, and galactic dust emission. The Sunyaev-Zel'dovich (SZ) effect also rises

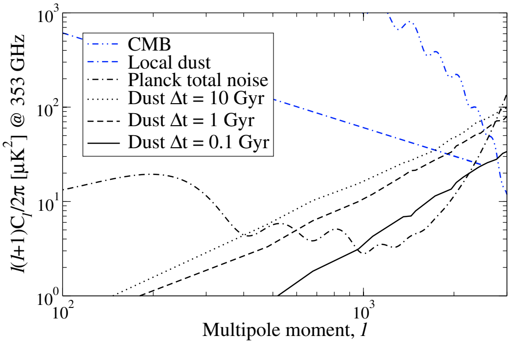

Fig. 4. Comparison between dust power spectrum, the Planck error limits and local dust ($T = 17$ K) at 353 GHz with binning 500. The error limits (total noise) consist of two parts; the CMB cosmic variance, which dominates for small ℓ, and the instrument noise, which dominates for high ℓ.

in the submillimeter range but the two central frequencies of the dust, 217 and 353 GHz, can be used for its identification since the SZ-effect drops more sharply at higher wave-lengths (the SZ-effect is practically null at 217 GHz, quite different from the early dust spectrum). The spectral shape of other foregrounds can be found in Aghanim et al. (2000, Fig. 1) where we can also see that the region around $\ell \sim 2000$ is the most favorable for dust detection.

4.2. Detectability with other instruments

There are several other instruments that might be used to detect the early dust: ALMA (Wootten 2003), BLAST (Devlin 2001), BOLOCAM (LMT) and (CSO) (Mauskopf et al. 2000), MAMBO (Greve et al. 2004), SCUBA (Borys et al. 1999), and SCUBA2 (Audley et al. 2004).

Using Eqs. (7) and (8) we have estimated the sensibilities of these detectors. The result is presented in Table 2. Since all of these instruments operate on a small patch in the sky we use $f_\mathrm{sky} = f_\mathrm{cut} = 10 \cdot FOV$, where *FOV* is the field of view of the instrument. The integration time was set to one hour and the noise per second, s_X, was calculated as $s_\mathrm{X} = NEFD/\sqrt{N_\mathrm{det}}$, where N_det is the number of detectors and *NEFD* is the noise equivalent flux density. The error was evaluated at the multipole moment $\ell \sim 1/FWHM$ (for BOLOCAM(LMT), ℓ was set to 20 000), and we used a bin-size of $L = \ell$. Note that ALMA is an interferometer and thus $E_\mathrm{instr} = f_\mathrm{sky}\frac{4\pi s_\mathrm{X}^2}{t_\mathrm{obs}} \cdot \frac{\ell(\ell+1)}{2\pi}$. Furthermore, the SCUBA2 array needs to be renormalized such that $NEFD = NEFD \times \sqrt{N_\mathrm{det}/(FOV/(\pi/4\cdot(FWHM/60)^2))}$. The resulting sensitivities $\sigma_\ell^\mathrm{instr}$ can be compared with the dust signal, as plotted in Fig. 6. As can be seen, BLAST, SCUBA and MAMBO are unable to detect the dust signal. However, BOLOCAM(LMT), ALMA, SCUBA2, and BOLOCAM(CSO) have good chances of detecting the radiation from the first dust. We also note that the curves are almost parabolic. In fact, for $1\,000 \lesssim \ell \lesssim 100\,000$ the curves can be fitted within ~10% as:

$$\begin{aligned}
\ell(\ell+1)C_\ell^\mathrm{Dust}/2\pi &\approx 2.13\times10^{-5}\times\ell^{1.92}, \ \Delta t = 10\ \mathrm{Gyr},\\
\ell(\ell+1)C_\ell^\mathrm{Dust}/2\pi &\approx 1.37\times10^{-5}\times\ell^{1.95}, \ \Delta t = 1\ \mathrm{Gyr},\\
\ell(\ell+1)C_\ell^\mathrm{Dust}/2\pi &\approx 4.02\times10^{-5}\times\ell^{1.98}, \ \Delta t = 0.1\ \mathrm{Gyr},
\end{aligned} \tag{9}$$

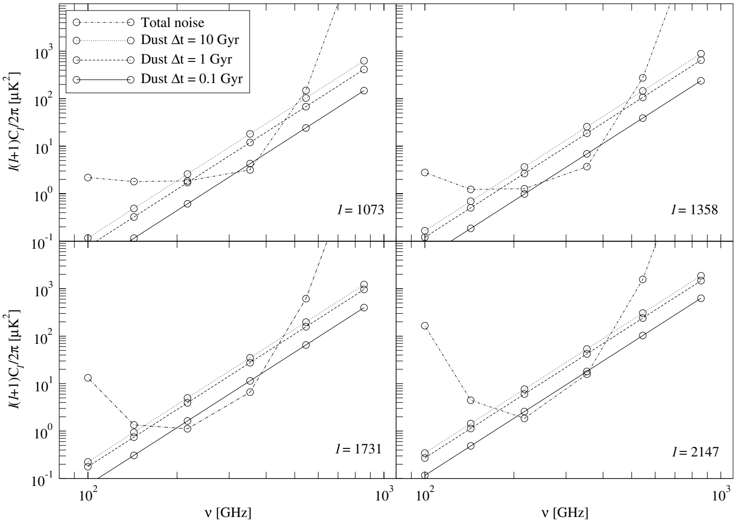

Fig. 5. Comparison between dust power spectrum and Planck error limits at $\ell = 1073$, 1358, 1731, and 2110 with binning 500. The error limits (total noise) consist of two parts; the CMB cosmic variance, which is constant at such μK^2-levels, and the instrument noise, which has the shape of an exponential×ℓ^2.

Table 2. Sensitivities, $\sigma_\ell^{\mathrm{instr}}$, for different (current and future) detectors. $NEFD$ = noise equivalent flux density, ν is the operating instrument frequency, N_{det} = number of detectors, $FWHM$ = full width at half max, FOV = field of view in units of arcmin^2, $\ell = 1/FWHM$, $\sigma_\ell^{\mathrm{instr}}$ is the instrument sensitivity in units of mK$^2_{\mathrm{CMB}}$. The instrument sensitivity was calculated with Eqs. (7) and (8) using $t_{\mathrm{obs}} = 1$ h, $f_{\mathrm{sky}} = f_{\mathrm{cut}} = 10 \cdot FOV$ and $L = \ell$.

Instrument	$NEFD$	ν	N_{det}	$FWHM$	FOV	ℓ	$\sigma_\ell^{\mathrm{instr}}$
	$\left[\frac{\mathrm{mJy}}{\sqrt{\mathrm{Hz}}}\right]$	[GHz]		[″]	[′²]	[10^3]	[$10^3\ \mu$K^2]
SCUBA	75	353	37	13.8	4.2	14	161
SCUBA2	25	353	5120	14.5	50	14	1.8
MAMBO	45	250	117	10.7	13	19	50
BLAST	239	600	43	59	85	3.5	424
BOLOCAM							
(CSO)	40	280	144	31	50	6.6	0.38
(LMT)	3	280	144	6	3.1	20	1.0
ALMA	1.5	353	1	13.8/2	0.085	24	8.0

in units of μK$^2_{\mathrm{CMB}}$. The dependency in ℓ, which is slightly different from an uncorrelated noise ℓ^2 behavior, means that large-scale correlations cannot be neglected. They mix differently at different epochs, depending on the dust lifetime parameter.

5. Conclusions

It seems that it is possible to detect the dust from the first generation of stars with the Planck satellite on small angular scales ($\ell \gtrsim 1000$). However, the detectability depends on the actual distribution of dust in the early universe, and also, to a large extent, on the dust lifetime.

The results are parametrized so that changing the frequency and the fraction of produced metals that become dust is only a matter of scaling the figures: $C_\ell \propto (\nu/353\mathrm{GHz})^4$ and $C_\ell \propto (f_{\mathrm{d}}/0.3)^2$. The spectrum of the early dust is compared to that of the primary CMB anisotropies, as well as that of the local dust. The unique spectral signature of the early dust will help in disentangling it from the CMB and the different foregrounds (local dust and extragalactic far infrared background).

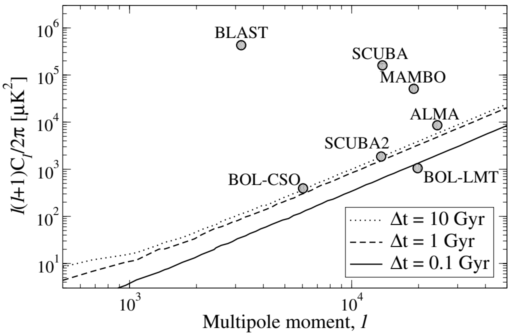

Fig. 6. Dust power spectrum as a function of multipole moment, ℓ, for different dust lifetimes. Estimated detection limits for different instruments are also included as small circles placed at $\ell \sim 1/FWHM$.

The spatial signature of the early dust is found to have $C_\ell \approx$ constant $\approx 10^{-5} - 10^{-4}\ \mu$K$^2_{\mathrm{CMB}}$ depending on the dust lifetime, Δt. Obviously, other signals that are correlated with the structures will also show a similar behavior in the power spectrum. Notably, the near infrared background from primordial galaxies could be correlated with the early dust.

The next generation of submillimeter instruments will be adequate to measure these early dust anisotropies at very small angular scales ($\ell \gtrsim 2000$). Our estimation shows that BOLOCAM, SCUBA2 and ALMA have a good prospect of finding the early dust. However, for these instruments, more detailed simulations are required in order to obtain a realistic DM and baryon distribution. A DM simulation on a smaller box, maybe $L = 50\ h^{-1}$ for PLANCK and smaller still for ALMA, would improve the results on the relevant angular scales, $\ell \gtrsim 1000$. This also means that the particles are smaller, giving a better level of detail. Furthermore, the distribution of dust relative to the DM can also be improved and it is even possible to include some semi-analytical results from the galaxy simulations in GalICS.

Acknowledgements. Finally, we wish to express our gratitude towards Eric Hivon who wrote the code to analyze the simulated signal and thus produce the dust power spectrum.

References

Aghanim, N., Balland, C., & Silk, J. 2000, A&A, 357, 1

Audley, M. D., Holland, W. S., Hodson, T., et al. 2004, in Astronomical Structures and Mechanisms Technology, Proc. SPIE, ed. J. Zmuidzinas, W. S. Holland, & S. Withington, 5498, 63

Bennett, C. L., Halpern, M., Hinshaw, G., et al. 2003, ApJS, 148, 1

Blaizot, J., Guiderdoni, B., Devriendt, J. E. G., et al. 2004, MNRAS, 352, 571

Blaizot, J., Wadadekar, Y., Guiderdoni, B., et al. 2005, MNRAS, 360, 159

Blaizot, J., Szapudi, I., Colombi, S., et al. 2006, MNRAS, 369, 1009

Borys, C., Chapman, S. C., & Scott, D. 1999, MNRAS, 308, 527

Boulanger, F., Abergel, A., Bernard, J.-P., et al. 1996, A&A, 312, 256

Cattaneo, A., Blaizot, J., Devriendt, J., & Guiderdoni, B. 2005, MNRAS, 364, 407

Cen, R. 2003, ApJ, 591, L5

Colless, M., Dalton, G., Maddox, S., et al. 2001, MNRAS, 328, 1039

Devlin, M. 2001, in Deep Millimeter Surveys: Implications for Galaxy Formation and Evolution, 59

Draine, B. T. 1990, in The Evolution of the Interstellar Medium, ASP Conf. Ser. 12, 193

Efstathiou, G. 2003, MNRAS, 343, L95

Eke, V. R., Cole, S., & Frenk, C. S. 1996, MNRAS, 282, 263

Elfgren, E., & Désert, F.-X. 2004, A&A, 425, 9

Greve, T. R., Ivison, R. J., Bertoldi, F., et al. 2004, MNRAS, 354, 779

Hannestad, S. 2003, J. Cosmology Astropart. Phys., 5, 4

Hatton, S., Devriendt, J. E. G., Ninin, S., et al. 2003, MNRAS, 343, 75

Ichikawa, K., Fukugita, M., & Kawasaki, M. 2005, Phys. Rev. D, 71, 043001

Komatsu, E., Kogut, A., Nolta, M. R., et al. 2003, ApJS, 148, 119

Lambda web-site: `http://lambda.gsfc.nasa.gov`. 1 March 2005

Mauskopf, P. D., Gerecht, E., & Rownd, B. K. 2000, in Imaging at Radio through Submillimeter Wavelengths, ed. J. G. Mangum, & S. J. E. Radford, ASP Conf. Ser., 217, 115

Ninin, S. 1999, Ph.D. Thesis, Université Paris 11

Oh, S. P., Cooray, A., & Kamionkowski, M. 2003, MNRAS, 342, L20

Spergel, D. N., Verde, L., Peiris, H. V., et al. 2003, ApJS, 148, 175

Subramanian, K., Seshadri, T. R., & Barrow, J. D. 2003, MNRAS, 344, L31

Szapudi, I., Bond, J. R., Colombi, S., et al. 2001, in Mining the Sky, 249

Tegmark, M. 1997, Phys. Rev. D, 56, 4514

The Planck collaboration 2005, Available at: `http://www.rssd.esa.int/SA/PLANCK/docs/Bluebook-ESA-SCI(2005)1.pdf`

Venkatesan, A., Nath, B. B., & Shull, J. M. 2006, ApJ, 640, 31

Wootten, A. 2003, in Large Ground-based Telescopes, Proc. SPIE, ed. J. M. Oschmann, & L. M. Stepp, 4837, 110

Paper III

Mass limits for heavy neutrinos

If fourth generation neutrinos exist and have a mass higher than 50 GeV they would produce a gamma ray signal due to annihilation within dense parts of the universe. We show that if the neutrino mass is $\sim 100 - 200$ GeV, this signal would already have manifested itself in data, and thus such masses can be excluded. We also show that in the edges of this region an eventual neutrino would give a small bump in the gamma ray spectrum.

Elfgren, Erik and Fredriksson, Sverker

Accepted for publication (December 10, 2007) in Astronomy and Astrophysics
(astro-ph/0710.3893)

Astronomy & Astrophysics manuscript no. CosmoNu2
December 19, 2007

© ESO 2007

Mass limits for heavy neutrinos

Erik Elfgren and Sverker Fredriksson

Department of Physics, Luleå University of Technology, SE-971 87 Luleå, Sweden

Received ¡date¿ / Accepted ¡date¿

ABSTRACT

Context. Neutrinos heavier than $M_Z/2 \sim 45$ GeV are not excluded by particle physics data. Stable neutrinos heavier than this might contribute to the cosmic gamma ray background through annihilation in distant galaxies, as well as to the dark matter content of the universe.

Aims. We calculate the evolution of the heavy neutrino density in the universe as a function of its mass, M_N, and then the subsequent gamma ray spectrum from annihilation of distant $N\bar{N}$ (from $0 < z < 5$).

Methods. The evolution of the heavy neutrino density in the universe is calculated numerically. To obtain the enhancement due to structure formation in the universe, we approximate the distribution of N to be proportional to that of dark matter in the GalICS model. The calculated gamma ray spectrum is compared to the measured EGRET data.

Results. A conservative exclusion region for the heavy neutrino mass is 100 to 200 GeV, both from EGRET data and our re-evalutation of the Kamiokande data. The heavy neutrino contribution to dark matter is found to be at most 15%.

Key words. Elementary particles – Neutrinos – (Cosmology:) dark matter – Gamma rays: observations

1. Introduction

The motivation for a fourth generation neutrino comes from the standard model of particle physics. In fact, there is nothing in the standard model stating that there should be exactly three generations of leptons (or of quarks, for that matter).

The present limits on the mass of a fourth generation of neutrinos are only conclusive for $M_N \lesssim M_Z/2 \approx 46$ GeV (Yao et al. 2006, p. 35). This limit is obtained from measuring the invisible width of the Z^0-peak in LEP, which gives the number of light neutrino species, as $N_\nu = 2.9841 \pm 0.0083$ (The LEP Collaborations 2001).

In Maltoni et al. (2000), a fourth generation of fermions is found to be possible for $M_N \sim 50$ GeV, while heavier fermions are shown to be unlikely. However, this constraint is only valid when there is a mixing between the generations (Novikov et al. 2002); and since this is not necessarily true, we will not take it for certain.

In the context of cosmology and astrophysics there are other contraints. Light neutrinos, with $M_N \lesssim 1$ MeV, are relativistic when they decouple, whereas heavier neutrinos are not. The light neutrinos must have $\sum m_\nu \lesssim 46$ eV in order for $\Omega_\nu h^2 < 1$ to be valid (Hannestad 2006b). For the dark matter (DM) content calculated by Spergel et al. (2003), the bound is $\sum m_\nu \lesssim 12$ eV. The number of light neutrino species are also constrained to $N_\nu = 4.2^{+1.2}_{-1.7}$ by the cosmic microwave background (CMB), large scale structure (LSS), and type Ia supernova (SNI-a) observations at 95% confidence (Hannestad 2006a).

Neutrinos heavier than about 1 MeV, however, leave thermal equilibirum before decoupling and therefore their number density drops dramatically, see for example Dolgov & Zeldovich (1981). This will be discussed in more detail in Sect. 2.

The most important astrophysical bound on heavy neutrinos comes from Kamiokande (Mori et al. 1992) and this will be considered separately in the end.

In Fargion et al. (1995), it is found that the mass range $60 \lesssim M_N \lesssim 115$ GeV is excluded by heavy neutrino annihilation in the galactic halo. However, according to Dolgov (2002, p. 57) this constraint is based on an exaggerated value of the density enhancement in our galaxy. Other works constraining the heavy neutrino mass include Fargion et al. (1998, 1999) and Belotsky et al. (2004). There has also been a study of the gamma ray spectrum of dark matter (DM) in general (Ando et al. 2007).

For an exhaustive review of modern neutrino cosmology, including current constraints on heavy neutrinos, see Dolgov (2002). It is concluded that there are no convincing limits on neutrinos in the mass range $50 \lesssim M_N \lesssim 1000$ GeV. A review of some cosmological implications of neutrino masses and mixing angles can be found in Kainulainen & Olive (2003).

In this paper we consider a stable fourth-generation heavy neatrino with mass $M_N \gtrsim 50$ GeV possessing the standard weak interaction. We assume that other particles of a fourth generation are heavier and thus do not influence the calculations.

We assume a ΛCDM universe with $\Omega_{tot} = \Omega_m + \Omega_\Lambda = 1$, where $\Omega_m = \Omega_b + \Omega_{DM} = 0.135/h^2$, $\Omega_b = 0.0226/h^2$ and $h = 0.71$ (Spergel et al. 2003), using WMAP data in combination with other CMB datasets and large-scale structure observations (2dFGRS + Lyman α). Throughout the article we use natural units, so that the speed of light, Planck's reduced constant and Boltzmann's constant equal unity, $c = \hbar = k_B = 1$.

If heavy neutrinos ($M_N \gtrsim 50$ GeV) exist, they were created in the early universe. They were in thermal equilibrium in the early stages of the hot big bang, but froze out relatively early. After freeze-out, the annihilation of $N\bar{N}$ continued at an ever decreasing rate until today. Since those photons that were produced before the decoupling of photons are lost in the CMB, only the subsequent $N\bar{N}$ annihilations contribute to the photon background as measured on earth.

The intensity of the photons from $N\bar{N}$-annihilation is affected by the number density of heavy neutrinos, n_N, whose mean density decreases as R^{-3}, where R is the expansion fac-

---

Send offprint requests to: Erik Elfgren, e-mail: `elf@ludd.ltu.se`

tor of the universe. However, in structures such as galaxies the mean density will not change dramatically, and since the number of such structures are growing with time, this will compensate for the lower mean density. Note that the photons are also redshifted with a factor R due to their passage through space-time. This also means that the closer annihilations will give photons with higher energy than the farther ones.

2. Evolution of neutrino density

Let us recapitulate the results of Dolgov & Zeldovich (1981).

The cosmic evolution of the number density, n_X, of a particle X can, in general, be written as

$$\dot{n}_X = -n_X^2 \langle\sigma v\rangle - 3H(t)n_X + \psi(t), \tag{1}$$

where $\langle\sigma v\rangle$ is the thermally averaged product of the mean velocity and total annihilation cross section for the particle, and $H(t) = \dot{R}/R$ is the Hubble constant. The term $-3H(t)n_X$ represents the expansion of the universe, and the production term is $\psi(t) = n_{Xeq}^2 \langle\sigma v\rangle$, where n_{Xeq} is the equilibrium concentration of particle X.

If we write $r_X = n_X/n_\gamma$, Eq. (1) can be expressed as

$$\dot{r}_X = -\langle\sigma v\rangle n_\gamma (r_X^2 - r_{Xeq}^2), \tag{2}$$

where

$$r_{Xeq} \approx \begin{cases} 1 & \text{if } \theta \equiv T/m_X > 1 \\ \frac{(2\pi)^{-3/2}}{2\cdot\zeta(3)/\pi^2} g_s \theta^{-3/2} e^{-1/\theta} & \text{if } \theta < 1. \end{cases} \tag{3}$$

Here $\zeta(3) \approx 1.2020569$ is the Riemann zeta function, T is the temperature, m_X is the mass of particle X and g_s is the number of spin states. For photons and electrons, $g_s = 2$, while for massless left-handed neutrinos, $g_s = 1$. For reference, $\frac{(2\pi)^{-3/2}}{2\cdot\zeta(3)/\pi^2} \approx \frac{1}{4}$.

The value of the relative equilibrium concentration, r_{Xeq}, is derived from

$$r_{Xeq} \equiv n_\gamma^{-1} n_{eq} = \frac{1}{2T^3\zeta(3)/\pi^2} \cdot \frac{1}{(2\pi)^3} \int \frac{4\pi p^2 dp}{e^{E/T}+1}, \tag{4}$$

where the expressions for n_γ and n_{eq} were taken from Dolgov (2002, Eq. 30).

According to Dolgov & Zeldovich (1981, Eq 2.9), freeze-out (equilibrium destruction) occurs when the rate of change of the equilibrium concentration due to the temperature decrease is higher than the reaction rates, which means that $2\langle\sigma v\rangle n_\gamma r_{Xeq} tT/m > 1$. Until freeze-out, the relative particle density follows the equilibrium density closely: $r_{fX} \approx r_{Xeq}$. Hence, the relative density at the moment of freeze-out is

$$r_{fX} = (2\langle\sigma v\rangle n_\gamma t_f \theta_f)^{-1} \approx r_{Xeq}, \tag{5}$$

where t_f and $\theta_f = T_f/m_X$ are the time and relative temperature at freeze-out.

As the temperature decreases, the production term r_{Xeq} will drop exponentionally, such that the relic concentration of X will be more or less independent of r_{Xeq}. With this approximation ($r_{Xeq} = 0$), Eq. 2 can be solved for $t \to \infty$:

$$r_{0X} \approx \frac{1}{2\langle\sigma v\rangle n_\gamma t_f \cdot (1+\theta_f)} = \frac{1}{2\langle\sigma v\rangle_f n_{\gamma f} \frac{3.68\cdot 10^{18}}{\sqrt{g_*(T_f)}} T_f^{-2}(1+\theta_f)}, \tag{6}$$

where we have used $tT^2 \approx 3.677\times 10^{18}/\sqrt{g_*}$ (Dolgov 2002, Eq. 37), with $g_*(T_f)$ from Kolb & Turner (1990, p. 65) being the number of relativistic species in thermal contact with the photons. Furthermore, $n_\gamma(t_0) = 2T_0^3\zeta(3)/\pi^2 \approx 0.24T_0^3$ is the photon density today, where the photon temperature today is $T_0 = 2.725$ K (Mather et al. 1999). According to the standard model of particle physics, $g_* = 106.75$ for $T \gtrsim 100$ GeV ($g_* \approx 200$ for supersymmetry models at yet higher temperatures). If we assume that $\theta_f \ll 1$ (which we will later show to be reasonable), we obtain $r_{0X} \approx r_{fX}\theta_f$, which differs by a factor two from the result of Dolgov & Zeldovich (1981, Eq. 2.11). This is natural if they consider the density of $n_{N+\bar{N}}$ since our r_{0X} is valid for N and $\bar{N}$ separately.

In order to take into account the increase in temperature due to entropy conservation after freeze-out of particle X, we must take

$$\left(\frac{n_{0X}}{\mathrm{m}^{-3}}\right) = r_{0X}\frac{43/11}{g_{*S}(T_f)} n_\gamma(t_0) \approx \frac{6.88\times 10^{-57}}{\langle\sigma v\rangle_f T_f(1+T_f/m_X)\sqrt{g_{*f}}}. \tag{7}$$

(In fact $g_{*f}^{-1/2}$ should be written $g_{*Sf}^{-1} \cdot g_{*f}^{1/2}$ but for $T_f > 0.1$ GeV, $g_{*Sf} = g_{*f}$.)

We now turn to the case of heavy neutrinos. Since we wish to avoid the lenghty calculations of the cross sections of heavy neutrinos (Enqvist et al. 1989), we use Fargion et al. (1995, Fig. 1 and Eq. 4) and solve for $\langle\sigma v\rangle$. We assume that they use $g_* = g_*(T_f) \approx g_*(M_N/30)$, but the exact value does not change the result in any significant way. The resulting $\langle\sigma v\rangle$ is presented in Fig. 1. The cross section drops from $M_N \sim 45$ GeV, where the Z^0 resonance peaks until the W^+W^- annihilation channel starts to dominate at $M_N \gtrsim 100$ GeV.

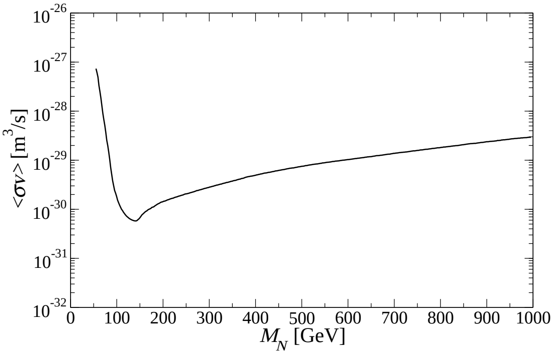

Fig. 1. The cross section times the velocity (in m^3/s) of heavy neutrino annihilation $N\bar{N}$ as a function of their mass (in GeV) at freeze-out, $T = T_f$.

According to Fargion et al. (1995), the cross sections of heavy neutrinos can be estimated using the annihilation channels

$$N\bar{N} \to Z^0 \to f\bar{f} \tag{8}$$

$$N\bar{N} \to Z^0 \to W^+W^-. \tag{9}$$

There are several other possible annihilation channels for $N\bar{N} \to W^+W^-$, like $N\bar{N} \to L\bar{L}$, H^0H^0, $Z^0Z^0 \to W^+W^-$ and also interference between L and Z^0, as well as between L and H^0. However, in the limit $s \to 4M_N^2$, which is valid for cosmological heavy neutrinos, the dominant channel is through s-channel $N\bar{N} \to Z^0$ (Enqvist et al. 1989, p. 656). Furthermore, the other annihilation products, $N\bar{N} \to H^0H^0$, Z^0Z^0, are suppressed with respect to W^+W^--production (Enqvist et al. 1989, p. 651, 656).

Hence, the above estimation of the $\langle\sigma v\rangle$ should be fairly accurate. If anything, it is slightly underestimated.

Using Eqs. 5 and 3, we can solve for $T_f = \theta_f \cdot M$. The result is presented in Fig. 2. Note that although it looks like a straight line, it really is slightly curved. We notice that $T_f/M_N \sim 1/30$, which shows our assumption $M_N \gg T_f$ to be valid. This is also in agreement with previous results, see e.g. Kolb & Turner (1990), where a value of $T_f/M_N \sim 1/20$ is quoted.

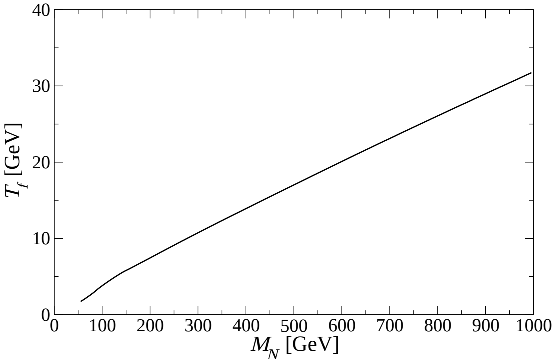

Fig. 2. The freeze-out temperature (in GeV≈ 1.16×10^{13} K) of heavy neutrinos as a function of their mass (in GeV).

We now return to Eq. 7 and apply it to the case of a heavy neutrino. We plot the resulting relative relic neutrino density as a function of the mass M_N in Fig. 3 using $\Omega_N = 2M_N \cdot n_N(T_0)/\rho_c$, where $\rho_c \approx 9.47 \times 10^{-27}$ kg/m^3 is the critical density of the universe. The resulting heavy neutrino density is very similar to the one obtained by Fargion et al. (1995, Fig. 1). The numerical simulation also shown in the figure will be the subject of the next section.

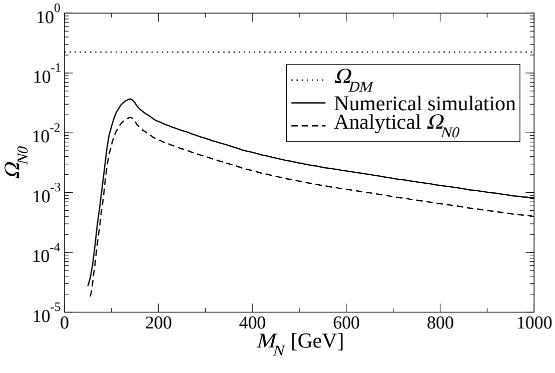

Fig. 3. The relic relative density of heavy neutrinos as a function of their mass (in GeV).

3. Numerical simulation of the neutrino density

For comparison, we evaluate the evolution of the heavy neutrino density numerically. Eq. 1 can be rewritten in terms of the temperature, T:

$$\frac{dn}{dT} = -\frac{dt}{dT}\left[3H(T)n(T) + \langle\sigma v\rangle\left(n(T)^2 - n_{eq}(T)^2\right)\right], \tag{10}$$

where

$$n_{eq}(T) = r_{eq} n_\gamma = 2T^3\left(\frac{M_N}{2\pi T}\right)^{3/2} e^{-M_N/T}, \qquad (T < M_N) \tag{11}$$

and the relation between time and temperature is given by

$$\frac{dt}{dT} = \frac{-1}{H(T)}\left(\frac{1}{T} + \frac{dg_{*S}/dT}{3g_{*S}}\right), \tag{12}$$

Here the Hubble constant is $H(T) = H_0\sqrt{\Omega(T)}$, where the total relative energy density of the universe is

$$\Omega(T) = \Omega_R(T) \cdot R^{-4} + \Omega_M \cdot R^{-3} + \Omega_k \cdot R^{-2} + \Omega_\Lambda. \tag{13}$$

The curvature term $\Omega_k = 0$ and the radiation density is

$$\Omega_R(T) = \Omega_R \frac{g_*(T)}{g_*(T_0)} \tag{14}$$

due to the reheating as particles freeze out. The reheating also means that $R = g_{*S}^{-1/3} T_0/T$ (Kolb & Turner 1990, p. 68). The number of relativistic species still in thermal contact with the photons, $g_{*S}(T)$, is given in Coleman & Roos (2003, Fig. 1). For the critical region $0.15 < T < 0.30$ GeV their Eqs. 8-9 have been used to calculate dg_{*S}/dT. This updated value of $g_{*S}(T)$ is needed to evaluate dg_{*S}/dT properly.

Using a fifth-order Runge-Kutta method with adaptive stepsize control, taken from Numerical Recipes (Press et al. 1992, Ch. 16.2), we solve for $n(T)$ in Eq. 10 using the initial condition $n_i = n_{eq}(T_i = M_N/15)$, which is well within the region of thermal equilibrium for the heavy neutrinos. The resulting relative relic neutrino density is presented in Fig. 3, where $\Omega_N = 2M_N \cdot n_N(T_0)/\rho_c$ as before. We notice that the peak of the curve is $\Omega_N(M_N = 140 \text{ GeV}) \approx 0.04$, which would then account for ~15% of the dark matter content of the universe.

For comparison, we plot the number density of heavy neutrinos (in m^{-3}) as a function of T for masses 50, 70, 90, 150, 500 and 1000 GeV in Fig. 4. As we can see, the transition between thermal equilibirum density and completely decoupled neutrino density is not sharp. This is one of the reasons for the difference between the analytical and the numerical relative density in Fig. 3. Another reason for the difference is the inclusion of the change in g_{*S} in the evaluation of dt/dT. The evolution of $g_{*S}(T)$ is the cause of the small "knee" in Fig. 4 seen at $T \sim 0.2$ GeV (the reheating from the quark-hadron transition). Furthermore, when electrons fall out of thermal equilibirum at $T \sim 1$ MeV there is another small knee, reducing again the heavy neutrino density somewhat.

4. Dark matter simulations

In Sect. 3, we calculated the mean density of neutrinos in the universe as a function of redshift and the mass of the heavy neutrinos. However, the neutrino annihilation rate, and thus the intensity from their gamma spectrum, is proportional to the square of the neutrino density. This means that inhomogeneities in the universe will tend to enhance the gamma ray signal.

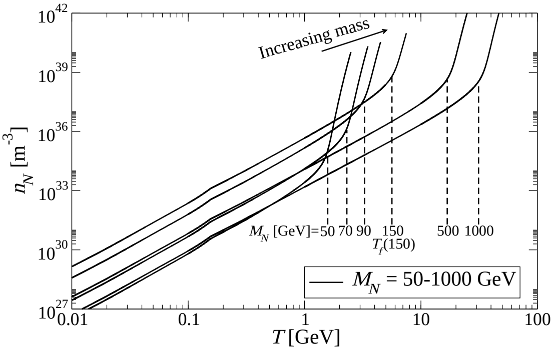

Fig. 4. The number density of heavy neutrinos (in m^{-3}) as a function of T for masses 50, 70, 90, 150, 500 and 1000 GeV (increasing from left to right in the upper right corner). The dashed vertical lines represent the calculated value of T_f in Fig. 2. Below $T = 0.01$ GeV, the curves evolve as $(T/T_0)^3 \cdot g_{*S}$.

In this section we describe how we calculate the inhomogeneities as a function of space and time, assuming only gravitational interaction between the dark matter consisting of heavy neutrinos and other DM particles. The clumping factor (also known as the boost factor) can then be used to calculate the actual intensity

$$\frac{dI}{dz} = C(z)\frac{dI_0}{dz}, \tag{15}$$

where dI_0/dz is the intensity contribution from redshift slice dz for a homogeneous universe and $C(z)$ is the enhancement due to the clumping at redshift z.

The clumping factor has been calculated in different settings before, ranging from Berezinsky et al. (2006) for local clustering giving a clumping factor of ~ 5 to Diemand et al. (2005) for mini-halos giving a clumping factor of two orders of magnitude. For a discussion about the accuracy of approximating the enhancement with a single clumping parameter, see Lavalle et al. (2006), though they focus on antiprotons.

The spatial and temporal distribution of DM in the universe is calculated with the GalICS program. The cosmological N-body simulation that we are referring to throughout this paper is done with the parallel tree-code developed by Ninin (1999). The initial mass power spectrum is taken to be a scale-free ($n_s = 1$) one, evolved as predicted by Bardeen et al. (1986) and normalized to the present-day abundance of rich clusters with $\sigma_8 = 0.88$ (Eke et al. 1996). The DM density field was calculated from $z = 35.59$ to $z = 0$, giving 100 "snapshots", spaced logarithmically in the expansion factor.

The basic principle of the simulations is to distribute a number of DM particles N^3 with mass M_{DM} in a box of size L^3. Then, as time passes, the particles interact gravitationally, clumping together and forming structures. When there are at least 20 particles together, it is considered to be a DM halo. It is supposed to be no other forces present than gravitation, and the boundary conditions are assumed to be periodic.

In the GalICS simulations the side of the box used was $L = 100h^{-1}$ Mpc, and the number of particles was set to 256^3, which implies a particle mass of $\sim 5.51 \times 10^9 h^{-1} M_\odot$. Furthermore, for the simulation of DM, the cosmological parameters were set to $\Omega_\Lambda = 2/3$, $\Omega_m = 1/3$ and $h = 2/3$. The simulations of the DM were done before the results from WMAP were published, which explains the difference between these parameters and the values used elsewhere in this paper, as stated in the introduction. Nevertheless, the difference is only a couple of percent and should not seriously alter the results.

Between the initial halo formation at $z \sim 11$ and the current epoch in the universe, there are 72 snapshots. In each snapshot a friend-of-friend algorithm was used to identify virialized groups of at least 20 DM particles. For high resolutions, it is clear that the mass resolution is insufficient. Fortunately, the first 20-particle DM clump appears at $z = 11.2$, while the bulk of the clumping comes from $z \lesssim 5$, where the lack of resolution is no longer a problem.

In order to make a correct large-scale prediction of the distribution of the DM, the size of the box would have to be of Hubble size, i.e., $\sim 3000h^{-1}$ Mpc. However, for a given simulation time, increasing the size of the box and maintaining the same number of particles would mean that we lose in mass resolution, which is not acceptable if we want to reproduce a fairly realistic scenario for the evolution of the universe.

We will make the approximation that our single box, at different time-steps, can represent the line of sight, and since we are only interested in the general properties of the dark matter clumping, this approximation should be acceptable.

4.1. Validity of simulation

GalICS is a hybrid model for hierarchical galaxy formation, combining the outputs of large cosmological N-body simulations with simple, semi-analytic recipes to describe the fate of the baryons within DM halos. The simulations produce a detailed merging tree for the DM halos, including complete knowledge of the statistical properties arising from the gravitational forces.

The distribution of galaxies resulting from this GalICS simulation has been compared with the 2dS (Colless et al. 2001) and the Sloan Digital Sky Survey (Szapudi et al. 2001) and found to be realistic on the angular scales of $3' \lesssim \theta \lesssim 30'$, see Blaizot et al. (2006). The discrepancy in the spatial correlation function for other values of θ can be explained by the limits of the numerical simulation. Obviously, any information on scales larger than the size of the box (~ 45') is not reliable. The model has also proven to give sensible results for Lyman break galaxies at $z = 3$ (Blaizot et al. 2004). It is also possible to model active galactic nuclei (Cattaneo et al. 2005).

Since it is possible to reproduce reasonable correlations from semi-analytic modelling of galaxy formation within this simulation at $z = 0 - 3$, we now attempt to do so also for somewhat higher redshifts.

4.2. Clumping of dark matter

We proceed to calculate the clumping factor $C(z)$. The inhomogeneities of the DM distribution can be calculated using the relative clumping of dark matter halos: $\bar{\rho}_i = \rho_i/\rho_{mean}$, where ρ_{mean} is the mean density of the dark matter in the universe and ρ_i is the mean density of DM halo i.

As matter contracts, the density increases, but since the gamma ray emitting volume also decreases, the net effect is a linear enhancement from the quadratic dependence on the density. This means that the DM halos will emit as:

$$\frac{I_{halos}}{I_0} = \frac{\sum_i m_i \bar{\rho}_i}{\sum_i m_i} \cdot C_{halo}, \tag{16}$$

where I_0 is the intensity for a homogeneous universe and the summation is done over all DM halos and thus $\sum_i m_i = m_{halos}$. The factor C_{halo} accounts for the modification from the form and properties of the halo itself. A simple conic DM distribution would give $C_{halo} = 1.6$. The more realistic distribution $\rho(r) = \rho_0 \cdot [(1+r)(1+r^2)]^{-1}$, where r is the radial coordinate relative to the halo radius, gives $C_{halo} = 1.1$. However, the radiation from within the denser part of the halo will also be subject to more absorption, and so for the sake of simplicity we use $C_{halo} = 1$. We notice that the average relative density over all the halos in the simulation is fairly constant, $\langle \bar{\rho}_i \rangle \sim 70$ for $z < 5$.

Simultaneously, the DM background (the DM particles that are not in halos) will decrease, both in density by a factor $(m_{tot} - m_{halos})/m_{tot}$ and because of their decreasing fraction of the total mass in the box m_{tot}:

$$\frac{I_{DM-background}}{I_0} = \left(\frac{m_{tot} - m_{halos}}{m_{tot}}\right)^2 . \qquad (17)$$

This means that the total clumping factor is

$$C = \frac{I_{halos}}{I_0} + \frac{I_{DM-background}}{I_0} = \frac{\sum_i m_i \bar{\rho}_i}{m_{tot}} + \left(\frac{m_{tot} - m_{halos}}{m_{tot}}\right)^2 , \qquad (18)$$

where the first term starts as unity whereafter it decreases and quickly becomes negligeable with respect to the second term, which starts at zero, but then rapidly increases. The total clumping is plotted in Fig. 5 along with the competing $(n_N/\mathrm{m}^{-3})^2$ effect, as well as the product, all as a function of the redshift z. The number density of heavy neutrinos in the figure is taken for the mass $M_N = 150$ GeV. We notice that the clumping enhancement remains ~ 30 for $z < 1$ and that the clumping is ~ 1 for $z > 5$. This is mainly due to the proportion of mass within the halos compared to the total DM mass. The clumping enhancement lies between the two extreme values by Berezinsky et al. (2006) and Diemand et al. (2005) quoted above.

In fact, the clumping factor can be even higher if other halo shapes are assumed with smaller radii (Ullio et al. 2002). The densities in the halos considered in the present work have been evaluated at the virial radius.

We also point out that before the reionization, at $z \gtrsim 5$, there is absorption from neutral hydrogen in the interstellar medium (ISM), also known as the Gunn-Petersen effect (Gunn & Peterson 1965). This means that photons from higher redshifts will be highly attenuated. For $z = 5.3$, the emission drops by roughly a factor of 10, and for $z \sim 6$ the opacity is $\tau_{eff} > 20$ (Becker et al. 2001). Hence, any gamma ray signal prior to this epoch would have been absorbed.

5. Photon distribution from $N\bar{N}$-collisions

In order to evaluate the photon spectrum from $N\bar{N}$-collisions we use PYTHIA version 6.410 (Sjöstrand et al. 2006). According to Enqvist et al. (1989, Eq. 13) the centre of mass energy squared is $E_{CM}^2 = 4M_N^2 + 6M_N T_f$ and $T_f \approx M_N/30$ as estimated above.

We generate 100,000 $N\bar{N}$ events for each mass $M_N = 50, 60, ..., 1000$ GeV and calculate the photon spectrum and mean photon multiplicity and energy. We assume that $N\bar{N}$ collisions at these energies and masses can be approximated by $\nu_\tau \bar{\nu}_\tau$ collisions at the same E_{CM}^2. This is obviously not equivalent, but $N\bar{N}$ cannot be directly simulated in PYTHIA. Nevertheless, with the approximations used in calculating $\langle \sigma v \rangle$, the only difference between $\nu_\tau \bar{\nu}_\tau$ and $N\bar{N}$ collisions (except in the cross section) is the t-channel production of W^+W^- through τ. However, since the heavy neutrinos are non-relativistic when they collide, the two Ws will be produced back-to-back, which means that the inclusion of the t-channel is unimportant.

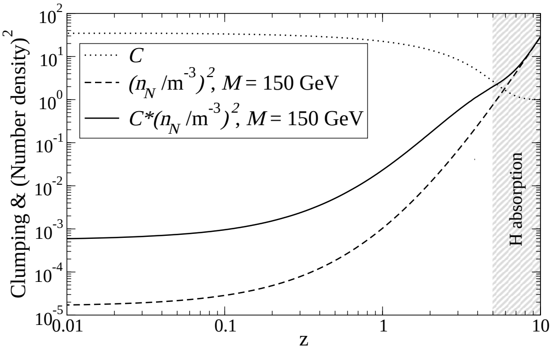

Fig. 5. The clumping factor (C, dotted line) compared to the competing effect of the decreasing heavy neutrino number density squared (n_N^2, dashed line) for $M_N = 150$ GeV and the product of the two (solid line). Different neutrino masses scale as in Fig. 4.

In order to verify this, we study the difference in the photon spectrum for W decay at 0 and 90 degrees, and despite an increasing difference between the two cases, even at $M_N = 1000$ GeV, the difference is not strong enough to change our conclusions.

The resulting photon distribution is presented in Fig. 6. We note that the photon energies peak at $E_{CM}/2$, which is natural since the decaying particles can each have at most half of the centre of mass energy. The curves continue to increase as $\propto E^{-1}$ as E decreases further. Note that the noise in the curves for lower E is due to lacking statistics for these rare events, but it does not affect the outcome of the calculations. We also calculate the mean photon energy and find it to be $\bar{E}_\gamma \approx 0.21 E_{CM}$ for all masses. The curve is normalized such that the integral over $\frac{dn_\gamma}{dE}$ is unity. The average number of photons, N_γ, produced for an $N\bar{N}$-collision is shown in Fig. 7. The sharp rise in the curve

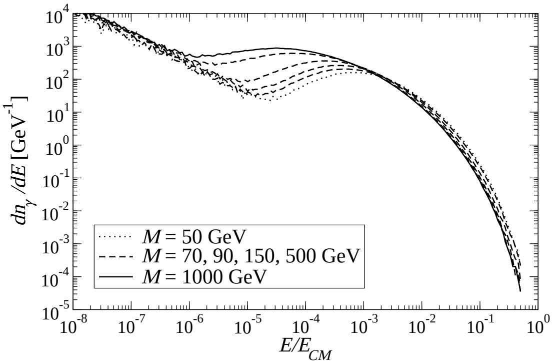

Fig. 6. The relative energy distributions of photons from $N\bar{N}$-collisions for heavy neutrino masses $M_N = 50, 70, 90, 150, 500, 1000$ GeV. $E_{CM} = 2M_N$ is the centre of mass energy.

at $M_N \sim 100$ GeV is due to the jets from the emerging W^+W^--production.

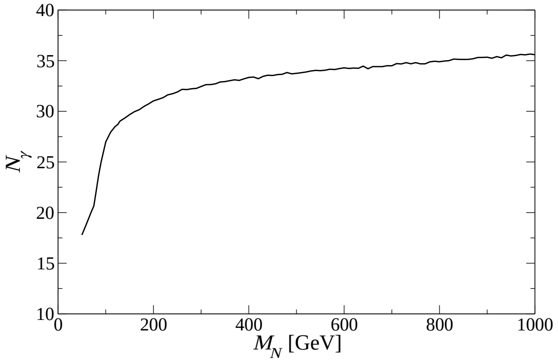

Fig. 7. The average number of photons produced for an $N\bar{N}$-collision as a function of heavy neutrino mass M_N in GeV.

6. Gamma ray spectrum

The $N\bar{N}$-collisions from the reionization at $z_i \sim 5$ until today give an integrated, somewhat redshifted, gamma spectrum for a heavy neutrino with a given mass:

$$I = \int_{T_i}^{T_0} C(T) \frac{n^2 \langle \sigma v \rangle}{4\pi} N_\gamma \frac{dn_\gamma}{dE}\Big|_{E\frac{T_0}{T}} \frac{dt}{dT} dT, \qquad (19)$$

where $C(T)$ is the clumping factor in Fig. 5 and $\frac{dn_\gamma}{dE}$ is the photon distribution in Fig. 6. $T_0 = 2.725$ K is the temperature of the CMB today and T_i is the reionization temperature, which we set to $T_i = 5 \cdot T_0$.

The resulting $E^2 I$ is presented in Fig. 8. When we compare the calculated heavy neutrino signal with data from EGRET (Sreekumar et al. 1998), we see that only neutrino masses around $M_N \sim 100$ or 200 GeV would be detectable, and then only as a small bump in the data around $E_\gamma \sim 1$ GeV. For intermediary neutrino masses, the signal would exceed the observed gamma ray data. In Fig. 9, the peak intensity for the different heavy neutrino masses is plotted, as well as EGRET data for the corresponding energy with error bars. The data represent the observed diffuse emission at high latitudes ($|b| > 10$ degrees), where first the known point sources were removed and then the diffuse emission in our galaxy was subtracted.

We have also compared the height of the curves, both with and without clumping, and the integrated difference is roughly a factor of 30.

7. Discussion and conclusions

The numerical calculation of the evolution of the heavy neutrino number density indicates that in the mass region $100 \lesssim M_N \lesssim 200$, the cosmological neutrinos would give a cosmic ray signal that exceeds the measurements by the EGRET telescope (Sreekumar et al. 1998). Note that the clumping factor for these limits is rather conservative. In Ullio et al. (2002), this factor is much larger, which would also produce a stronger limit on the heavy neutrino mass.

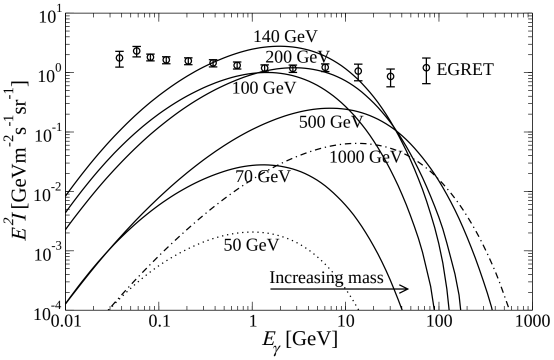

Fig. 8. Cosmic gamma radiation from photons produced in $N\bar{N}$-collisions as a function of photon energy for neutrino masses $M_N = 50, 70, 100, 140, 200, 500, 1000$ GeV. The dotted line represents $M_N = 50$ GeV and the dot-dashed $M_N = 1$ TeV. The solid lines are the masses in between. The circles represent data from EGRET (Sreekumar et al. 1998), with error bar, as derived for extragalactic sources.

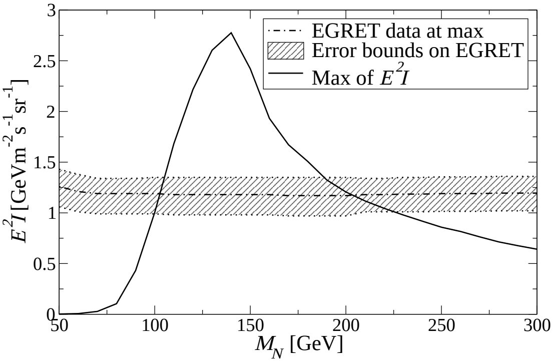

Fig. 9. Maximum cosmic gamma radiation from photons produced in $N\bar{N}$-collisions as a function of neutrino mass (in GeV). The marked region is excluded since $\Omega_N > \Omega_{DM}$ within. The data are taken at the energy corresponding to the maximum in Fig. 8. with error bars.

We can also compare our neutrino density with the results from the Kamiokande collaboration (Mori et al. 1992). We scale the neutrino signal in their Fig. 2 to Ω_N/Ω_{DM}, where we use $h_0 = 0.71$, $\Omega_m = 0.2678$ and $\Omega_b = 0.044$. This is shown in Fig. 10, where we compare our numerical results for the relic neutrino density to the observed muon flux in the Kamiokande detector. This gives an exclusion region of $80 \lesssim M_N \lesssim 400$ GeV. Our analytical results, which are comparable to the traditional relic neutrino densities, is about a factor two lower, giving an exclusion region of $90 \lesssim M_N \lesssim 300$ GeV. The model that gives these limits (Gould 1987) is rather complicated and not verified experimentally, so these results cannot be taken strictly. Note also that in the three-year WMAP analysis (Spergel et al. 2007), the value of Ω_{DM} depends on which other data the WMAP data are combined with. For WMAP+CFHTLS Ω_{DM} can be as high as 0.279 and for WMAP+CBI+VSA it can be as low as 0.155. The higher of these possibilities would give an exclusion region of $85 \lesssim M_N \lesssim 350$ GeV. The lower boundary value would give

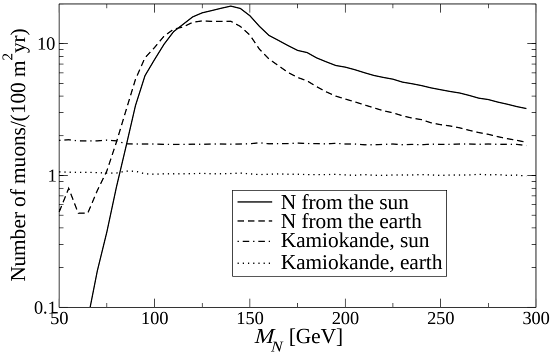

Fig. 10. Predicted signal from enhanced $N\bar{N}$ annihilation in the earth and the sun compared to the measured signal in the Kamiokande. On the y-axis: the number of muons (per 100 m^{2}year) produced by muon neutrinos resulting from heavy neutrino collisions in the sun and the earth, as evaluated by Mori et al. (1992), but scaled to our $\Omega_N(M_N)$. On the x-axis: the heavy neutrino mass in GeV.

an exclusion region of $75 \lesssim M_N \lesssim 500$ GeV. A conservative limit based on the Kamiokande data gives the exclusion region $100 \lesssim M_N \lesssim 200$ GeV.

If a heavy neutrino exists with a mass $M_N \sim 100$ GeV or $M_N \sim 200$ GeV it would give a small bump in the data at $E_\gamma \sim 1$ GeV. Currently the data points are too far apart and the error bars too large to neither exclude nor confirm the eventual existence of such a heavy neutrino. Most of this part of the gamma ray spectrum is usually attributed to blazars, which have the right spectral index, ~ 2 (Mukherjee et al. 1997).

We note that there could be an enhancement in the signal due to the higher DM densities within galaxies compared to the mean density in the halos. On the other hand, from within galaxies there will also be an attenuation due to neutral hydrogen, thus reducing the enhancement. There will also be a certain degree of extinction of the signal due to neutral hydrogen along the line of sight, but even if we assume complete extinction above $z = 4$ the resulting spectrum decreases with only about 20%.

We are also aware of the ongoing debate concerning the antiprotons – whether or not the DM interpretation of the EGRET gamma excess is compatible with antiproton measurements (Bergström et al. 2006; de Boer et al. 2006). We note the argument by de Boer that antiprotons are sensitive to electromagnetic fields, and hence their flux need not be directly related to that of the photons, even if they too were produced by $N\bar{N}$ annihilation.

In the advent of the Large Hadron Collider, we also point out that there may be a possibility to detect the existence of a heavy neutrino indirectly through the invisible Higgs boson decay into heavy neutrinos (Belotsky et al. 2003).

It will of course be interesting to see the results of the gamma ray large area space telescope (GLAST). It has a field of view about twice as wide (more than 2.5 steradians), and sensitivity about 50 times that of EGRET at 100 MeV and even more at higher energies. Its two-year limit for source detection in an all-sky survey is 1.6×10^{-9} photons cm^{-2} s^{-1} (at energies > 100 MeV). It will be able to locate sources to positional accuracies of 30 arc seconds to 5 arc minutes. The precision of this instrument could well be enough to detect a heavy neutrino signal in the form of a small bump at $E \sim 1$ GeV in the gamma spectrum, if a heavy neutrino with mass ~100 or 200 GeV would exist.

There are also some other possible consequences of heavy neutrinos that may be worth investigating. The DM simulations could be used to estimate the spatial correlations that the gamma rays would have and to calculate a power spectrum for the heavy neutrinos. This could be interesting at least for masses $M_N \sim 100$ GeV and $M_N \sim 200$ GeV. The annihilation of the heavy neutrinos could also help to explain the reionization of the universe. Another possible interesting application of heavy neutrinos would be the large look-back time they provide (Silk & Stodolsky 2006), with a decoupling temperature of $\gtrsim 10^{13}$ K (Enqvist et al. 1989).

Acknowledgements. E. E. would like to express his gratitude to Konstantine Belotsky, Lars Bergström, Michael Bradley, Alexander Dolgov, Kari Enqvist, Kimmo Kainulainen and Torbjörn Sjöstrand for useful discussions and helpful comments and explanations. We are both grateful to the GalICS group, who has provided the complete dark matter simulations and finally to the Swedish National Graduate School in Space Technology for financial contributions.

References

Ando, S., Komatsu, E., Narumoto, T., & Totani, T. 2007, Phys. Rev. D, 75, 063519
Bardeen, J. M., Bond, J. R., Kaiser, N., & Szalay, A. S. 1986, ApJ, 304, 15
Becker, R. H., Fan, X., White, R. L., et al. 2001, AJ, 122, 2850
Belotsky, K., Fargion, D., Khlopov, M., Konoplich, R., & Shibaev, K. 2003, Phys. Rev. D, 68, 054027
Belotsky, K., Fargion, D., Khlopov, M., & Konoplich, R. V. 2004, ArXiv High Energy Physics - Phenomenology e-prints, hep-ph/0411093
Berezinsky, V., Dokuchaev, V., & Eroshenko, Y. 2006, Phys. Rev. D, 73, 063504
Bergström, L., Edsjö, J., Gustafsson, M., & Salati, P. 2006, J. Cosmology Astropart. Phys., 5, 6
Blaizot, J., Guiderdoni, B., Devriendt, J. E. G., et al. 2004, MNRAS, 352, 571
Blaizot, J., Szapudi, I., Colombi, S., et al. 2006, MNRAS, 369, 1009
Cattaneo, A., Blaizot, J., Devriendt, J., & Guiderdoni, B. 2005, MNRAS, 364, 407
Coleman, T. S. & Roos, M. 2003, Phys. Rev. D, 68, 027702
Colless, M., Dalton, G., Maddox, S., et al. 2001, MNRAS, 328, 1039
de Boer, W., Gebauer, I., Sander, C., Weber, M., & Zhukov, V. 2006, ArXiv Astrophysics e-prints, astro-ph/0612462
Diemand, J., Moore, B., & Stadel, J. 2005, Nature, 433, 389
Dolgov, A. D. 2002, Phys. Rep., 370, 333
Dolgov, A. D. & Zeldovich, Y. B. 1981, Rev. Mod. Phys., 53, 1
Eke, V. R., Cole, S., & Frenk, C. S. 1996, MNRAS, 282, 263
Enqvist, K., Kainulainen, K., & Maalampi, J. 1989, Nuclear Physics B, 317, 647
Fargion, D., Khlopov, M. Y., Konoplich, R. V., & Mignani, R. 1995, Phys. Rev. D, 52, 1828
Fargion, D., Khlopov, M. Y., Konoplich, R. V., & Mignani, R. 1998, Soviet Journal of Experimental and Theoretical Physics Letters, 68, 685
Fargion, D., Konoplich, R., Grossi, M., & Khlopov, M. 1999, ArXiv Astrophysics e-prints, astro-ph/9902327
Gould, A. 1987, ApJ, 321, 571
Gunn, J. E. & Peterson, B. A. 1965, ApJ, 142, 1633
Hannestad, S. 2006a, Journal of Cosmology and Astro-Particle Physics, 1, 1
Hannestad, S. 2006b, Progress in Particle and Nuclear Physics, 57, 309
Kainulainen, K. & Olive, K. A. 2003, in Neutrino Mass, ed. G. Altarelli & K. Winter, 53–+
Kolb, E. & Turner, M. 1990, The Early Universe (Oxford: Westview Press), xlii + 547
Lavalle, J., Pochon, J., Salati, P., & Taillet, R. 2006, ArXiv Astrophysics e-prints, astro-ph/0603796
Maltoni, M., Novikov, V. A., Okun, L. B., Rozanov, A. N., & Vysotsky, M. I. 2000, Physics Letters B, 476, 107
Mather, J. C., Fixsen, D. J., Shafer, R. A., Mosier, C., & Wilkinson, D. T. 1999, ApJ, 512, 511
Mori, M., Hikasa, K., Nojiri, M. M., et al. 1992, Physics Letters B, 289, 463
Mukherjee, R., Bertsch, D. L., Bloom, S. D., et al. 1997, ApJ, 490, 116
Ninin, S. 1999, PhD thesis: Université Paris 11
Novikov, V. A., Okun, L. B., Rozanov, A. N., & Vysotsky, M. I. 2002, Physics Letters B, 529, 111
Press, W. H., Teukolsky, S. A., Vetterling, W. T., & Flannery, B. P. 1992, Numerical Recipes in C: The Art of Scientific Computing (New York, NY, USA: Cambridge University Press)

Silk, J. & Stodolsky, L. 2006, Physics Letters B, 639, 14
Sjöstrand, T., Mrenna, S., & Skands, P. 2006, Journal of High Energy Physics, 5, 26
Spergel, D. N., Bean, R., Doré, O., et al. 2007, ApJS, 170, 377
Spergel, D. N., Verde, L., Peiris, H. V., et al. 2003, ApJS, 148, 175
Sreekumar, P., Bertsch, D. L., Dingus, B. L., et al. 1998, ApJ, 494, 523
Szapudi, I., Bond, J. R., Colombi, S., et al. 2001, in Mining the Sky: Proc. of the MPA/ESO/MPE Workshop, ed. A. Banday, S. Zaroubi, & M. Bartelmann, 249
The LEP Collaborations. 2001, ArXiv High Energy Physics - Experiment e-prints, hep-ex/0112021
Ullio, P., Bergström, L., Edsjö, J., & Lacey, C. 2002, Phys. Rev. D, 66, 123502
Yao, W.-M., Amsler, C., Asner, D., et al. 2006, Journal of Physics G Nuclear Physics, 33, 1

Paper IV

Are there indications of compositeness of leptons and quarks in CERN LEP data?

The implications of a substructure of fermions are investigated within a particular preon model, and possible signal characteristics are evaluated at the fairly “low” energies of the existing CERN LEP data.

Elfgren, Erik and Fredriksson, Sverker
Submitted to Physical Review D
(hep-ph/0712.3342)

Are there indications of compositeness of leptons and quarks in CERN LEP data?

Erik Elfgren* and Sverker Fredriksson†
Department of Physics
Luleå University of Technology
SE-97187 Luleå, Sweden

The "preon-trinity" model for the compositeness of leptons, quarks and heavy vector bosons predicts several new heavy leptons and quarks. Three of them can be produced in e^+e^- annihilations at CERN LEP energies, since they can be created out of a system of three preons and their antipreons, where three preons form a heavy lepton or quark, while the other three go into a normal lepton or quark. In fact, these new particles are predicted to be lighter than the top quark, while the top itself cannot be produced this way, due to its particular preon substructure. The empirical situation is analyzed, and the most likely masses are estimated.

PACS numbers: 12.60.Rc, 13.35.Hb, 14.65.Ha

I. INTRODUCTION

New generations of leptons and quarks, as compared with those prescribed by the so-called standard model (SM), have been searched for at the three main high-energy laboratories, *i.e.*, CERN LEP, DESY HERA and the Fermilab Tevatron. A general conclusion is that no statistically significant signals have been found [1]. This goes for both a fourth generation of leptons and quarks, *e.g.*, a b' quark, and excited versions of the normal ones, *e.g.*, e^* and ν^*. From an experimental point of view there is not much difference between the two approaches. A fourth generation is believed to mimic the normal three, while excited leptons and quarks are believed to couple to other particles exactly like the unexcited versions, except for kinematic effects of the higher masses.

The existence of any of these would be a strong evidence for a substructure of leptons and quarks in terms of preons. Excitations are hard to imagine without an inner structure of the excited object, and yet another generation of leptons and quarks would also be difficult to reconcile with the idea that they are all fundamental.

There are indeed already several phenomenological, and logical, arguments in favour of a substructure of leptons, quarks and heavy vector mesons in terms of preons [2–4]. It even seems as if the standard model itself contains several prophecies of preons [3] among its many seemingly unrelated bits and pieces. The "preon-trinity" model [5] was inspired by such arguments, as well as by models for the three-quark structure of light baryons [6, 7], by early preon models [2, 8–10] and by the concept of diquarks [11].

The aim of this publication is to reanalyze the data from, above all, the (closed) CERN LEP facility, in order to look for signals of new leptons and quarks, as prescribed by the preon-trinity model. As it turns out, some of the criteria used in the existing experimental searches are not valid in the model. Above all, the predicted new leptons and quarks are *not* just heavier versions of the old ones. They have their own unique features, which should be confronted with the data.

TABLE I: The "supersymmetric" preon scheme.

charge	$+e/3$	$-2e/3$	$+e/3$
spin-1/2 preons	α	β	δ
spin-0 (anti-)dipreons	$(\bar{\beta}\bar{\delta})$	$(\bar{\alpha}\bar{\delta})$	$(\bar{\alpha}\bar{\beta})$

II. THE MODEL

The main ingredients are that there exist three absolutely stable species (flavours) of spin-1/2 preons, called α, β and δ, with electric and colour charges, and that these also tend to form tightly bound spin-0 dipreons. Thanks to the choice of preon charges, inspired by the ones of the original three-quark model, the scheme gets an attractive supersymmetric balance between preons and *anti*-dipreons, as summarised in Table I.

It is then prescribed that leptons are built up by one preon and one dipreon. Quarks consist of one preon and one anti-dipreon, and heavy vector bosons of one preon and one antipreon. The results are shown in Table II. There is an obvious $SU(3)$ preon-flavour symmetry in the scheme, just like with quark flavours in the first quark model. The stability of preons means that the total preon flavour is absolutely conserved, unlike the quark flavour in the quark model.

One can make about a dozen observations about leptons, quarks and heavy vector bosons. Most of these provide qualitative explanations of some seemingly disjunct ingredients of the SM, *e.g.*, the mixings of some quarks, neutrinos and heavy vector bosons, and the (partial) conservation of three lepton numbers, all being consequences of preon flavour conservation [5].

The most notable difference from the SM is the set of new leptons, quarks and heavy vector bosons predicted

---

*Electronic address: `elf@ltu.se`

†Electronic address: `sverker@ltu.se`

TABLE II: Composite states in the preon model: *leptons* as a preon and a dipreon, *quarks* as a preon and an anti-dipreon, and *heavy vector bosons* as a preon and an antipreon.

	$(\beta\delta)$	$(\alpha\delta)$	$(\alpha\beta)$	$(\bar\beta\bar\delta)$	$(\bar\alpha\bar\delta)$	$(\bar\alpha\bar\beta)$	$\bar\alpha$	$\bar\beta$	$\bar\delta$
α	ν_e	μ^+	ν_τ	u	s	c	Z^0/Z'	W^+	Z^*
β	e^-	$\bar\nu_\mu$	τ^-	d	X	b	W^-	Z'/Z^0	W'^-
δ	$\nu_{\kappa 1}$	κ^+	$\nu_{\kappa 2}$	h	k	t	$\bar Z^*$	W'^+	Z''/Z'

by the model. These contain a δ preon that does not belong to a dipreon, and are to be found in the bottom row of Table II, plus in the right-most column. They must all have such high masses that they have escaped discovery, *except* the t quark, which is most probably the quark below b in Table II. This indicates that also the other new quarks and leptons have masses in the region $100 - 200$ GeV. There is a good chance that $\nu_{\kappa 1}$, κ, $\nu_{\kappa 2}$, h and k (earlier called "g" [5]) are all *lighter* than the top quark. It must be stressed though that the model is entirely defined by this scheme, and has not (yet) been complemented with a preon dynamics. Hence exact masses, branching ratios and life-times of quarks and leptons cannot be reproduced or predicted. However, experience tells that lepton masses are lower than that of "corresponding" quarks. In addition, there is a trend among the known quarks of Table II that the masses increase from left to right. All in all, one can therefore expect the mass relations $M_{\nu_{\kappa 1}} < M_{\nu_{\kappa 2}} < M_t$, $M_h < M_k < M_t$, and $M_\kappa < M_k$, which means that CERN LEP energies would suffice for the reactions discussed in this study, and that signs of compositeness might hence exist in old data.

In the following, only the relevance of the model to existing data from the CERN LEP facility will be discussed. For other details of the model, such as the argument that the odd X quark, with charge $-4e/3$, is not expected to exist as a bound system, the reader is referred to Ref. [5]. General arguments that preons should exist are given in Refs. [2, 3].

III. THE REACTIONS

Any system of a certain preon flavour and its anti-flavour can be produced in e^+e^- annihilation, as long as the energy suffices. As can be seen in Table II, there are three new leptons/quarks that carry the same net preon flavour as a lighter partner. These pairs are $\nu_{\kappa 2} = \delta(\alpha\beta) \leftrightarrow \nu_e = \alpha(\beta\delta) \leftrightarrow \bar\nu_\mu = \beta(\alpha\delta)$, $h = \delta(\bar\beta\bar\delta) \leftrightarrow c = \alpha(\bar\alpha\bar\beta)$ and $k = \delta(\bar\alpha\bar\delta) \leftrightarrow b = \beta(\bar\alpha\bar\beta)$.

As long as the masses of these leptons and quarks are not too high, e^+e^- annihilation can therefore result in the production of the pairs $\nu_{\kappa 2}\bar\nu_e$, $\nu_{\kappa 2}\nu_\mu$, $h\bar c$ and $k\bar b$:

$$e^+e^- \to \delta(\alpha\beta) + \bar\alpha(\bar\beta\bar\delta) = \nu_{\kappa 2} + \bar\nu_e, \tag{1}$$

$$e^+e^- \to \delta(\alpha\beta) + \bar\beta(\bar\alpha\bar\delta) = \nu_{\kappa 2} + \nu_\mu, \tag{2}$$

$$e^+e^- \to \delta(\bar\beta\bar\delta) + \bar\alpha(\alpha\beta) = h + \bar c, \tag{3}$$

and

$$e^+e^- \to \delta(\bar\alpha\bar\delta) + \bar\beta(\alpha\beta) = k + \bar b. \tag{4}$$

(and the corresponding antiparticles). For the sake of simplicity, reactions with additional particles in the final state, *e.g.*, photons, will not be discussed here. All final particles will hence be assumed to come from hadronisation or decay of the quarks or leptons listed above.

It is notable that the top quark, $t = \delta(\bar\alpha\bar\beta)$, has no such partner, and hence there is no "single-top production" in e^+e^- reactions.

Since $e^- = \beta(\beta\delta)$, *all* processes of interest are transitions from the original preon system $\beta(\beta\delta)\bar\beta(\bar\beta\bar\delta)$ to the intermediate one $\alpha\bar\alpha\beta\bar\beta\delta\bar\delta$. This, in turn, can split up in many different ways, among which are the four different pairs listed above.

The transition

$$e^+e^- = \beta(\beta\delta)\bar\beta(\bar\beta\bar\delta) \to S^* \to \alpha\bar\alpha\beta\bar\beta\delta\bar\delta \tag{5}$$

can take place via a number of intermediate systems S^*. Examples are one or more photons, a suitable combination of gluons (or "hypergluons"; the possible quantas of a hypothetical preon interaction [2]), a preon-antipreon pair ($\beta\bar\beta$, after the annihilation of $(\beta\delta)(\bar\beta\bar\delta)$) or a dipreon-anti-dipreon pair ($(\beta\delta)(\bar\beta\bar\delta)$, after the annihilation of $\beta\bar\beta$).

The latter should be less likely, because it seems as if a dipreon always stays together, once it has been created [5]. Hence the only new particles that can be produced from the annihilation of $\beta\bar\beta$ would be through the creation of a $\delta\bar\delta$ pair. This would result in either $e^+e^- \to \nu_{\kappa 1}\bar\nu_{\kappa 1}$ or $h\bar h$, with only superheavy final leptons or quarks. They can occur only if $M_{\kappa 1}, M_h < E_{LEP}/2$, where E_{LEP} is the total LEP energy (≤ 209 GeV). In that case they might be seen through the decay products of the two neutrinos or quarks.

The model also allows for production processes like

$$e^+e^- \to \nu_e + \nu_\mu \tag{6}$$

(but *not* of different *charged* leptons, like $e^+\mu^-$). However, due to the neutrino helicities, this can happen only for annihilation in a total spin-0 state. Therefore, this final state cannot be produced in, *e.g.*, Z^0 decay, which means that it cannot be restricted by the well-known "three-generation" data from Z^0 decay [1]. However, the decay

$$Z^0 \to \bar\nu_e + \nu_{\kappa 2}, \tag{7}$$

should, in principle, be possible, and similarly for the final states with quarks in reactions (3) & (4). They have not been seen, so their masses must exceed $M_Z/2$.

IV. ANALYZING THE CERN LEP DATA

We will start by discussing the $\nu_{\kappa 2}$ decay channels of interest for an analysis of LEP data. It is important to keep in mind that lepton numbers are not exactly conserved in our model, and that there is no fourth lepton number connected to the predicted new leptons. The observed lepton number conservation is in our model equivalent to "dipreon number conservation", *i.e.*, the three usual lepton numbers are conserved in leptonic processes only to the extent that the tightly bound dipreons are left intact. In normal leptonic decays and "low-energy" reactions this must be the case, because all imaginable dipreon-breaking processes violate energy conservation. However, the heavy leptons *must* decay through a reshuffling of the preons inside a dipreon, and would hence change the normal lepton numbers. An example is $\kappa^+ \to \mu^+ + \nu_e + \bar{\nu}_\tau$, violating all three lepton numbers. In addition, the three neutrinos on the diagonal of Table II might mix into new mass eigenstates, since they have identical preon net flavours. This is equivalent to neutrino oscillations, which do not conserve lepton numbers. Lepton number conservation might also be violated in normal leptonic collisions, if the energy is high enough to break up existing dipreons. As argued in [5] we think that the energy scale for new preon processes is a few hundred GeV rather than TeV (as the top quark seems to be an example of a "superheavy" three-preon state). The "TeV scale" often mentioned in discussions of compositeness is rather the expected momentum-transfer scale for revealing substructure in deep-inelastic scattering of leptons and quarks.

The most interesting decay channel for the lightest heavy neutrino is

$$\nu_{\kappa 2} \to e^-/\mu^+ + W^{+/-}, \tag{8}$$

followed by

$$W \to q_1\bar{q}_2, \tag{9}$$

or in terms of preon processes:

$$\delta(\alpha\beta) \to \beta(\beta\delta)/\alpha(\alpha\delta) + (\alpha\bar{\beta})/(\bar{\alpha}\beta). \tag{10}$$

The decay into two quark jets gives an opportunity to find the invariant mass of the neutrino. The W is most probably real if the neutrino mass is reasonably well above the W mass. Hence one should restrict the analysis to events where the estimated invariant mass of the two hadron jets is close to the W mass. The main background to this process is $e^+e^- \to W^+W^-$ followed by one $W \to \ell + \bar{\nu}$ and the other $W \to q_1\bar{q}_2$, where ℓ is e or μ.

The analysis hence requires a standard-model Monte Carlo simulation, where one looks for an excess of events within an interval of invariant masses around some value below 175 GeV (the top mass). If such an excess is seen, the "extra events" should have a few characteristics, typical for our model, but not for the standard-model background events:

- there would be a threshold effect at the total e^+e^- energy $\sqrt{s} = M_{\nu_{\kappa 2}}$, rather than at the W^+W^- threshold.
- the charged lepton would always be back-to-back to the W (*i.e.*, the cms of the two hadron jets) in the rest system of the $\nu_{\kappa 2}$. This, in turn, has a speed given by kinematics only, *i.e.*, by $\sqrt{s}$ and $M_{\nu_{\kappa 2}}$.
- at first sight it seems as if the $\nu_{\kappa 2}$ would decay as willingly to an electron as to a muon in accordance with, *e.g.*, W decay. However, the situation is a bit more complicated, since e^- and μ^+ (not μ^-) are on equal footing in our model. They have *opposite* dominant helicity components in the ultra-relativistic limit. Although we do not know the dynamics of the heavy-neutrino decay, we suspect that its decay favours an outgoing charged lepton with positive helicity, *i.e.*, the μ^+ (and μ^- in $\bar{\nu}_{\kappa 2}$ decay). Intuitively, this seems in accordance with the helicities of the decay $W^+ \to \mu^+ + \nu_\mu$.

These predictions are best investigated by the CERN OPAL collaboration. It has so far published searches for, among others, heavy neutral leptons at $\sqrt{s}$ values up to 183 GeV [12–14]. A similar analysis at the highest LEP energies is underway [15].

The main conclusion so far from OPAL is that no signs of a heavy neutral lepton have been found at LEP energies up to 183 GeV. This result is summarised as 95% CL lower mass limits for various channels (decay modes), the values being typically around 90 GeV.

However, the OPAL analyzes contain some extra assumptions, not necessarily valid for our model. For instance, a new heavy neutrino is supposed to belong to a new "fourth family", and be produced toghether with its own antineutrino. This is not the case in our model. In the search for excited versions of the normal neutrinos it is supposed that the couplings are as prescribed by the standard model. Any differences between a normal neutrino and its excited partner is assumed to be due to the different masses only. We therefore look forward to a less model-dependent analysis of *all* available OPAL data along the directions outlined above, including the most recent ones beyond 200 GeV.

Next we consider the decay channel

$$\nu_{\kappa 2} \to e/\mu + W, \tag{11}$$

followed by

$$W \to e/\mu + \nu_e/\nu_\mu. \tag{12}$$

Now the invariant neutrino mass cannot be derived. The only signal of a new neutrino would therefore be an excess of events compared to what is expected from the standard model in the channel

$$e^+e^- \to \ell_1^+\ell_2^- + invisibles. \tag{13}$$

Here also the ALEPH collaboration can contribute to the analysis, although it focuses on W-pair production at various LEP energies [16–20]. This means that there are several experimental cuts in order to assure that each event produces a W-pair, which might naturally eliminate alternative processes, such as the one we are interested in.

Looking at the totality of ALEPH data, for all W decay modes, the ones taken at the lowest three LEP energies [16–18] are consistent with a small "excess" of events in some kinematic bins, but only on the 0.5σ to 1σ level. The case is weakened by the fact that other bins show similar "deficits" in comparison to Monte Carlo simulations of the standard model, hinting at a mere statistical effect. In addition, ALEPH does not find any relevant deviation from lepton universality, *e.g.*, an excess of muons, according to our speculation above that a heavy neutrino would prefer muonic decays.

At the LEP energy of 189 GeV the ALEPH statistics is much better, and the possible deviations from the standard model are even smaller, on the order of 0.2σ at the most.

The only aspect of the ALEPH data that can give some support to a closer analysis along our prediction is the fact that there is a clearer excess of events in kinematic regions outside the ("acoplanarity") cuts used to define W-pair production, especially for LEP energies up to 183 GeV. Obviously, these regions are expected to contain events with other configurations than just a W pair, but it is not clear to us why the simulations do not describe the data so well.

We now analyze the different neutrino decay mode

$$\nu_{\kappa 2} \to \nu_e/\nu_\mu + \gamma(\gamma), \tag{14}$$

or in terms of preon processes:

$$\delta(\alpha\beta) \to \beta(\alpha\delta)/\alpha(\beta\delta) + \gamma(\gamma). \tag{15}$$

Hence the full events of interest are

$$e^+e^- \to \nu\bar{\nu} + \gamma(\gamma). \tag{16}$$

The signal is one or more high-energy gammas, and a deviation in the production cross-section and the phase-space distribution of gammas, as compared to expectations from the standard model.

Such studies have been made by the DELPHI collaboration [21–23], in events with just photons (plus "invisibles"), and at LEP energies up to 189 GeV. Parts of the DELPHI analysis focus on the possibility of a new generation of heavy neutrinos.

The results are summarised as the distribution in "missing mass" of the invisibles recoiling against the gamma(s). The possible deviations of this distribution from the standard-model expectation are presented as upper production cross-section limits of a heavy "neutral object". However, this analysis is built on the idea that the heavy neutrino is "stable", and hence identical to one of the outgoing neutrinos in the process given above. Provided that its mass is fairly high, and that only high-energy gammas are studied, the "missing mass" would be a good measure of the neutrino mass. A theoretical analysis of expected event rates for such a production of a 50 GeV neutrino at LEP is presented in [26].

If we stay with the case of a highly unstable neutrino, where the gammas come from its decay (and not from its production), there is a simple relation, in the one-gamma case, between the "missing mass" (MM) of the DELPHI analysis and the mass ($M_{\kappa 2}$) of $\nu_{\kappa 2}$. Assuming that its decay products, γ and a light neutrino, are aligned along its spin direction, we get:

$$M_{\nu_{\kappa 2}} = \sqrt{E_{LEP}^2 - MM^2}. \tag{17}$$

There is no such simple relation for two-gamma decays, since we do not know the dynamics behind the decay. Intuitively, it seems likely that the "missing mass" distribution would anyway peak at the same value as for the one-gamma decays, but there might also be a second peak due to the fact that the gammas can radiate in the same or in opposite directions in the $\nu_{\kappa 2}$ rest system. The only data points that deviate by more than 1σ from the standard-model result in [23] are at $MM \approx 135$ GeV in both the 2γ data and in parts of the one-gamma data (from the HPC calorimeter). This value corresponds to a $\nu_{\kappa 2}$ mass of around 140 GeV. There is also a similar excess at $MM \approx 165$ GeV in the 2γ data, possibly corresponding to a 110 GeV neutrino. However, a signal would be smeared out, since the data are summarised over several LEP energies. No significant excess is seen in the one-gamma case when the data are summed from all (three) DELPHI calorimeters.

The detailed analysis of "limits of compositeness" in [23] is not of much value for judging our ideas, because it is built entirely on predictions from a rather specific preon model [27]. These model predictions rely, for instance, on the existence of additional, composed bosons with unknown (high) masses.

Finally, one might ask if the lightest of the superheavy neutrinos, the $\nu_{\kappa 1}$, might be *stable*, and hence correspond to the hypothetical "dark-matter" neutrino analyzed in [28] and elsewhere. Since it is most probably the lightest of the superheavy particles, it can perhaps be pair-produced at LEP as $\nu_{\kappa 1}\bar{\nu}_{\kappa 1}$ (but it cannot be created together with a light partner). However, there is no particular reason for a stable $\nu_{\kappa 1}$. All superheavy leptons and quarks *must* decay through the break-up of their dipreons. Otherwise the top quark would be stable, and so would the heavy lepton κ. The $\nu_{\kappa 1}$ would indeed decay to, for instance, an e^- through the same preon processes as for $t \to b$, as can be seen in Table II.

A new, heavy quark can be studied in two different ways. One can either look for an excess of events with a high missing mass that recoils against the normal quark. Or one can try to identify the decay products of the new quark, and derive their invariant mass.

The first method should, in principle, be simpler than the second one, since it takes only to identify a c or b jet and measure its energy. Assuming that no other particles have been produced than a pair of one new and one normal quark, and that the mass of the latter can be neglected, one gets the relation

$$E_q = \frac{E_{LEP}^2 - M^2}{2E_{LEP}}, \qquad (18)$$

between the mass M of the new quark and the energy E_q of the recoiling normal quark. In practice, jet energies are measured, and the relation between the initial quark energy and that of its final hadronic jet is not simple. In order to search for the h (or k), quark data are needed for jets typical for c (or b) quarks. Unfortunately, most LEP data on heavy flavours are taken at the Z^0 peak. Superheavy quarks would give broad peaks in the jet energy spectrum according to Eq. (18), on top of the background, which would most probably come from $e^+e^- \to W^+W^-$ followed by $W \to q_1\bar{q}_2$.

The second method, *i.e.*, to look for decay products of the heavy quark or lepton, is the conventional one. The two quarks h and k do not decay like the t, and cannot be discovered as a result of the search for single-top production. However, k is identical to the hypothetical fourth-generation b' quark, which has been searched for in many experiments [1]. It decays like $k \to b + x$, through $\delta(\bar{\delta}\bar{\alpha}) \to \beta(\bar{\beta}\bar{\alpha}) + x$, where x can be a γ, a Z^0 or a gluon. According to [24] the bZ^0 or cW channels should dominate the decay of a "b'", so one way to find it would be to analyze the recoiling mass against a b and a Z^0 jet, or a c and a W jet. However, their analysis is built on production of $b'\bar{b}'$ *pairs*, unlike in our model. And so is the recently published experimental search by the DELPHI collaboration [25]. We instead suggest that the analysis is remade for $b'\bar{c}$ production, which would require other kinematical cuts than in [25].

In conclusion, we argue that there might still be room for signatures of composite quarks and leptons in the CERN LEP data, provided that these are analyzed with slightly different methods in comparison to what has been done so far.

We acknowledge useful communications with R. Tenchini from the ALEPH collaboration, J. Timmermans and S. Ask from the DELPHI collaboration, as well as D. Plane from the OPAL collaboration. E.E. is grateful to the Swedish National Graduate School of Space Technology for financial support, and S.F. would like to thank the Max Planck Institut für Kernphysik, CERN and Indiana University for hospitality and stimulating feedback during visits where these ideas were presented and discussed.

---

[1] *Review of Particle Physics*, W.-M. Yao *et al.*, J. Phys. **G33**, 1 (2006).
[2] I.A. D'Souza, C.S. Kalman, *Preons* (World Scientific, Singapore 1992).
[3] S. Fredriksson, in Beyond the Desert 2003, Springer Proc. in Physics **92**, 211 (2004), Ed. H.-V. Klapdor-Kleingrothaus; arXiv:hep-ph/0309213.
[4] C.S. Kalman, Nucl. Phys. Proc. Suppl. **142**, 235 (2005).
[5] J.-J. Dugne, S. Fredriksson and J. Hansson, Europhys. Lett. **57**, 188 (2002).
[6] M. Gell-Mann, Phys. Lett. **8**, 214 (1964).
[7] G. Zweig, report CERN-TH-412 (1964), unpublished.
[8] H. Harari, Phys. Lett. **86B**,83 (1979).
[9] M.A. Shupe, Phys. Lett. **86B**, 87 (1979).
[10] H. Fritzsch and Mandelbaum, Phys. Lett. **102B**, 319 (1981).
[11] M. Anselmino, E. Predazzi, S. Ekelin, S. Fredriksson and D.B. Lichtenberg, Rev. Mod. Phys. **65**, 1199 (1993).
[12] G. Alexander *et al.*, Phys. Lett. **B385**, 433 (1996).
[13] K. Ackerstaff *et al.*, Eur. Phys. J. **C1**, 45 (1998).
[14] G. Abbiendi *et al.*, Eur. Phys. J. **C14**, 73 (2000).
[15] D. Plane, private communication.
[16] R. Barate *et al.*, Phys. Lett. **B401**, 347 (1997).
[17] R. Barate *et al.*, Phys. Lett. **B415**, 435 (1997).
[18] R. Barate *et al.*, Phys. Lett. **B453**, 107 (1999).
[19] R. Barate *et al.*, Phys. Lett. **B484**, 205 (2000).
[20] A. Ealet *et al.*, report ALEPH 2001-013 (2001), contributed paper to several conferences in 2001.
[21] P. Abreu *et al.*, Eur. Phys. J. **C6**, 371 (1999).
[22] P. Abreu *et al.*, Eur. Phys. J. **C8**, 41 (1999).
[23] P. Abreu *et al.*, Eur. Phys. J. **C17**, 53 (2000).
[24] S.M. Oliveira and R. Santos, Phys. Rev. D**68** 093012 (2003); Acta Phys. Polon. **B34**, 5523 (2003).
[25] J. Abdallah *et al.*, Eur. Phys. J. **C51**, 249 (2007).
[26] A. Ilyin *et al.*, Phys. Lett. **B503**, 126 (2001).
[27] H. Senju, Prog. Theor. Phys. **95**, 455 (1996), and references therein.
[28] E. Elfgren and S. Fredriksson, Astronomy and Astrophysics, to be published; arXiv:astro-ph/0710.3893.

Paper V

Using Monte Carlo to optimize variable cuts

Optimization for finding signals of exotic particles are made by carefully choosing cuts on variables in order to reduce the background while keeping the signal. A method is proposed for optimizing these cuts by the use of cuts chosen with a Monte Carlo method.

Elfgren, Erik
Submitted to Physics Letters B
(hep-ph/0712.3340)

Using Monte Carlo to optimize variable cuts

Erik Elfgren

Abstract

A Monte Carlo method to optimize cuts on variables is presented and evaluated. The method gives a much higher signal to noise ratio than does a manual choice of cuts.

There are two important methods for refining a signal over background ratio: likelihood analysis and cut-based analysis. Likelihood analysis has the advantage of not discarding any potential signal. However, it is not as straightforward to evaluate its statistical significance compared to the cut-based analysis. Cut-based analysis on the other hand, cuts away parts of the signal in order to reduce the background evenmore.

Traditionally, variable-cuts have been sought with the help of good sense and some experimentation.

In this letter I address an automatical method for searching for optimal cuts. I have used only one simulated set of data, fairly large, and many different backgrounds. The simulated data are heavy leptons with masses $100-200$ GeV done at center-of-mass energies of $183-209$ GeV to correspond to the OPAL experiment at LEP.

The method is simple: Initially, determine which of the variables are most relevant and what their ranges are. If possible, find some minimum cuts that will leave the signal intact, while still reducing the background. This can significantly reduce the time spent on each iteration below.

The cut optimization then has the following general algorithm:

(1) Choose a random variable and change the cut randomly with a value between 0 and $T * max$, where T is initialized as $T_i = 100\%$ and max as the maximum value of the variable.
(2) If this change leaves us with a higher $S/\sqrt{B}$-value, keep it, otherwise discard it.

Email address: `elf@ludd.ltu.se` (Erik Elfgren).

Preprint submitted to Elsevier Science *20 December 2007*

(3) Decrease T and restart from the beginning

A problem with this method is that it might get stuck in a local minimum somewhere. This can be remedied by storing the final cuts and the $S/\sqrt{B}$-value and then reinitializing the process, iterating until a satisfying $S/\sqrt{B}$-value is obtained. The method can be parametrized by ΔT, the change in T per iteration, T_i, the initial value of T and N_{it}, the number of reinitializations.

Our test case is described in general in [1] and in particular in [2]. A short resumé follows here. The signal we are looking for is $e^+e^- \rightarrow \bar{\nu}N \rightarrow \nu lqq$ and the main variables are the lepton energy E_l, the missing energy, E_ν, the invariant mass of l and ν, the invariant mass of the N $(= q, q, l)$ and the lepton type ($l = e, \mu$ or τ). Both the signal events and the background events were subject to the full OPAL detector simulation [3] as well as some basic cuts to ensure a good quality [4]. The miminum cuts mentioned above were set to $E_l, E_\nu \geq 5$ GeV. The Monte Carlo generator EXOTIC [5] was used to generate the $e^+e^- \rightarrow \bar{\nu}N$ signal. The following masses were simulated $M_N = 100, 110, 120, 130, 140, 150, 160, 170, 180, 190, 200$ GeV and for each mass the energies $E = 183, 189, 192, 196, 200, 202, 204, 205, 206, 207, 208$ GeV for all $M_N < E$. The total number of signal events surviving the initial cuts were about 350 for each pair of (E, M_N). A variety of MC generators was used to study the multihadronic background from SM, see [2] and references therein. The relevant backgrounds are $qq\gamma$ (KK2f+PYTHIA 6.125), $llqq$, $eeqq$, $qqqq$, $ee\tau\tau$ (grc4f 2.1) and $\gamma\gamma qq$ (HERWIG).

The traditional cut based analysis left us with some $\sim 5 - 15$ signal events and $\sim 5 - 10$ background events, i. e., $S/\sqrt{B} \sim 5$. On the other hand, the MC based method often managed to completely remove the background, while still preserving ~ 50 signal events. There are several ways to improve the value of $S/\sqrt{B}$ but they all come at the cost of longer execution time. The different improvements were:

- Use high T_i value
- Use smaller ΔT for each iteration
- Increase the number of iterations, N.
- Change more variables than one, before recomputing $S/\sqrt{B}$

For most of these improvements, the general behaviour was that

$$\frac{S}{\sqrt{B}} \sim 5.1 \times t^{0.37} \tag{1}$$

where t is the time in seconds. The only exception was in increasing the number of variables, which was not profitable. The $S/\sqrt{B}$ is illustrated in Fig. 1. The values have been averaged over ten different optimization runs. For the dot-

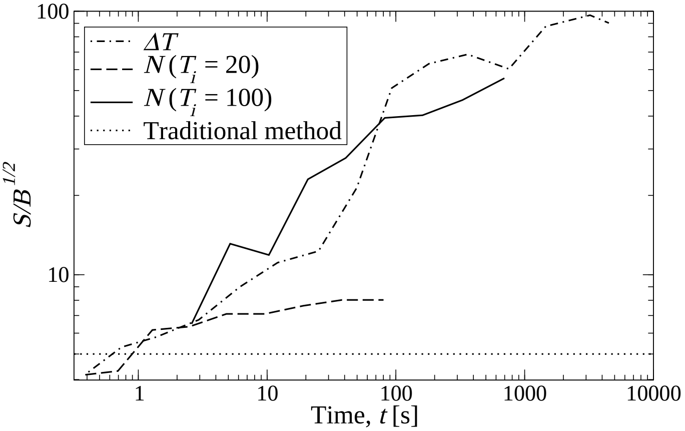

Fig. 1. Comparison of changes in some parameters. The dot-dashed curve represents changing ΔT, the dashed and solid curves represent changing N_{it} with two different $T_i = 20, 100$ GeV and the dotted line is the approximate result of the traditional cut based analysis.

dashed curve, the step ΔT is modified from $2^4 - 2^{-10}$ and divided by two each time. The values of $T_i = 20\%$ and $N_{it} = 2$. We notice that the curve is levelling out asymptotically. The solid and the dashed lines both have $\Delta T = 10$ and the number of iterations goes from $N_{it} = 2$ to 512, multiplied by two each time. Furthermore, $T_i = 20\%$ for the dashed line and $T_i = 100\%$ for the solid one.

I acknowledge support from the Swedish National Graduate School of Space Technology and I thank F. Sandin for many useful discussions.

References

[1] The OPAL Collaboration, G. Abbiendi, et al., Search for unstable heavy and excited leptons at LEP2, European Physical Journal C 14 (2000) 73–84.

[2] E. Elfgren, Heavy and excited leptons in the opal detector?, Master's thesis, Université de Montréal (2002).

[3] J. Allison, et al., The detector simulation program for the OPAL experiment at LEP, Nuclear Instruments and Methods in Physics Research A 317 (1992) 47–74.

[4] G. Alexander, et al., Measurement of the Z^0 line shape parameters and the electroweak couplings of charged leptons, Z. Phys. C52 (1991) 175–208.

[5] R. Tafirout, G. Azuelos, EXOTIC - A heavy fermion and excited fermion Monte Carlo generator for e^+e^- physics, Computer Physics Communications 126 (2000) 244–260.